Doctoral Dissertation
Doctoral Program in Mechanical Engineering (35th Cycle)

# Development of an innovative procedure to assess the crashworthiness of composite materials

By

**Lorenzo Vigna**

******

**Supervisor(s):**
Prof. Davide Salvatore Paolino, Supervisor
Prof. Giovanni Belingardi, Co-Supervisor

**Doctoral Examination Committee:**
Prof. Valentina Lopresto, Referee, University of Naples Federico II
Prof. Simonetta Boria, Referee, University of Camerino

Politecnico di Torino
2023

# Declaration

I hereby declare that the contents and organization of this dissertation constitute my own original work and does not compromise in any way the rights of third parties, including those relating to the security of personal data.

Lorenzo Vigna

2023

* This dissertation is presented in partial fulfillment of the requirements for **Ph.D. degree** in the Graduate School of Politecnico di Torino (ScuDo).

*Dedicated to Elena*

# Acknowledgment

The work reported in this dissertation has been proposed and financed by the company ITW Test and Measurement Italia s.r.l. – Instron CEAST Division. I would like to thank the company and all its employees for their interest and their support from the financial, technical and human point of view. A special thank to Dr. Giuseppe Galizia and Dr. Andrea Calzolari that followed the full project from the first steps to the revision of this dissertation, and to all the other employees of the Italian site of Instron for their professionality, availability and sympathy.

This work would not have been possible without the DIMEAS department of Politecnico di Torino, first my academic supervisor Prof. Davide Paolino (not just a guide during the project, but the only one that could have convinced me in starting this PhD), and Prof. Giovanni Belingardi, a really important reference for me in the field of crashworthiness of composites. I would like to acknowledge also the support, the ideas, the help and the friendship I got from all the guys of the PoLiVe research group.

Thanks also to all the people from different companies, universities, and research centers from all around the world that have supported my work with suggestions, ideas and… a lot of specimens to be tested. Special thanks to Iman Babaei and Ravin Garg for beginning this work and creating a solid base for the development of the testing fixture and procedure. I would like to also acknowledge the help from the MS students Riccardo Destefanis and Enio Colonna from Politecnico di Torino and the BS student Nicholas Damiano from McMaster University in developing some critical parts of the project.

Last but not least, thanks to Elena, my parents, my brother Davide and my sister Rachele, all my family and friends that have supported and advised me during these three long – but not too long – years.

# Abstract

The crashworthiness of a vehicle is defined as the capability of protecting the passengers from injuries due to high decelerations occurring in case of crash. This is achieved including specific structures (called crash boxes or crash absorbers) in the body-in-white with the aim of absorbing the kinetic energy of the vehicle by deforming in a controlled way. While these structures are today manufactured mainly with ductile metals, composite materials are progressively substituting them in high performance structures for crashworthiness applications thanks to the high Specific Energy Absorption (SEA), that allows for a significant reduction of the weight of the vehicle. Some composite structures show very high SEA, in many cases higher than metals, but their diffusion in crashworthiness applications is slowed down by their complex behavior during crash failure.

From many researches carried out in last decades it is known that different structures made of the same material can show, in a crash test, very different failure modes and levels of energy absorption. This is due to the complexity of failure mechanisms occurring during crash, that involve delamination, fiber fracturing and interface debonding.

In this work, the development of an innovative testing procedure to assess the crashworthiness of composite materials is reported. The test is based on the use of flat specimens to characterize the crash behavior of the material applying an in-plane load using a drop tower testing machine. The design and development of a clamping device to avoid the buckling of the specimen is presented together with many experimental results that prove the effectiveness of the testing procedure. Results are then compared to those obtained with specimens made of the same material but with different geometries to investigate the effect on the failure mode and the level of energy absorption of the material.

The testing procedure has two main objectives: first, have a standard method to measure the SEA and other properties of the material with the aim of material screening and properties comparison; second, to have useful experimental results to feed the material cards of finite element software with the aim of predicting the behavior of complex components by simulation. For this reason, part of the work

involved the use of finite element models to investigate in depth the behavior of the material and to test the predictive capabilities of material cards optimized with the results of the crashworthiness test on flat coupons.

The outcome of this work is a testing procedure able to evaluate the SEA of composite flat coupons in splaying or tearing failure mode. The results obtained with the tearing failure mode are higher than those obtained with the splaying failure mode, but lower than those obtained on self-supporting sinusoidal specimens with small curvature radii; this means that a different failure mechanism is taking place, but even more effective failures can happen in different structure geometries, thus signifying that both the splaying and tearing test can give a conventional result useful for materials comparison and material card optimization but not representing the maximum or minimum SEA achieved by the material.

The predictive capabilities of the finite element models after the calibration of parameters based on the experimental results are not satisfactory and require deeper investigation to obtain good predictions on the behavior of complex components. This is due to the high complexity of the failure mechanisms that have been observed experimentally and strongly influence the energy absorption level of the material. Further work will be aimed at finding more complex material models and more advanced techniques for material parameters identification able to reproduce the experimental observations more accurately.

# Contents

# List of Figures

# List of Tables

# Chapter 1

# Introduction

The CMH-17 Composites Material Handbook defines the crashworthiness as the capability of a vehicle *to eliminate injuries and fatalities in relatively mild impacts, and to minimize them in all severe collisions* [1]. This aim can be achieved by means of active methods (e.g., automatic braking in case of risk of impact) or by means of passive methods. This second way requires a proper design of the body in white (BIW) of the vehicle to achieve four goals:

- maintaining a survival volume for the passenger avoiding the intrusion of external bodies
- providing adequate occupant restraint
- including some structural elements (known as crash boxes or crash absorbers) with the aim of dissipating the kinetical energy of the vehicle by deforming in a controlled manner in case of impact.
- allowing for a safe post-crash egress from the craft [1].

The crash box is then a sacrificial element that must provide a controlled deceleration of the vehicle avoiding excessive peaks that could cause injuries to passengers. International standards define the testing conditions and the requirements in terms of maximum deceleration allowed. The crash box should then provide a controlled force and deceleration during its deformation and a certain length of deformation to dissipate a proper level of kinetic energy of the vehicle. A typical solution consists of the introduction, in specific areas of the vehicle, of metallic structure with approximately tubular shape like the two crash boxes in Figure 1.

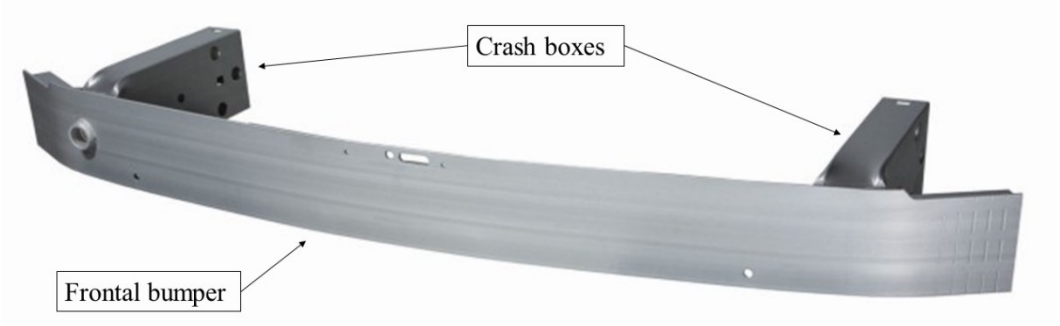


Figure 1: Typical aluminum frontal automotive structure made of a bumper and two crash boxes [2].

If ductile metals are employed, the structure typically deforms folding progressively, and the ductile deformation of the material grants the absorption of the impact energy (Figure 2). Following the automotive trends that aim at lightweighting and reduction of the emissions of vehicles, an improvement that is taking place during last years is the substitution of metals with composite materials to reduce the overall weight of the vehicle. However, composite materials for crashworthiness applications have some peculiar behaviors that require a more complex design process and that will be described in section 2.1.

Figure 2: Aluminum specimen for impact energy absorption evaluation and deformed shape after compression test.

The perspectives in terms of lightweighting and metal substitution are excellent for next future, also thanks to new composites that are under development to improve recyclability (thermoplastic matrixes and fibers, chopped recycled fibers) and to decrease their carbon footprint (natural origin fibers). A case study in 2012 quantified in 19% the possible decrease of the weight of a vehicle substituting metals in critical areas and 23% the possible total weight of composites in a car [3]. These percentages are continuously increasing and today the massive application of composites to standard automotive production is taking place. On the other end, the complex behavior of composites during crash failure, the necessity to build complex numerical models with fine tuning of the material cards, and the absence of a standard method to evaluate the energy absorption of the material are slowing down this trend.

Between the numerous testing standards available for the mechanical characterization of composites, the standard compression test (ASTM D3410 [4]) allows to evaluate the compression resistance of the material, but not its energy absorption during progressive failure. Similarly, existing standards for impact tests like the puncture test (ASTM D3763 [5], ASTM D5628 [6], ISO 6603 [7, 8]) and the Compression After Impact test (ASTM D7136 [9] and D7137 [10]) provide information on the damage tolerance and residual resistance after damage of the material, but are not adequate to evaluate the energy absorption during crash. Several discussions on the creation of a standard test to assess the crashworthiness of composites took place in last years, but due to the complexity of the matter still there is no sufficient agreement to get to an international standard [11, 12].

The objective of the present work is to develop a testing procedure to assess the crashworthiness of composite materials using composite samples. The first part of the work consisted of the design of a testing fixture to perform in-plane compression tests on composite samples, considering all the peculiar aspects of this test. From the test it is possible to evaluate the level of energy absorption of the material. The fixture was used to fully characterize a carbon/epoxy material, considering the effect of the different failure modes and testing conditions (loading rate and testing temperature). Comparative tests were carried out using specimens with different geometries and on a full-scale component, both made of the same material. The results of crashworthiness tests were then used to tune the material card in LS-Dyna and to test the predictive capabilities of the FEM simulation of a component.

# Chapter 2

# Literature review

## 2.1 Crashworthiness of composite materials

Polymer matrix composite materials can be very effective for crashworthiness applications thanks to the combination of high energy absorption and low density. Considering the indicator of the Specific Energy Absorption (SEA, see section 2.1.1 for details), that corresponds to the ratio between energy absorbed during the failure and mass of the failed material, many composite structures have been observed to be more effective than metallic ones [13, 14]. This is clearly visible in Figure 3, that summarizes the results of many researches available in the literature. Another important aspect that comes out from Figure 3 is the absence of a general trend in the results of the different composite materials as a function of the fiber type or of the fiber volume fraction. This is true also for other characteristics of the composite, like the matrix type, the production process, the presence of defects, the layup sequence, the geometry of the crash box.

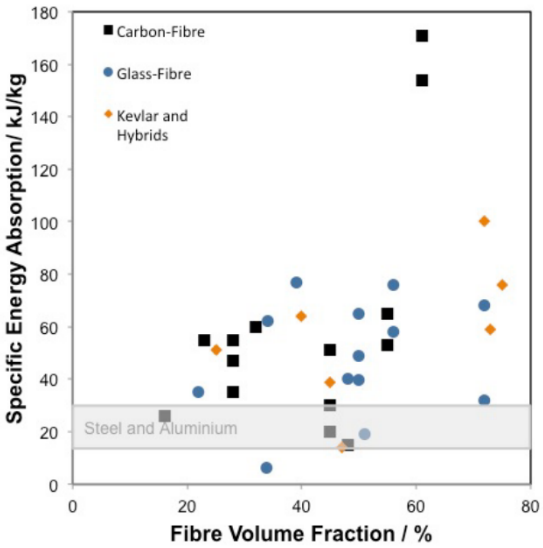


Figure 3: Specific Energy Absorption of some composite structures compared to typical values of metallic structures [14].

Due to the absence of a standard test method to evaluate the crashworthiness of composite materials and the extremely high number of parameters involved, it is difficult to make a comparison between researches carried out following different methods [11]. Given the increasing interest on vehicle lightweighting and the consequent necessity of understanding the effect of the various parameters on the energy absorption capability of the material, the agreement on a standard test method is today more and more necessary.

An important difference between the behavior of a metallic crash box and of a composite crash box is the failure mode. While ductile metals absorb energy mainly through plastic deformation, composite materials usually show a brittle behavior, with consequently low energy absorption in tensile condition. Things are different in compression conditions, when composites can have several failure modes depending on several conditions like the geometry, the matrix and fibers used, the production process, the load conditions. Farley and Jones [15] and Hull [16] carried out the first research on the failure of composite materials in crash conditions, identifying the following failure modes:

- Tearing or transverse shearing
- Splaying or lamina bending

- Fragmentation or fracturing
- Local buckling or folding.

In these studies, a strong dependence of the SEA from the failure mode was found, with tearing and fragmentation failure modes resulting as the most efficient energy absorbing mechanisms, while splaying and local buckling resulted less efficient. A deeper description of these failure modes is reported in section 2.1.2. On the same material, different failure modes can take place depending on the constraint and loading conditions, and the same material can show different value of SEA depending on the failure mode. The failure mode and the corresponding level of energy absorption are something difficult to predict before performing a test, even with the help of a finite element model. A successful FEM simulation needs extensive parameter tuning of the material card of the composite to match the experimental data, and the predictive capabilities of these models are still under question.

All these considerations support the necessity of a standard method to assess the crashworthiness of composites. Main goals of the proposed testing method are:

- Have a measurement of the SEA of the material to compare different materials
- Allow to account for the different failure modes that can happen on the same material during a crash test
- Provide useful data to tune the material card parameters of explicit FEM codes, allowing the prediction of the behavior of complex structures during crash.

### 2.1.1 Performance indicators for crashworthiness

Crashworthiness tests typically consist of compression tests on specimens, components, or complete structures. The load can be applied quasi-statically or dynamically using a high-speed compression machine or under impact conditions, i.e., by means of an impact against a mass having known initial speed. The typical result is a force-displacement curve (Figure 4), through which it is possible to calculate the SEA, that is the most used indicator of the crashworthiness of the material [14]. The curve is typically divided in three parts:

- The first part consists of an increase of the force value corresponding to the elastic initial loading of the specimen and finishes with a peak that corresponds to the initiation of the failure of the specimen. This peak can be smoothed and lowered in height, and the risk of a sudden failure avoided, creating a failure trigger in the specimen with a change in the geometry that locally weakens the structure and initiates the failure.
- The central part consists of a stable value of the force that corresponds to the progressive failure of the specimen.
- The final part usually consists of a decrease of the force at the end of the test.

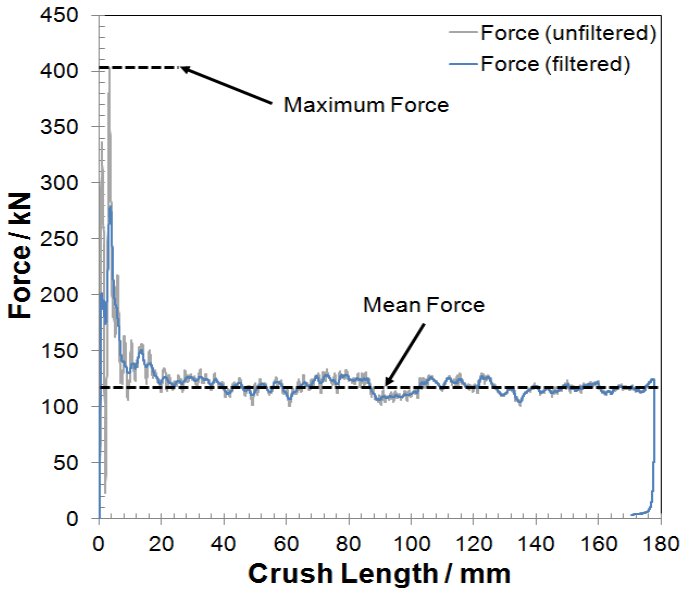


Figure 4: Example of a force-displacement curve acquired during a compression test on a specimen [14].

To compare the results of different tests, some performance indicators are used. A first indicator is the SEA, that corresponds to the ratio between energy absorbed and crushed mass:

$$SEA = \frac{E}{\rho A \delta} = \frac{\int_0^{\delta} F d\delta}{\rho A \delta} = \frac{F_{mean}}{\rho A}, \quad (1)$$

where $F$ is the acquired force signal, $E$ is the energy absorbed during the test, $\rho$ is the material density, $A$ the cross section of the specimen, $\delta$ the final crash displacement and $F$ the crush force. It is also known as specific sustained

crush stress (SSCS). A higher SEA allows to obtain higher crash force and lower weight of the component. To get a result that is a real property of the material, it is important to evaluate SEA in a part of the force-displacement curve where the failure is stable (not changing in time) and not influenced by unwanted factors (e.g., the failure trigger that intentionally reduces the material strength). A simpler formula can be obtained through some simplifications as proposed by Cutting et al. [17]:

$$SEA = \frac{F_{mean}}{\rho A} = \frac{F_{mean}}{\frac{m_s}{Al}A} = \frac{F_{mean}l}{m_s}, \quad (2)$$

that simplifies the SEA calculation as it only requires the average crash force acquired during the test $F_{mean}$, the total length of the specimen $l$, and the total mass of the specimen before the test $m_s$. Using Eq. (2), it is not necessary to measure the density of the material $\rho$ and the cross section of the specimen $A$, that can be difficult to measure in case of specimens with complex cross sections. As a drawback, the cross-section $A$ of the specimen must be constant.

Another performance indicator is the crash force efficiency (CFE), that corresponds to the ratio between mean crash force and peak force and indicates the effectiveness of a structure in absorbing a high amount of energy maintaining low peak forces that can be dangerous for the passengers:

$$CFE = \frac{F_{mean}}{F_{peak}}. \quad (3)$$

Another performance indicator for the comparison of performance of different structures or materials is the sustained crush stress (SCS), that needs to be evaluated in the stable crash region of the force-displacement curve:

$$SCS = \frac{F_{mean}}{A}. \quad (4)$$

These indicators can be used to describe the performance of specimens or structures, independently from the material. Typical values will vary depending on the structure and on the material.

### 2.1.2 Failure modes

Different failure modes can occur during a crash test on a composite material, due to the complex internal structure made of fibers and matrix that can behave in very different ways during the failure. The failure is the result of several phenomena:

- Interface debonding between matrix and fibers
- Fibers failure under tensile or compression load, that can have brittle aspect (sudden failure typical of carbon and glass fibers) or ductile aspect (Kevlar or thermoplastic fibers)
- Matrix failure under tensile, compression or shear load, that can have brittle aspect (with strong fragmentation, typical of thermosets) or ductile (plastic deformation, typical of thermoplastics)

Farley and Jones [15] and Hull [16] carried out the first research on the failure of composite materials in crash conditions, identifying four failure modes:

- Tearing or transverse shearing when the crack grows inside the fabric layers causing the rupture of both matrix and fibers (Figure 5a); the fibers failure results in high energy absorption.
- Splaying or lamina bending when the laminate bends, causing delamination between the layers that consists of debonding and matrix breaking with the rupture of few or no fibers (Figure 5b).
- Fragmentation or fracturing when the formation of several small fragments occurs, and both matrix and fibers are breaking (Figure 5c).
- Local buckling or folding when there is local bending of the structure, a behavior similar to the plastic folding of ductile metals (Figure 5d).

In these studies, a strong dependence of the SEA from the failure mode was found, with tearing and fragmentation failure modes resulting as the most efficient energy absorbing mechanisms, while splaying and local buckling resulted less efficient. Several parameters influence the failure mode of a crushed component or specimen. Splaying is the typical failure mode in flat or low-curvature geometries made with long fiber materials, while tearing and fragmentation are more typical of corner elements. Folding is instead typical of polymeric or natural fibers, that show a ductile behavior in compression conditions.

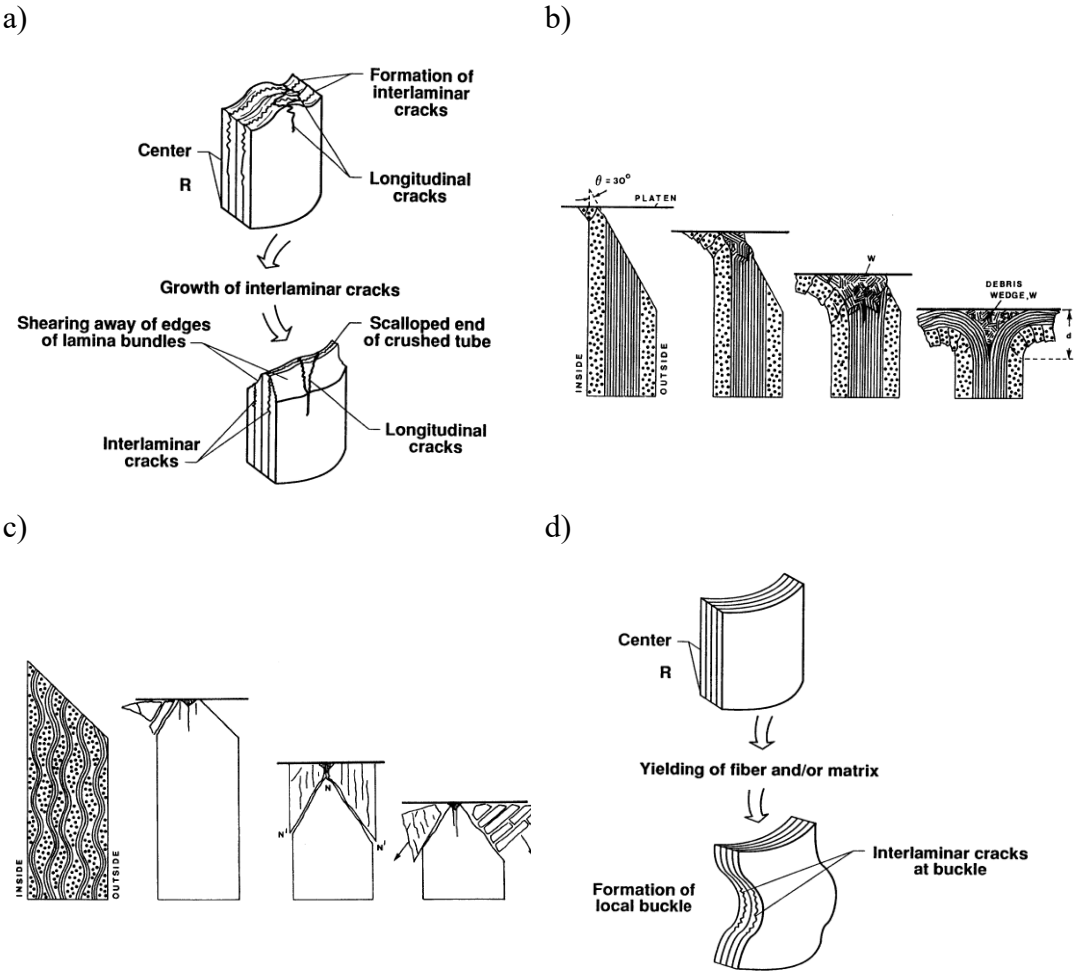


Figure 5: a) Transverse shearing failure mode as described by Farley and Jones [15]; b) Splaying failure mode as described by Hull [16]; c) Fragmentation failure mode as described by Hull [16]; d) Local buckling failure mode as described by Farley and Jones [15].

The proposed categorization is a simplification of the real failure phenomenon, that can be very complex and involve different coexisting failure mechanisms, and is probably one of the causes of the characteristic oscillation of the force-displacement curve acquired during crash tests [18]. Some changes in the failure mode in the same crash test are shown for example in Figure 6.

a) b)

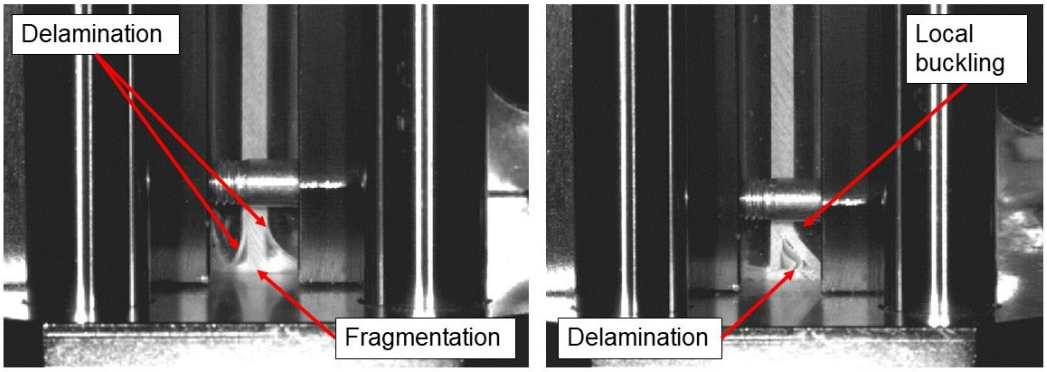


Figure 6: Different failure modes in different moments of the same test on glass fiber flat specimen a) First moments of the test b) Final moments of the test. The failure mode is a combination of splaying, fragmentation and local buckling [18].

Different failure modes can be triggered by different structure geometries and have different effectiveness in terms of energy absorption, even for the same material. This results in the experimental evidence that structures with different level of curvature can cause different levels of SEA even if made of the same material [19]. For this reason, the failure mode is an important parameter to be considered in the proposed testing method.

### 2.1.3 Material properties affecting the energy absorption

Many researches have been focused on the investigation of the effect of several factors on the SEA, SCS or CFE of composite structures. Focusing on the SEA, which is the main parameter to assess the crashworthiness of the material, it can be influenced by factors related to the material itself or to the testing conditions. Furthermore, the interaction between different factors and the absence of a standard method that allows to compare different studies make the research on this subject quite difficult. The most influent parameters identified in the literature, that it is necessary to take into account to define a standard testing procedure, are described in this section.

Fibers are one of the elements that strongly influence the mechanical properties of a composite, and this regards the crashworthiness of the material as well. The most common fibers used for crash structures are carbon, glass and aramid, but new research trends are trying to introduce thermoplastic fibers to improve recyclability or natural fibers to reduce the carbon footprint of composite structures. Due to the actual state of the research, where there is no standard procedure to measure the SEA of composite materials, it is difficult to clearly state which fiber gives the best performance. The plot in Figure 3, taken from [14], reports the results of tests found in literature, carried out using different specimens and in several testing conditions. What is clear from the plot in Figure 3 is that several composites showed a SEA higher than what was found in typically used metals (aluminum and steel), and this is mainly due to the lower density of composites. Some articles report tests where different fibers were compared in the same testing conditions, but also in this case the strong interaction with the other influent factors makes the choice of the most effective fiber for crashworthy design very difficult. Farley and Jones [15] carried out an extensive research on the effect of different fibers finding a correlation between fiber's stiffness and SEA, but they found also a strong interaction with other parameters like the choice of the matrix or the layup angle of the fibers. Despite their better impact damage tolerance, aramid fibers usually have lower crush characteristics than carbon fibers [20]. Also hybrid aramid-carbon specimens showed lower specific energy absorption than fully carbon composites [21]. Reason of this can be the lower compressive resistance and the plastic behavior of the aramid fibers, that determines a progressive folding failure mode that causes the lower energy absorption [13]. Considering the failure mode, while carbon and glass fibers tend to give brittle failure of the material, with splaying or tearing, aramid fibers usually cause ductile deformation with folding of the structure [15, 22]. Most of the researches available in the literature, are referred to long fibers, even if chopped fibers are suitable for automotive applications because of their lower price and possibility to be manufactured from recycled fibers [23, 24].

Another important element influencing the crashworthiness of composites is the matrix, even if its effect is again something difficult to understand. This is mainly due to the several parameters that characterize the different plastics, to the interaction with other factors (e.g., different fibers will bond in different ways to the matrix). In general, it is possible to state that the dependence of the absorbed energy from the choice of the matrix is lower than from the choice of fiber's architecture [25]. Good results are usually obtained with thermosetting resins,

between which the most used in high performance applications is epoxy, but other polymers like polyester or vinyl ester gave good results as well. The brittle behavior of many thermosets causes fragmentation of the matrix with good energy absorption during the stable crush of the material. Thermoplastic materials, instead, due to their more ductile behavior, do not show fragmentation, causing the folding of the structure and consequently lower energy absorption. An important exception are the carbon-PEEK composites, that showed the higher energy absorption found in literature [14]. This was explained because of the high toughness of the PEEK matrix [13], and, in general, polymeric matrixes with higher fracture toughness have shown better performances during crash [25]. Furthermore, as typical of composite materials, a good adhesion between the matrix and the fiber is necessary to get the best performance. The surface treatment of the fibers is then very important in order to assure a good bonding and get high specific energy absorption [26].

Regarding long fibers or oriented short fibers, another important parameter is the fiber architecture. Three main parameters describe the fiber architecture of a composite: fiber volume fraction, use of unidirectional fibers or fabric, direction of the fibers respect to the crash direction. In tests carried out on tubes, specimens made of woven fabric showed slightly better results than those analogously made of unidirectional layers [27]. The SEA of fabric tubes was found about 10% higher than in unidirectional tubes, and the reason of this behavior could be related to the more tridimensional orientation of the fibers. In [28] the tubes with an amount of circumferential fibers were found to have a SEA almost double than those having only axial fibers. An increased SEA can be obtained with a higher percentage of axial fibers up to a certain limit, followed by a drop for higher values. The behavior was found dependent on the crush speed, with an optimal condition to maximize the SEA around 80% in quasi-static conditions and 50% in dynamic conditions [16]. In another research, the winding angle of tubes made using the filament-winding technique showed an optimal behavior with an angle of 70° with respect to the axial direction, and a decrease for different angles [16]. Several other configurations and stacking sequences were tested by other researchers obtaining results that are sometimes difficult to compare. In another research, several layups were compared, and a layup consisting of a combination of 8 layers of axial fibers and 2 layers of fabric that demonstrated to have the higher SEA [21]. Regarding the proportion between fibers and matrix volume, an increase of SEA with the volume of fibers was found, even if its effect is influenced by many other parameters [14]. In some applications, a technique used

to increase the energy absorption is the design of sandwich structures including Kevlar honeycomb cores, as usually happens in motorsport [29].

A failure trigger is an element of a structure for crashworthiness necessary to start a stable failure avoiding excessive peak forces and sudden failures like buckling, typically causing low level of energy absorption. To achieve high levels of energy absorption the failure should start in a specific area of the structure and then propagate to the remaining part in a stable and progressive way, deforming or fragmenting the highest quantity of material possible. While in crash boxes the geometry itself is generally designed to trigger the failure in a specific area (e.g., a conical structure starts failing from its vertex, where the local stress is maximum), a specific trigger element is present on specimens for SEA evaluation. The simplest way to trigger the failure requires a chamfer to reduce the thickness of the laminate. With this trigger the crash force rapidly increases from zero (initial contact) up to a peak (corresponding to a displacement close to the chamfer depth), then stabilizes to a lower value when the stable crash condition is reached. The chamfer angle was found to be influent on the peak force [30]. The chamfer can be machined or the same effect can be obtained with a progressive reduction of the laminate thickness, reducing the number of layers [31]. Other trigger geometries presented in literature consist of cuts in the direction of the laminate, like V-shaped trigger [32–34], sawtooth trigger [35–37] or cuts with different geometries [38, 39]. Another possible approach is to force the material flow during failure in the desired direction in order to obtain the desired failure mode. To achieve this it is possible to use an external device that forces the flow of crashed material in the wanted direction [40, 41].

### 2.1.4 Effect of the testing conditions on the energy absorption

An important aspect to be taken into account when discussing about crash tests on polymer matrix composites is the impact velocity. It is widely known that the strain rate affects the behavior of polymers and consequently of polymer matrix composites [42, 43]. While the effect of impact velocity on impact tests has been deeply investigated [44, 45], only few papers deal with the effect of impact velocity on crashworthiness tests. Farley [20] found no effect of the crashing speed on carbon/epoxy tubes and an increase of the SEA in Kevlar/epoxy. Duong et al. found no effect of impact speed on the SEA of two carbon/epoxy laminates with different layups [46]. In the available literature,

many researches were carried out with quasi-static loading rates, and a deep investigation on the effect of loading rate in many different materials has not been developed yet.

Another important parameter that affects the mechanical performance of polymers and polymer matrix composites is the temperature. This happens also in crashworthiness tests, where the SEA was found to be dependent on the testing temperature but also on the matrix type. In short carbon fiber samples, while epoxy showed a decrease of SEA both at high and low temperatures, ABS and PPS showed an increasing trend of SEA with the decrease of temperature [24].

Testing rate and temperature are then two important parameters to be considered when testing the crashworthiness of composites, and that need to be specified in a testing standard. Some experimental results on testing rate and temperature are presented in Section 4.

## 2.2 Testing of composite materials in crash conditions

Given the complex behavior of composites for crashworthiness applications, the testing phase is today critical in order to obtain a well-designed crash box. Crash tests can give useful information for the design of the component or for numerical model calibration. Tests can be carried out on components or material samples, in different conditions (strain rate, temperature etc.), or according to different techniques (high strain rate compression, quasi-static compression, drop tower impact, sled impact).

Different kinds of results are obtained from crashworthiness tests. First, crash tests are used for validation of components or structures, verifying the level of energy absorption and that the crash force peak is low enough to avoid injuries to passengers. Secondly, tests on components or specimens are useful to characterize the material or the structure, giving results like SEA, SCS, CFE, average crash force or peak force (see Section 2.1.1). These results are useful to build material databases and to compare different composite laminates. Finally, the force-displacement curves can be used to tune the material cards of finite element models by means of curve matching algorithms.

### 2.2.1 Building block approach

The typical design process of a complex system like a vehicle follows the building block approach, usually represented by the pyramid in Figure 7, that asks for different tests to be performed at increasing levels of complexity.

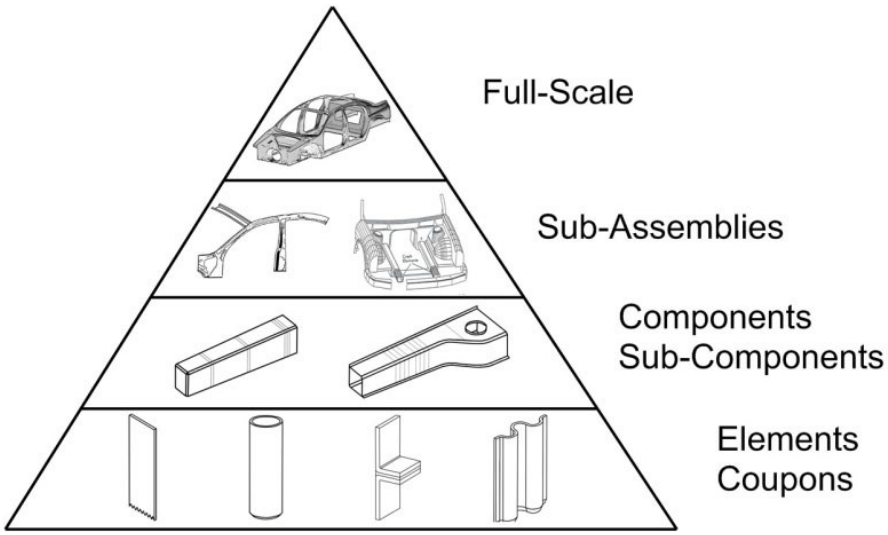


Figure 7: Schematic representation of the building block approach applied to the design of a vehicle [12].

Moving from the base of the pyramid in Figure 7, the complexity of the design and the cost of testing increase.

- The base of the pyramid consists of coupons and elements. Coupons are intended as samples to characterize the material by means of standard or custom tests to find the mechanical properties required for the design. The elements are again material samples but are characterized by shapes and production process more similar to that of the final component, then giving results more similar to those obtained during the component testing. Tests on coupons and elements are usually low-cost respect to those carried out on components, and the results are used for material screening or to build databases for numerical modeling. Both coupons and elements do not find place on the final product.
- The second floor of the pyramid is populated by components and sub-components, the simplest parts that find place on the final product.

The production and testing at prototype level of components is significantly more complex and expensive than at coupon level.

- Sub-assemblies are simple structures made of more components, and their testing is usually very expensive. Sub-assemblies testing is performed close to the end of a project.
- Test of a full-scale model is usually performed for the final validation of the design, as the production cost of a full prototype is very high (in particular if the testing requires the destruction of the prototype like in a crash test). If the results of the test are not good enough, modifications to the design causes very high cost and delays to the project.

It is easy to understand how it is convenient to spend time and resources in tests performed at coupon and element level, where the cost of samples is low, and an extensive use of simulation can help to predict the behavior of components, assemblies or full-scale product. For this reason, a part of the work presented here is aimed at testing the predictive capabilities of numerical models built from the data acquired during coupon crash testing (Chapter 5).

### 2.2.2 Coupons

There is a wide literature on crashworthiness tests on composite materials, and due to the absence of a standard method, several different coupons have been used to measure SEA and other crashworthiness properties.

The first tests were carried out on circular tubes to be loaded along their axis because they can stably lay on a plane during the test and are easy to be manufactured by filament winding, pultrusion or hand-layup using a mandrel. [15, 16, 28]. For the same reasons, this specimen is today still very common, and non-circular cross sections have been also used for material characterization [21–23, 26, 27, 47]. The failure modes obtained with these tests depend on the material as shown by some examples in Figure 8. A mixed splaying/tearing failure mode is typically obtained with long fibers brittle materials, while progressive folding is obtained with more ductile materials.

a) b) c)

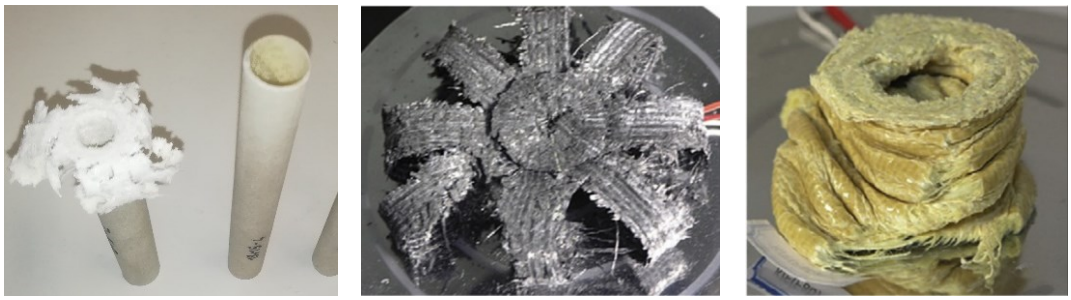

Figure 8: Tubular specimens: a) glass fiber/epoxy tube showing brittle behavior, with a mixed tearing/splaying failure; b) carbon/epoxy specimen showing brittle behavior with a mixed tearing/splaying failure [22]; c) Kevlar/epoxy tube after compression showing plastic-like folding failure mode [22].

In some researches, tapered tubes have been also used [47–49]. The tapered geometry is more complex to be obtained due to the need of a conical mold and a more difficult layup process but it has the advantage of being more similar to real structures. It is not unusual, indeed, to find tapered impact attenuator structures to have the failure starting in the desired point (i.e., the smallest cross section, where the stress is maximum with same crash force). Another effect of the tapered shape is the increasing crash force due to the increasing cross section (Figure 9).

a) b)

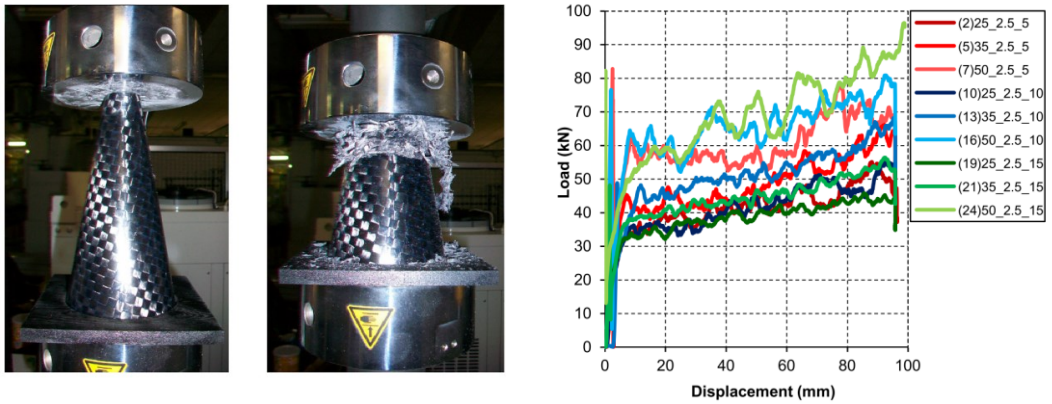


Figure 9: a) Conical carbon/epoxy specimen before and after compression test [48]; b) Force-displacement curves obtained on different conical specimens with the characteristic increasing trend of the force due to the increasing cross section where failure takes place [48].

This happens also in real structures having tapered shape like the side-impact attenuators in Formula 1 racing [32, 50]. Focusing on material characterization, a tapered shape means a variable cross section during the test, that needs to be taken into account to calculate the stress from the force signal or the volume for density and SEA calculation. For this reason, the material characterization using a tapered specimen is more complex.

Another solution that can be found in the literature consists of open section specimens of various kind, some of which have been reported in Figure 10. The section is again constant, and the open section geometry allows to obtain these specimens through several production processes using a mold or simply cutting the desired shape from a larger tube [19]. An open section, compared to closed section, has the same self-supporting characteristics but gives the possibility of easily using another production process like compression molding, that allows to manufacture thermoplastic specimens very rapidly [24, 51].

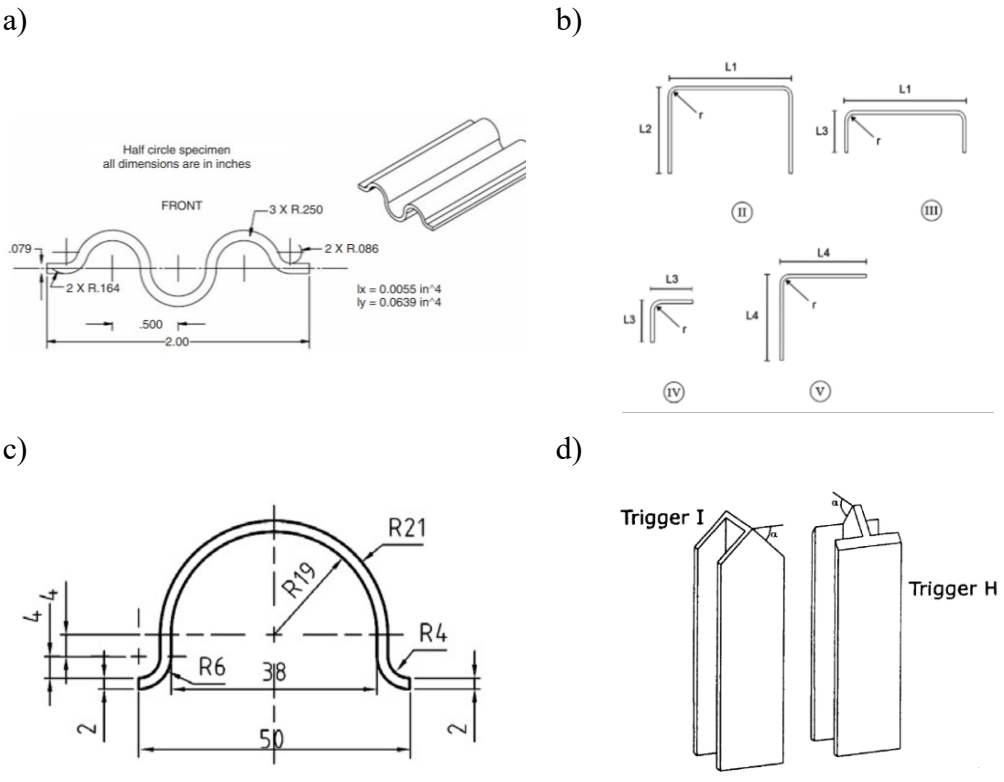


Figure 10: a) Sinusoidal specimen proposed by Feraboli [52]; b) Angular and C-shaped cross sections [19]; c) Omega section [53]; d) I-section specimens [39].

Comparisons between different open section specimens is difficult because the cross section geometry has a strong effect, as pointed out by Feraboli on corner and C-shaped specimens [19] and on corrugated specimens with different curvatures [52]. Between the various open-section specimens available in the literature, the waved geometry was used by several authors [54], but it is worth considering also the Omega shape [53], the I shape [39], or the hat shape [55].

Finally, crashworthiness tests can be carried out using flat specimens. The first advantage of the flat geometry is the independence from the specimen shape. Neglecting the typical dispersion of crash tests on composites, all the plane specimens made of the same material should give the same result if tested under the same conditions (i.e., applying the same constraints). A flat specimen also overcomes several manufacturing complexities as it can be simply cut from a flat plate by milling or waterjet as it is normally done for specimens for standard characterization tests (tensile, compression etc.). This makes it also the less expensive available specimen type, as it simply requires a plane mold for curing several specimens with a single cure cycle thus minimizing wastes. On the other hand, testing the crashworthiness of composites using a flat specimen necessarily requires an anti-buckling fixture with a specific design in order to get acceptable results. More details on anti-buckling fixtures are given in the following.

### 2.2.3 Anti-buckling fixtures for test of flat panels

The first idea of a crash test of a composite laminates using a flat specimen was proposed by Lavoie and Morton working for NASA in 1993 [35]. This design consisted of four supporting columns (two for each side) with the task of maintaining the specimen in vertical position and avoiding its buckling (Figure 11). The specimen has a rectangular shape with a steeple, or a saw-tooth trigger machined on one of the shorter edges to start the failure. The trigger is positioned on a flat surface, against which the failure happens, and a compression load is applied on the other edge by means of a flat plate that distributes uniformly the pressure on the full cross section.

a) b)

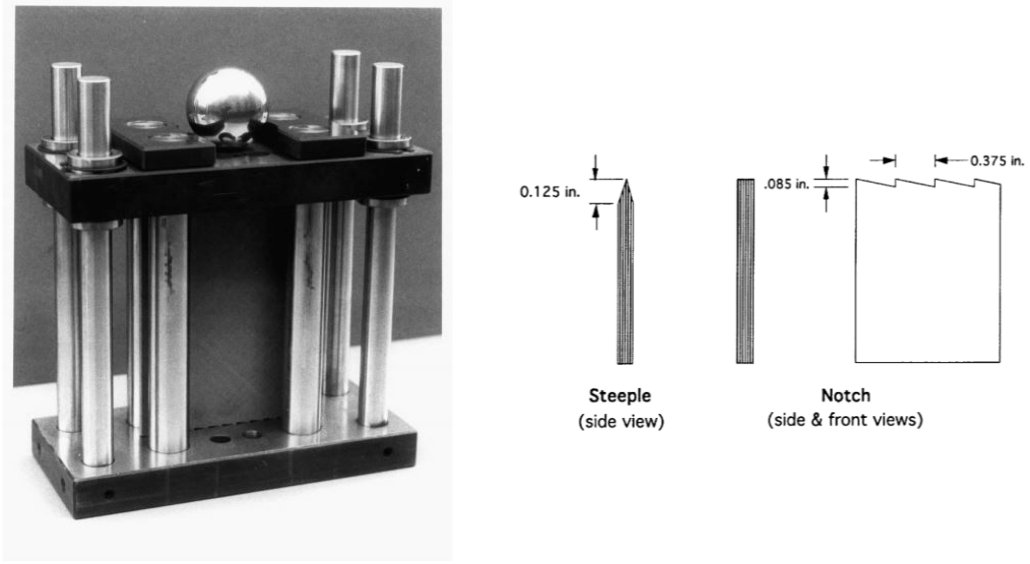


Figure 11: a) Anti-buckling fixture for crashworthiness test proposed by Lavoie and Morton [35]; b) Plain specimens for crashworthiness tests [35].

A similar fixture was proposed by Dubey and Vizzini substituting the supporting columns with knives to reduce the friction and facilitate the debris flow during crash [56], and a similar fixture was also proposed by Daniel et al. [57].

An improvement of the setup was suggested by Cauchy Savona and Hogg (2006, Queen Mary University of London, Figure 12) to accommodate specimens with different thicknesses allowing a translation of the knifes driven by screws [25, 58]. The torque imposed to the fastening screws should be limited to avoid excessive friction force during the test that causes overestimation of the energy absorption properties of the material.

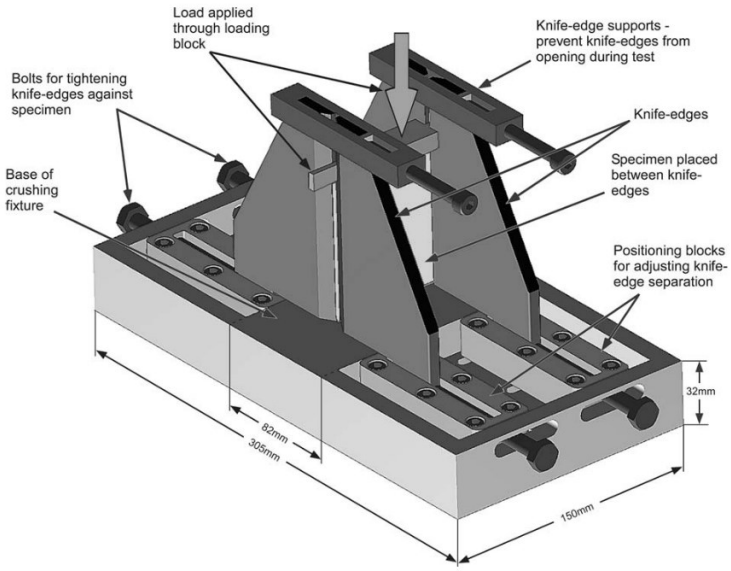


Figure 12: Anti-buckling fixture for crashworthiness test of flat specimen proposed by Cauchy Savona and Hogg [58].

All these fixtures have in common two couples of supporting columns or knives that constraint the full height of the specimen. This imposes a constraint in the lower part of the specimen, where the failure takes place, that affects the energy absorption evaluation because it introduces tearing close to the supports, a failure mode that differs from what is obtained on the other areas (splaying) causing higher energy absorption. Furthermore, the supports act as a constraint to the debris flow thus causing an increase of the crash force. For these reasons, an overestimation of the SEA of the material is usually detected.

To overcome these issues, a different approach was proposed by Jacobs et al. from University of Tennessee (Figure 13), with rolling supports instead of the anti-buckling columns to minimize the friction force and a crash area specifically designed to trigger a bending failure mode with an imposed bending radius [59, 60]. Several different materials were characterized using this fixture between 2003 and 2006 [23, 61, 62], but due to the limitation to the study of the bending failure mode, new testing fixtures were proposed during following years.

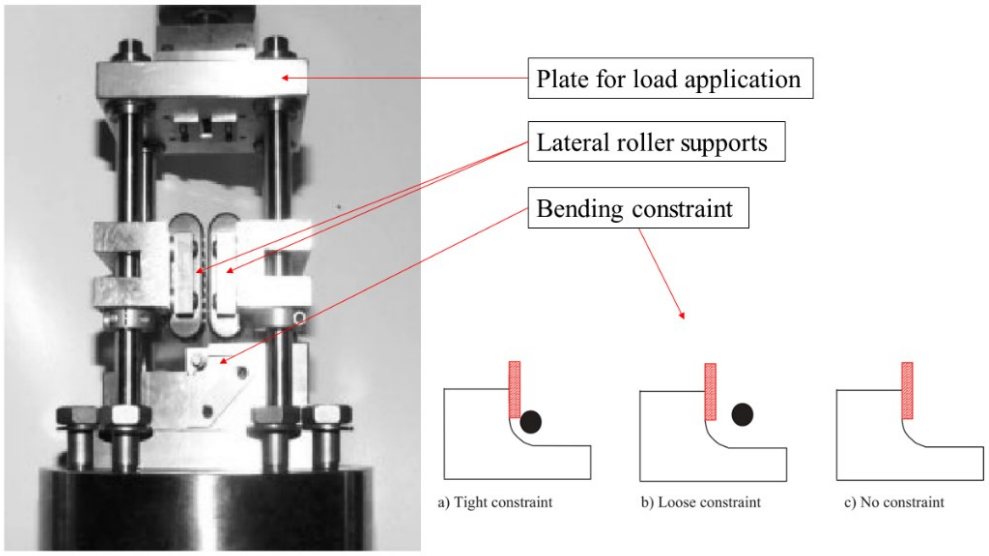


Figure 13: Anti-buckling fixture for crashworthiness test of flat specimen proposed by Jacob et al. [60].

An innovative modification to the NASA fixture was proposed by the company Engenuity, leaving a certain height of specimens unsupported in the failure area (Figure 14a) [63]. In this way, the lower constraint of the specimen avoids tearing and gives space for the debris flow, allowing the desired splaying of the material. The test is performed under a drop tower machine to have high strain rate and the force is applied to the specimen by means of a metallic plate that distributes the force on the upper edge of the specimen. Another innovative feature introduced by Engenuity is the use of pins in the lower part of the support specifically located to constrain the specimen in the failure area suppressing the splaying and triggering a tearing failure, allowing in this way the study of different failure mechanisms using the same specimen geometry (Figure 14b) [64, 65]. Engenuity uses the results obtained from this fixture and from other tests to build material models that can be used in their CZone plugin in Abaqus [63].

a) b)

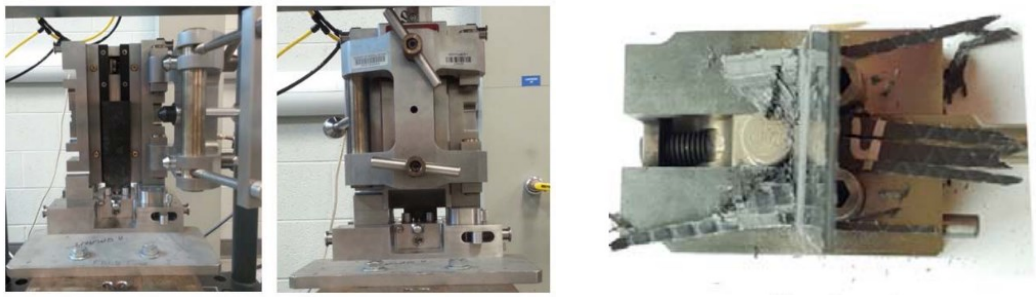

Figure 14: a) anti-buckling fixture for crashworthiness test designed by Engenuity [64]; b) specimen tested in tearing failure mode using the fixture of Engenuity [64].

A different improvement of the NASA fixture was proposed by Feraboli in 2009 [36]. The new fixture (Figure 15a) has a screw-driven clamping mechanism to test specimens with different thicknesses, adjustable supporting knives to study the effect of the unsupported height on the SEA, and an upper plate guided by four columns to distribute the load from the testing machine to the upper edge of the specimen. The specimen has rectangular shape with saw-tooth or steeple edge to trigger the failure. Two materials were tested showing different behaviors at various unsupported heights, observing how the failure mode changes from mixed tearing/splaying (zero unsupported height, like in the NASA fixture) to splaying failure mode with lower SEA (unsupported height from 3 to 13 mm) and buckling with very low SEA (unsupported height higher than 13 mm). The test results obtained on flat specimens (Figure 15b) were compared to those obtained on C-shaped, corner and sinusoidal specimens, confirming that the flat geometry is responsible of the lower SEA because of the splaying or buckling failure mode [19, 52].

a) b)

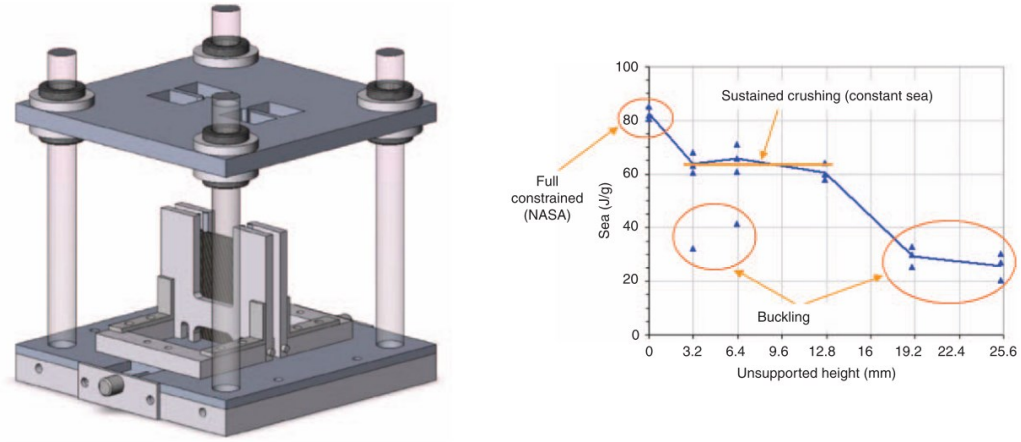


Figure 15: a) anti-buckling fixture for crashworthiness test on flat panel designed by Feraboli [36]; b) SEA of a carbon/epoxy flat specimen as a function of the unsupported height [36].

Many fixtures with similar characteristics were later designed by other authors. A fixture designed at University of Toulouse was used to study the delamination of composites with different triggers [66] and under impact loading conditions [46], pointing out some issues related to the peak force and how it depends on the failure trigger and on the impact condition. Results comparable to those obtained by Feraboli have been obtained also from a fixture designed at University of Tokyo [33, 67].

A later approach proposed by Feindler at TU Munich [68] overcomes the idea of having a specimen sliding between supports and requires clamping the specimen on three of its edges and loading on one of the shorter edges. In Figure 16 it is possible to see how the specimens fails in a mixed mode, with splaying in the central part and tearing at the edges of the impactor.

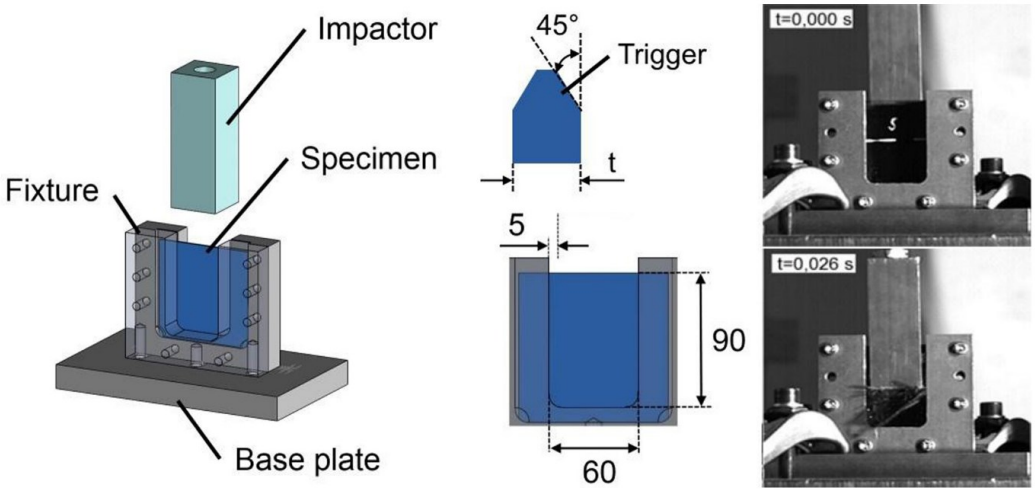


Figure 16: Test setup for mixed splaying/tearing test proposed by Feindler [69].

The fixture was used for parameter identification of FEM models [69] and a procedure to identify the contribution of the two different fracture mechanisms has been proposed performing tests with different impactor widths (Figure 17) and finding good correlation with results obtained testing corner and C-shaped specimens [70–72].

a) b)

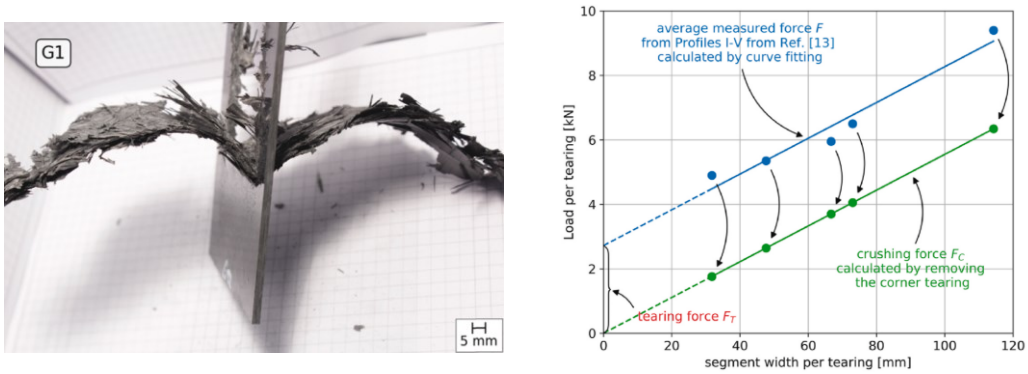


Figure 17: a) Failure mode obtained with the fixture developed at TU Munich [72]; b) schematic representation of the procedure to identify the tearing and splaying components of the crash force [72].

A different approach proposed by Bru et al. [34] and later used by Dalli et al. [32] consists of rigidly clamping the specimen leaving an unsupported height that reduces during the test due to the absence of sliding between the specimen and the testing fixture (Figure 18).

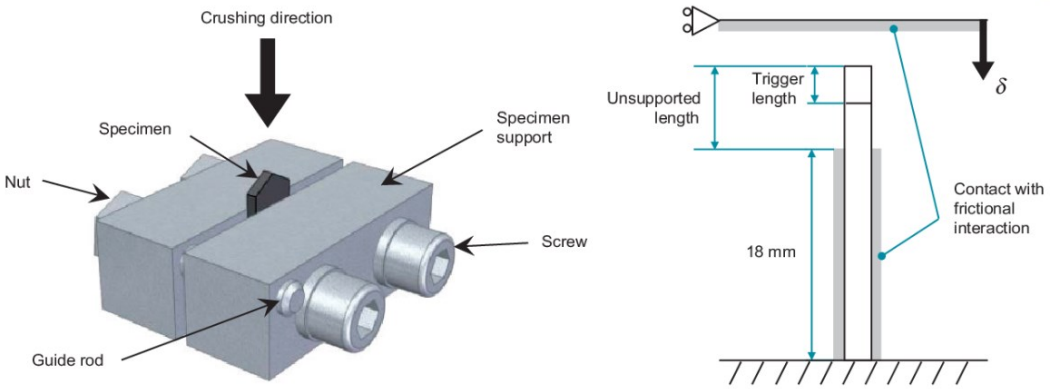


Figure 18: Test setup with specimen clamping and non-constant unsupported height proposed by Bru et al. [34].

Since the unsupported height must be limited to avoid buckling of the specimen, the usable crashing distance is short and mostly influenced by the failure trigger, so the crash force is calculated on a very small distance (less than 10 mm) compared to what is done using other testing fixtures (up to 40 mm as done by Feraboli [36]). Another drawback is that, having a non-constant unsupported height, the constraint condition inevitably changes during the test, causing variations in the failure mode and crash force.

### 2.2.4 Towards a standard method for testing the crashworthiness of composites

Despite all the efforts of many researchers during last decades, some of which have been presented in the previous pages, today there is no standard procedure or

norm available to assess the crashworthiness of composites [11]. This is because the crash failure of composites is a complicate matter, with the level of energy absorption influenced by several factors like the geometry, the physical constraints, and the failure mode. Several consortia have worked to get to a standard testing procedure, for example the Crashworthiness Working Group of the CMH-17 (Composite Materials Handbook) in parallel with ASTM Committee D-30 on Composite Materials [1] or the Energy Management Working Group of the Automotive Composites Consortium (ACC), as well as publicly financed projects like the report *Crash Safety Assurance Strategies For Future Plastic and Composite Intensive Vehicles* founded by US governmental departments [12], but due to the lack of agreement today there is still no standard procedure widely recognized.

An acceptable standard method for coupons testing must then guarantee a number of features:

- Define a coupon geometry
- Define parameters that univocally describe the crashworthiness performance of the material to build properties databases
- Take into account all the possible variables linked to the material (layups, thicknesses, production processes, matrixes and fibers…)
- Obtain repeatable and reproducible results
- Permit to reproduce different failure modes and evaluate their influence on the energy absorption
- Allow for testing at different strain rates and temperatures
- Provide useful data for the design and simulation of composite components.

The core of the following work is to investigate all the cited features to propose a testing procedure that could be proposed as a standard testing method for the assessment of the crashworthiness of composites.

## 2.3 Crash simulation of composite structures

The structural FEM simulation of composites is a complex field due to many peculiar features like the presence of matrix and fibers, the anisotropy, the several fracture mechanisms. Focusing on crash, the progressive failure of composites is

very complex to be simulated due to the contemporary presence of more fracture mechanisms that require the use of complex algorithms, some of which today still under development, to be described. Explicit simulation can be conducted on several software between which the most used in industry and research are LS-Dyna, Radioss, Abaqus and Pam-Crash.

Due to the high cost of experimental studies on components for crashworthiness, and the excellent energy absorption properties of composites, their crash simulation is gaining today growing interest to get to a faster and cheapest development of these components [73]. The simulation can be of help in this process, but careful calibration of simulation parameters based on experimental results is necessary to get sufficiently accurate results. For this reason, and for the wide possibilities offered by FEM software in terms of available algorithms and parameters, a broad literature has been developed by several authors in last decades [74]. The main achievements and modeling strategies are described in the following pages with particular focus on the LS-Dyna software, that was used for the simulation work described in Chapter 5.

### 2.3.1 Modeling approaches

Seen the complex behavior of the crash failure of composites, several are the possible approaches to the simulation of this problem. A first difference can be identified in the scale of the phenomenon investigated [75]:

- Microscale when fibers and matrixes are modeled using solids elements; this approach is the most detailed because can consider the intralaminar interaction of fibers and matrix, but can be applied to a very small portion of material
- Mesoscale when each ply is modeled, and several plies are bonded by cohesive, shell or solid elements; this approach is less detailed than the previous one, but more computationally efficient and allows to model components studying their intralaminar behavior.
- Macroscale when a single shell or solid layer describes the full laminate; even if most software allows to set up the correct stacking sequence, the intralaminar behavior is lost, but in a good model the results related to load and energy are accurate and computational time is strongly reduced.

Microscale and mesoscale models are typically used in research to study the micro damages in the material, while macroscale models are more adequate to simulate the behavior of larger components and structures for the easier setup and lower calculation effort, and typically find place in industries. Once chosen the best approach regarding the scale of the investigated phenomenon, several possibilities are still available to set up the model, starting with the material model.

Several material models are available in LS-Dyna to simulate the damage of composites [76]. While material model 22 (MAT_22) is not adequate for crash simulation because it does not implement a crashfront algorithm, one of the most used is MAT_54, based on the Chang-Chang failure criterion [77] and used by several authors with good results [29, 64, 78–84]. MAT_54 applies the so-called crashfront algorithm, that means that the element close to a failed element start reducing their strength according to a SOFT parameter, and this behavior is necessary to allow the progressive crashing of the laminate; the correct setup of the SOFT parameter is crucial to have an accurate result [85]. The model MAT_58 is based on the Hashin failure criterion [86] and uses a nonlinear stress-strain curve. Even if less frequently used than MAT54 due to the higher number of parameters to be set up, with calibrated parameters the accuracy is good [80] and represents the failure mode better than MAT54 thanks to the nonlinear behavior [82]. Some material cards have been developed more recently to take in consideration the matrix failure even in a single shell or solid layer (MAT_161, MAT_162, MAT_261, MAT_262); due to the recent availability of these models, the high number of parameters required and the good results generally achieved with MAT_54 and MAT_58, a low number of researches on these models is available [80, 87].

A more diffused approach when the interlaminar behavior of the material and the energy absorbed by delamination is of interest consists of modeling the layup of the material using more shell or solid layers bonded by TIEBREAK contacts (i.e. bonded contacts where failure is modeled [64, 88]) or COHESIVE elements (i.e. elements with a fracture mechanics based behavior [89]).

An influent parameter on structural simulations is the mesh size; a mesh sensitivity test is typically a good way to check the robustness of the modeling. A general trend, starting from a coarse mesh, sees the average crash force increasing and the peak force decreasing with finer meshes, up to a stabilization at constant

values (mesh convergence). The convergence is reached with mesh sizes that depend on the specific case study, and a compromise with calculation time needs to be reached. Another important choice is related to the element formulation, due to the several possible choices available in LS_Dyna; the element formulation can influence both the results and calculation time, and the fully integrated element formulation is often a good choice [78].

Boundary conditions and contacts need to be chosen to represent at best the situation under study. An AUTOMATIC_SINGLE_SURFACE with correct input parameters is usually the best choice to model the contact between all the parts that can get in contact during the simulation, including self-contact [90]. An important role is played by the realistic choice of the friction coefficient, as friction is responsible of a non-negligible portion of energy dissipation. A trigger needs to be included in some cases to act as failure initiator, and can replicate the real trigger geometry that can be found on the simulated component (e.g. a thickness reduction or a specific geometry) or have a different nature due to the possibilities given by the FEM software (deletion of some elements or change in the material properties).

A long discussion would be necessary to describe the effect of the most important material card parameters on the simulation of the crash failure. Focusing only on the simpler models (MAT54 and MAT58), Feraboli et al. [78] and Boria [82] identified the compressive strength XC, the compressive strain-to-failure DFAILC and the SOFT parameter related to the crashfront algorithm as the most influent on the failure process. Similar conclusions were drawn by Cherniaev et al. that used the optional parameter SLIMC1 (stress limit factor in longitudinal compression) finding it influent as well [80]. When delamination is modeled using TIEBREAK contacts or COHESIVE elements, the mode 1 fracture toughness is the main parameter controlling the energy absorbed by delamination.

### 2.3.2 Optimization of material cards

Because of the complex behavior of composites during their failure, after the initial setup of the model several runs are usually necessary to adjust the parameters and get a sufficiently accurate result. While this is the only way to deal with some non-physical parameters that cannot be directly obtained from

experimental data (e.g. SOFT or SLIMC1), in some cases it is necessary to modify some parameters that can be obtained from experiments (e.g. DFAILC, the compressive strain-to-failure) because of their strong influence on the energy absorption in the model. The simplest approach is to modify the input parameters observing their effect on the result looking for a good fit with available experimental data. This trial-and-error approach was effectively used by several authors [78–80, 82] and is useful to understand the effect of the parameters on the results, but is inevitably less robust and subjected to the perceptions and observations of the researcher.

In modern software specific packages have been included to automatically run parameters tuning applying several possible optimization algorithms. Optimization strategy has been recently used by several authors for parameter identification or optimum design identification [84, 91–94]. Focusing on the optimization of material cards for crash simulation, the typical approach requires to compare the force-displacement curves acquired from experiments and numerical models. The parameters in the material card are automatically modified until the matching of the two curves is sufficiently good. This procedure is called *curve matching* and consists of the minimization of a function that can be the mean square error, the area between the two curves or any other function defined by the user. Parameters are modified using a *Design of Experiment* technique and results are extracted from each design point. A mathematical model representing the distribution of the results (*metamodel*) is built and the best combination of values is calculated choosing one between the several available algorithms.

The LS-Opt software has been developed to run several kind of studies and optimizations based on LS-Dyna models and gives the possibility to set up a curve matching procedure applying *Single Stage Optimization*, *Sequential Response Surface Method with domain reduction*, or *Efficient Global Optimization* [95]. A high number of parameters can be set up to get to a robust and fast parameter identification, and no standard procedure to set up this calculation is today available.

### 2.3.3 Predictive capabilities of FEM models

The calibration of the material card requires the matching between the results of the FEM simulation and experimental results. After a good matching is obtained,

the capability of the tuned material card to predict the behavior of a different structure or load case is something that today is generally considered not accurate. A new tuning of the material card based on new experimental results obtained testing a prototype of the new structure is usually performed in the industrial field. The reason of this is the complex failure and post-failure behavior of composites, that is not accurately described by the available algorithms because of the several failure mechanisms occurring at microscopic level and influencing the macroscopic behavior of the material and its energy absorption.

Few examples of prediction of the behavior of composites structure after calibration of the material cards are available in the literature. Good prediction of the crash test of some components of a Formula One car were obtained by Bisagni et al. after calibration of the material cards based on experimental crash tests on tubes [50]. Good results achieved with the C-Zone software implemented in Abaqus were described with few details by Lescheticky et al. [63]. Liu and Xia proposed a characterization procedure for a carbon fiber composite that allowed to build a material card that successfully predicted the axial crash of a waved specimen [81]. Dalli et al. proposed a set of crash tests on tubular and flat coupons from which a material card able to predict in Abaqus the crash of the side impact attenuator used in Formula One was obtained, even if several issues to be further investigated before getting to a procedure widely accepted in the industry were pointed out [32]. Despite the good results achieved so far, all the cited papers report different procedures based on different tests, confirming the lack of agreement and the absence of a standard procedure for this kind of predictions.

## 2.4 Previous work carried out at Politecnico di Torino

To further develop the idea of a standard crash test on composite specimens, a research group at Politecnico di Torino started working on the design of a new fixture for compression testing on flat composite plates and related testing procedure. This work moved the first steps from the research of the PhD students Iman Babaei and Ravin Garg, whose research achievement are summarized in this chapter. The research was carried out in the framework of the ICONIC project, which has received funding from the European Union's Horizon 2020 research and innovation program under the Marie Skłodowska-Curie grant. The project

later found the interest and the collaboration of the CEAST division of the Instron company, that supported the design and prototyping of the testing fixture. The research of Iman Babaei was related to the design of a testing fixture and procedure to test the crashworthiness of composite materials [37, 96], while the work of Ravin Garg aimed at improving the FEM simulation strategies based on the experimental results [97, 98].

### 2.4.1 First design of an anti-buckling fixture

The most promising way to get to a standard procedure for a crashworthiness testing procedure was identified as the use of flat specimens to avoid the issues linked to the curvature of the specimen and the lower cost of the sample, that can be easily cut from a larger cured plate like the specimens needed for standard characterization tests (tensile, compression, shear, flexural etc.). A flat plate needs an anti-buckling fixture to be tested in compression condition, and the starting point was identified in the Feraboli fixture to study the splaying failure mode [36]. The specimen (Figure 19) was defined as a rectangular shape with dimensions 150 mm x 100 mm and saw tooth trigger as proposed in the literature [35–37]. The dimensions of the plate were chosen to be consistent with the CAI (Compression After Impact) standard test (ASTM D7136 [9] and D7137 [10]).

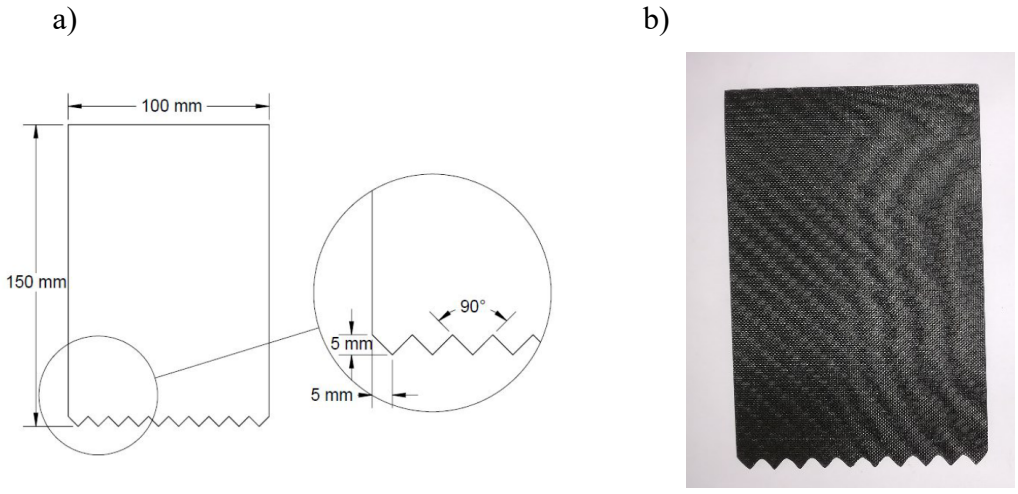


Figure 19: a) geometry of the specimen and trigger proposed in [96]; b) a carbon fiber/epoxy flat specimen for crashworthiness assessment.

The following requirements were identified for the design:

- Splaying failure mode avoiding buckling and tearing
- Thickness of the specimen between 2 mm and 10 mm
- Optimize the design for impact testing
- Capability of withstand impacts up to 1800 J and 220 kN
- Manual clamping through screw-driven mechanism
- Automatic specimen centering

The first design of the fixture is reported in Figure 20 with the description of the most important components. The design was optimized for testing in impact conditions in an Instron 9450 drop tower testing machine. The specimen is clamped between four anti-buckling steel columns (two for each side) whose dimension and position was optimized through FEM simulations [37]. The columns can be moved vertically to have different unsupported heights (from 0 mm to 20 mm) and study the effect of this parameter on the crashing failure. The specimen is positioned with the saw-tooth trigger in the lower part, where a portion of it is left unsupported, in contact with a steel plate against which the failure happens. The clamping force necessary to assure the contact between the specimen and the anti-buckling columns is given through a screw-driven vise mechanism that assures the centering of the specimen respect to the base of the tower and the impactor. A steel plate, guided by four external columns in a configuration similar to the Feraboli fixture [36], distributes the load from the impactor, that has an hemispherical head with 20 mm diameter, on the full upper edge of the specimen.

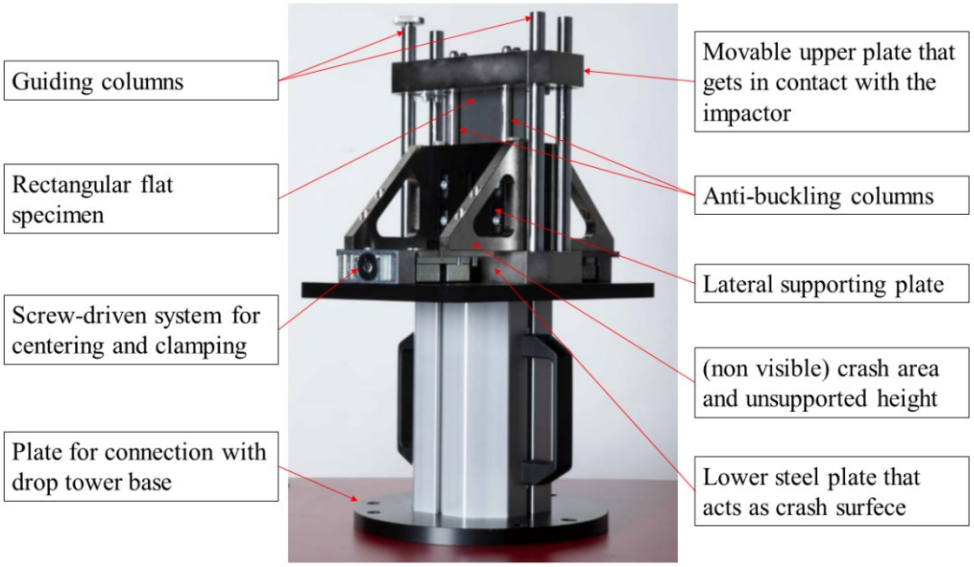


Figure 20: first design of the anti-buckling fixture proposed by Politecnico di Torino and Instron [37].

The fixture was positioned in the testing chamber of a Instron 9450 drop tower, that can guarantee impact energies ranging from 0.59 J to 1800 J, and impact velocities from 0.77 m/s to 24 m/s [99]. The machine was equipped with a striker with strain-gauge load cell with maximum force of 222 kN, and the force was sampled at a frequency of 1 MHz. From the acquired force signal, given the initial condition of the impact (the impactor mass and velocity), it was possible to calculate the displacement of the dropped mass, that corresponds to the crashed length of the specimen [18]:

$$\delta(t) = \delta_0 + v_0 t + \frac{gt^2}{2} - \int_0^t \left( \int_0^t \frac{F(t)}{m} dt \right) dt, \tag{5}$$

where $F(t)$ is the acquired force, $\delta_0$ and $v_0$ are the initial displacement (null when the first contact with the sample is taken as reference) and velocity (imposed by the testing machine), $t$ is the time from the first contact with the sample, $m$ is the dropped mass (that comprises striker, weight carrier and additional weights) and $g$ the acceleration of gravity. The area under the force-displacement curve is then the energy acquired by the failure process of the specimen, and can be used for the calculation of the SEA according to Equation 1.

The tests were recorded using a Photron FASTCAM Mini AX 2 high-speed camera, having a resolution of 1024×1024 pixels at 6400 fps that can be reduced to achieve higher frame rates. The high-speed videos (Figure 21) are fundamental to understand the crashing process and have been useful to propose further improvements of the testing fixture.

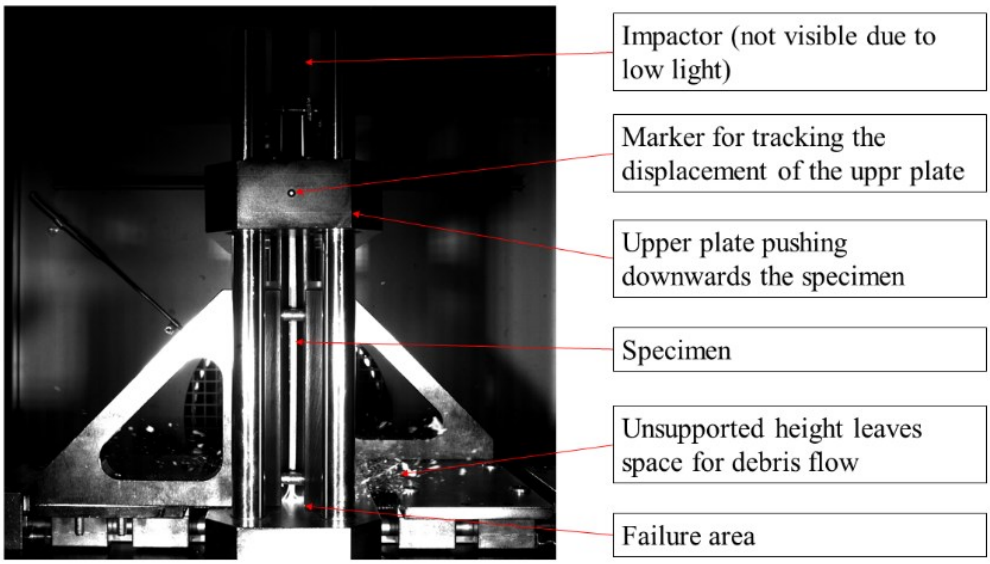


Figure 21: frame acquired through high-speed camera during a crash test on a glass fiber/epoxy specimen.

A typical force-displacement curve is represented in Figure 22 with the indication of the main characteristics. The contact between the impactor and the upper plate causes an initial high peak due to the inertia of the upper plate. The force then falls to zero, corresponding to a loss of contact between the two components, and later grows again to a lower peak before finally stabilising oscillating around a constant value. The first part of the curve is neglected because of the influence of the impact between upper plate and impactor, that hides the real behaviour of the specimen under compression failure; the peak force is actually an inertial peak, and evaluating it as the peak of the crash force generated by the specimen is definitely not correct. To avoid the influence of the first contact, only the part of curve where the force is stable is considered for the

evaluation of the energy absorption and SEA. The very last part of the curve is again neglected to avoid possible effect due to the very low speed and kinetic energy available at the end of the stroke. It is possible to see how the displacement starts reducing when the force falls to zero, and this is due to the rebound of the impact mass due to the release of the elastic energy accumulated in the non-crashed part of the specimen.

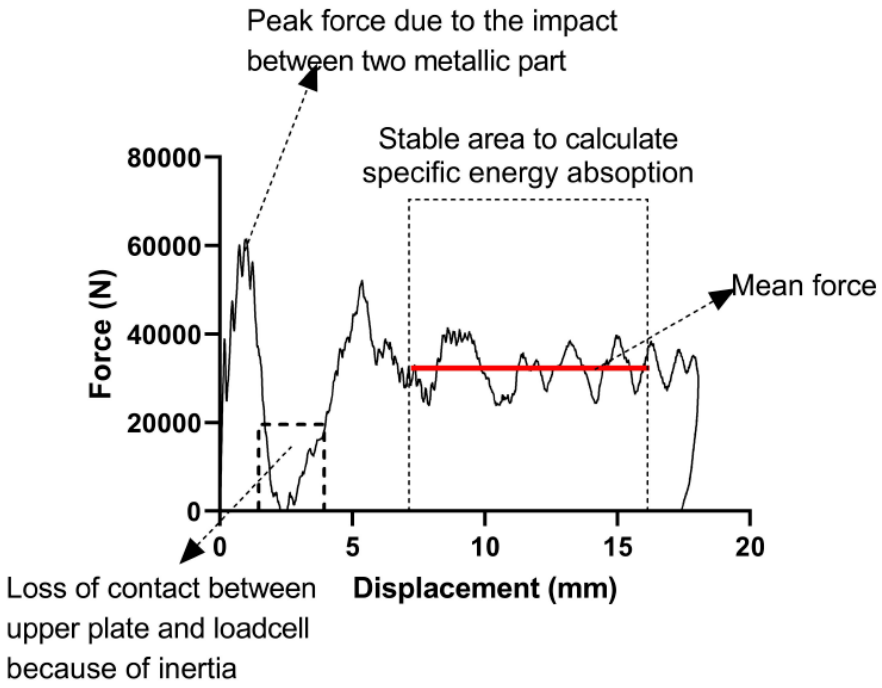


Figure 22: typical force-displacement curve obtained from the newly developed anti-buckling fixture [96].

## 2.4.2 Experimental results

The fixture described in section was used as a part of a wider study devoted to the mechanical characterization of a typical composite material used for crashworthiness applications. The chosen material is a carbon fiber reinforced epoxy laminate built stacking several layers of the Microtex GG630T-37 prepreg [100]. The prepreg consists of carbon fiber 2x2 twill fabric having a weight of 630 g/m$^2$ coated with E3–150 high toughness epoxy resin with resin content 37% in

volume [101]. The layup direction was 0°/90° for all the layers, that were positioned on proper molds and cured in autoclave covered by vacuum bag. The layup preparation and autoclave cure of the material were always performed by the company Carbon Mind srl [102] following the same process to assure the comparability of results (curing process in Figure 23).

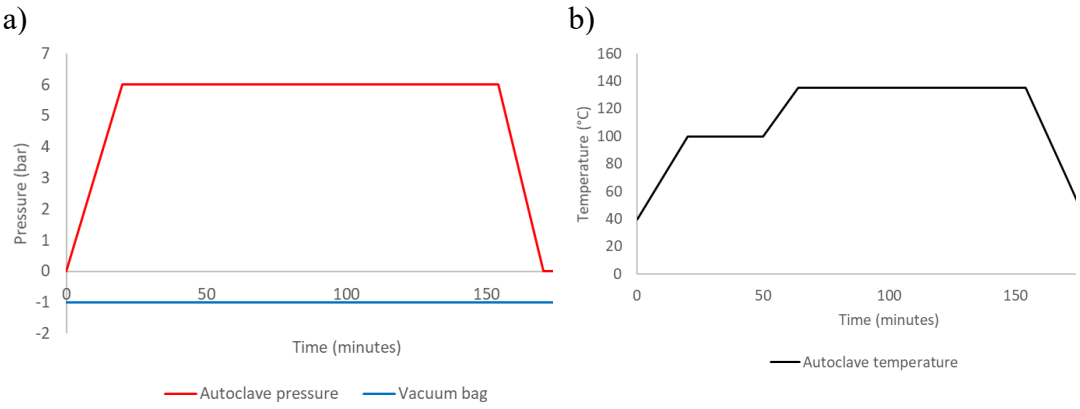


Figure 23: Cure cycle the Microtex GG630T-37 prepreg, provided by Carbon Mind srl: a) pressure; b) temperature.

The GG630T-37 material was characterized in three different steps, starting from the lower level of the building block approach:

- Standard mechanical characterization of the laminate according to ASTM norms
- Crashworthiness tests on flat samples
- Crash test on a full component.

The first characterization step was the measurement of the mechanical properties by means of standard quasi-static tests. The tests were carried out on a Instron 8801 hydraulic testing machine in the laboratories of Politecnico di Torino, and the results are summarized in Table 1.

**Table 1**: Mechanical properties of GG630T-37 carbon/epoxy laminate [96]

| Property | Value | Standard |
|---|---|---|
| **Density** | 1.47 kg/dm$^3$ | |
| **Tensile modulus** | 59.8 ± 2.2 GPa | ASTM D3039 |
| **Tensile strength** | 946 ± 37.5 MPa | ASTM D3039 |
| **Compressive modulus** | 57.8 ± 1.5 GPa | ASTM D3410 |
| **Compressive strength** | 325 ± 13.1 MPa | ASTM D3410 |
| **Shear modulus** | 3.7 ± 0.3 GPa | ASTM D3518 |
| **Shear strength** | 59 ± 0.4 MPa | ASTM D3518 |
| **Flexural modulus** | 70.0 ± 2.1 GPa | ASTM D790 |
| **Flexural strength** | 624 ± 48.1 MPa | ASTM D790 |
| **Poisson's ratio** | 0.074 ± 0.006 | ASTM D3039 |
| **Yield strain** | 0.017 ± 0.001 | ASTM D3039 |

As a second step, compression tests were performed on flat samples using the fixture and the Instron 9450 drop tower in the Instron CEAST laboratory as described in section 2.4.1. The effect of the impact mass and velocity was studied finding a SEA of about 45 kJ/kg and no dependence on the investigated factors in the chosen ranges. The failure mode (Figure 24) was splaying for all the specimens, with small variations from one specimen to another.

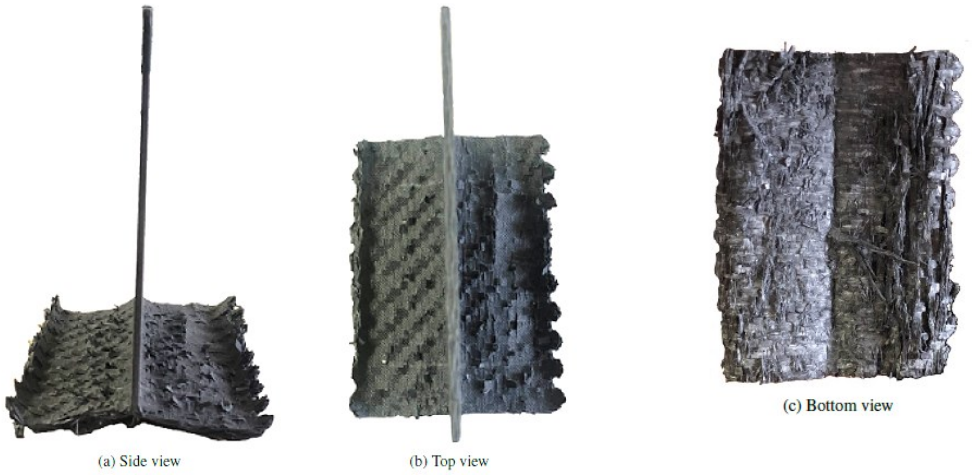


Figure 24: Splaying failure mode found on GG630T-37 carbon/epoxy specimens after crashworthiness test [96].

The results are summarized in the two plots in Figure 25, that shows the force-displacement curves as a function of the impact mass and velocity, and in Table 2, that shows how the variation of the SEA in the explored testing conditions is negligible.

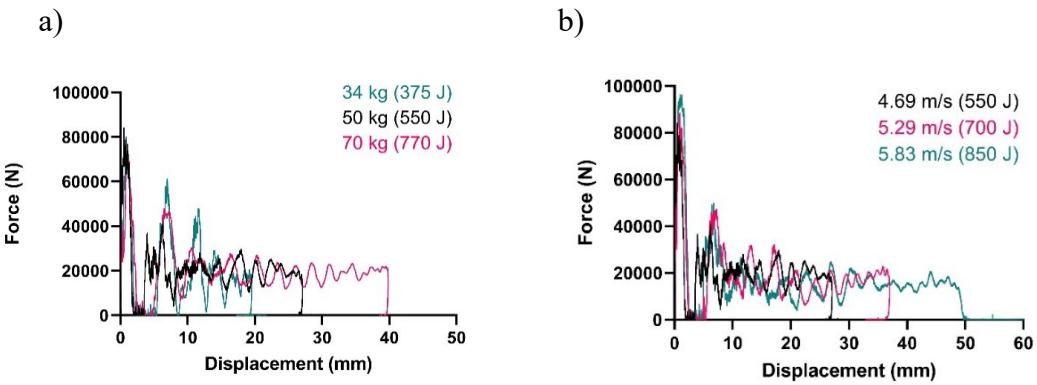


Figure 25: a) force-displacement curves at same impact velocities of 4.69 m/s and different impact masses and energies [37]; b) force-displacement curves at same impact mass of 50 kg and different impact velocities and energies [37].

**Table 2**: Summary of crashworthiness tests carried out on the carbon/epoxy laminate in [96].

| Material | Impact energy (J) | Impact mass (kg) | Impact velocity (m/s) | SEA (kJ/kg) |
|---|---|---|---|---|
| **GG630T-37 carbon fiber epoxy** | 374 | 34 | 4.69 | 45.5 |
| | 550 | 50 | 4.69 | 46.2 |
| | 770 | 70 | 4.69 | 45.9 |
| | 700 | 50 | 5.29 | 45.4 |
| | 850 | 50 | 5.83 | 45.0 |

Similar results were obtained on a glass fiber fabric/epoxy resin laminate with thickness of 3 mm, commercially available under the name NEMA FR4 [103]. Specimens were cut by milling from larger plates. The main mechanical properties are given in Table 3.

**Table 3**: Mechanical properties of NEMA FR4 carbon/epoxy laminate. The density was measured by the authors, while the other properties are given by the supplier of the material [104].

| Property | Value | Standard |
|---|---|---|
| **Density** | 2.07 kg/dm$^3$ | |
| **Tensile modulus** | 24 GPa | ISO 178 |
| **Tensile strength** | 300 MPa | ISO 527 |
| **Flexural strength** | 500 MPa | ISO 178 |
| **Compressive strength** | 500 MPa | ISO 604 |

The results of crashworthiness tests in Table 4, with SEA showing again small variations depending on the testing condition. An important difference with the GG630 carbon fibrer/epoxy is the higher SEA of the glass fiber composite.

**Table 4**: Summary of crashworthiness tests carried out on the glass fiber/epoxy laminate in [96].

| Material | Impact mass (kg) | Impact velocity (m/s) | SEA (kJ/kg) |
|---|---|---|---|
| **NEMA FR4 glass fiber/epoxy** | 34 | 4.69 | 50.9 |
| | 50 | 4.69 | 48.9 |
| | 70 | 4.69 | 50.7 |
| | 70 | 3.96 | 51.3 |
| | 70 | 5.34 | 49.7 |

Another investigation performed using the NEMA FR4 glass/epoxy samples is related to the unsupported hight in the range 5 mm to 35 mm. As previously noticed by Feraboli [36], the results show a plateau of the SEA as a function of the unsupported height due to the splaying failure mode, and a reduction of the SEA and increase of scattering for high values of unsupported height, as described in Figure 26. This behavior is due to the introduction of new failure mechanisms like a longer crack due to the lower constraint that appears with unsupported height of 20 mm and bending, that stars occurring when the unsupported height grows up to 35 mm because of the longer unsupported part of the specimen.

a) b)

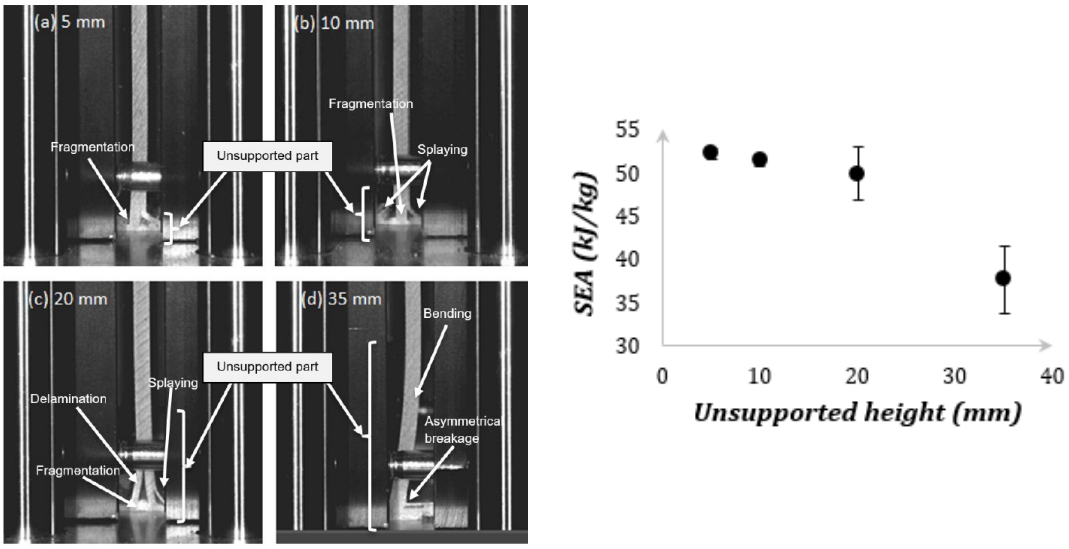


Figure 26: a) Effect of the unsupported height on the failure mode on 3 mm-thick glass/epoxy specimens. While the splaying failure is similar with unsupported height equal to 5 mm and 10 mm, a longer crack is visible with unsupported height 20 mm, and bending appears with unsupported height 35 mm [37]; b) trend of SEA as a function of the unsupported height.

Moving to the component level of the building block approach, an impact attenuator designed for a Formula SAE car was built using the same GG630T-37 carbon/epoxy material and tested to study the behavior of the material on a real component, where the constraints are different, there are curvature radii and inclined surfaces and the failure is triggered by the geometry itself. The attenuator has a tapered structure with the lower section oriented toward the front of the vehicle. The stacking sequence is always 0°/90° and the thickness increases from two plies in the frontal area to three plies in the central part and four plies in the rear part, as explained in Figure 27a; this solution, together with the tapered structure, triggers the failure mode of Figure 27b, making sure that the failure starts in the frontal part and the force increase is sufficiently smooth to avoid high peaks that could cause injuries to the passenger.

a) b)

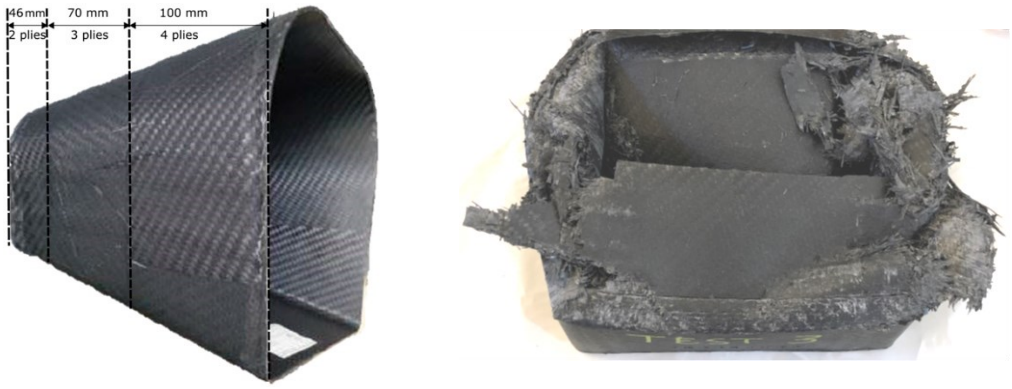


Figure 27: a) Impact attenuator for a Formula SAE car made of GG630T-37 carbon/epoxy material [98]; b) impact attenuator after impact with mass 300 kg and velocity 7.7 m/s [96].

The attenuators were tested in quasi static compression conditions (10 mm/min) and under a 300 kg falling weight load at impact speeds ranging from 7.1 to 8 m/s, obtaining the force-displacement curves in Figure 28.

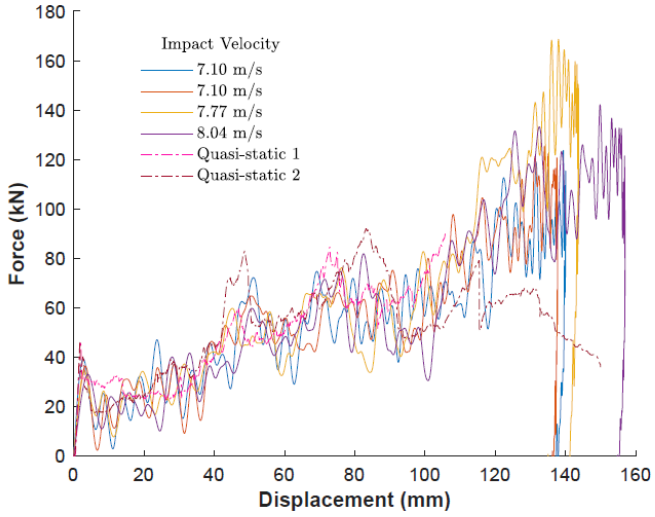


Figure 28: Force-displacement curves acquired during quasi-static and drop weight compression tests on the carbon fiber impact attenuators [96].

The SEA of the material calculated considering the total energy absorbed during the test and the mass of the crashed material (27.8 kJ/kg in quasi-static conditions and 23.7 kJ/kg under impact load) results significantly lower than in coupon testing (45 kJ/kg.). This is an effect of the crashing process of the demonstrator, that involved not only splaying but also tearing, fragmentation, bending and buckling. In particular, buckling in the flat walls due to the sloped geometry left large parts of material unfractured, causing a lower energy absorption.

### 2.4.3 Prediction of the behavior of a complex structure based on coupon level experimental results

The results obtained from the tests presented in the previous pages were used by Ravin Garg to simulate the behavior of the material by means of an explicit FEM simulation [97, 98]. The material properties of the GG630T-37 of the carbon/epoxy laminate obtained through standard ASTM tests in Table 1 were used to set up a material card to simulate the crashworthiness test on flat plates. Some of the parameters required by the material card are not measurable by experiments and needed to be found by means of a parameter identification procedure based on a curve matching algorithm. After a good correspondence between the experimental force-displacement curve and the simulated one was obtained, the tuned material card was used to simulate the behavior of the impact attenuator without modifying any parameter and showing good results. Several modeling strategies were adopted on the Radioss FEM software to find the most effective, and the results are summarized in the following.

The first modeling approach was aimed at building the simplest model possible to reduce the calculation time (macro scale model). The specimen was modeled as a single shell layer and the same solution was adopted for the upper and lower plates of the fixture; the anti-buckling columns were instead modeled as solid. The CRASURV formulation of material law 25 in Radioss was used to model the composite specimen, and property type 11 was used to define the layup of the CFRP laminate allowing for modelling the element type, thickness, layer position and orthotropic direction of each ply. The specimen was modeled using 4

nodes quadrilateral shells adopting a 4 mm mesh size as it was considered the best trade-off between accuracy and calculation efficiency. Fully integrated Batoz shell element formulation was used. The Johnson–Cook elastoplastic material model was used for the steel parts. Contact modelling was defined using the node-to-element (Type 7) and surface-to-surface (Type 24) contacts as described in Figure 29.

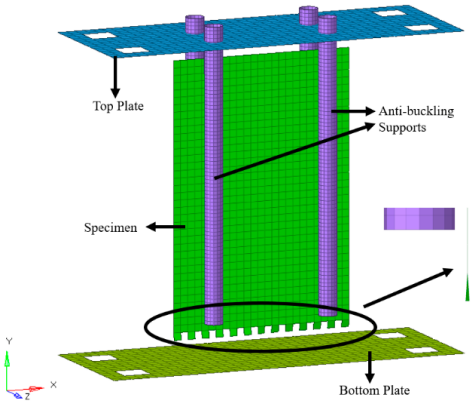


| Component | Material (Numerical Material Law) |
|---|---|
| Top Plate (Rigid Body) | C40 Steel (Johnson–Cook Elastoplastic Law 2) |
| Specimen | Carbon fibre reinforced epoxy (CRASURV Law 25) |
| Supports (Rigid Body) | C40 Steel (Johnson–Cook Elastoplastic Law 2) |
| Bottom Plate (Rigid Body) | C40 Steel (Johnson–Cook Elastoplastic Law 2) |

| Component Pair | Contact Model | Friction Co-ef |
|---|---|---|
| Top Plate + Specimen | Node-to-element (Type 7) | 0.3 |
| Supports + Specimen | Surface-to-surface (Type 24) | 0.3 |
| Base + Specimen | Node-to-element (Type 7) | 0.3 |
| Specimen Self Contact | Node-to-element (Type 7) | 0.2 |
| Top Plate + Supports | No contact defined | -- |

Figure 29: Single shell FEM model of the crashworthiness test on flat specimens [98].

A different model (meso scale model) was built modeling the flat specimen as four layers of shell elements bonded by three layers of cohesive elements (Law 59 Connect) to model the delamination behavior, that cannot be represented by a single shell element model. A strain-based failure criterion was preferred to an energy-based approach, because an energy-based criterion requires data from double cantilever beam (DCB) and end-notched flexure (ENF) tests, which were not available. The number of elements and the calculation time increased substantially using this modeling technique.

The HyperStudy optimization software was used for the identification of the non-available parameters of the material card. An automatic identification procedure was chosen as it is a more robust and repeatable approach compared to trial-and-error approaches adopted in several previous publications [78, 80, 82]. The optimization setup requires to set the unknown variables and their boundaries, in this case:

- $W_{p\_max}$: Global maximum damaging work per unit volume
- $W_{pmax\_c1}$: Compressive maximum damaging work per unit volume in 1 direction
- $\sigma_{res\_c1}$: Compressive residual stress in 1 direction
- $W_{pmax\_c2}$: Compressive maximum damaging work per unit volume in 2 direction
- $\sigma_{res\_c2}$: Compressive residual stress in 2 direction
- $W_{pmax\_t12}$: Shear maximum plastic damaging per unit volume in 12 direction
- $\tau_{res\_t12}$: Shear residual stress in 12 direction.

The damage work is the parameter controlling the failure of the element, while the residual stress is required to define the softening behavior. Given that the studied material is a fabric, the same material properties are considered in 1 and 2 directions, then $W_{pmax\_c1} = W_{pmax\_c2}$ and $\sigma_{res\_c1} = \sigma_{res\_c2}$. The failure criterion controls the element deletion depending on the minimum of the global and directional damaging work values; therefore, it was necessary to optimize only $W_{p\_max}$. The number of parameters to be optimized reduced then to three: $W_{p\_max}$, $\sigma_{res}$ and $\tau_{res\_t12}$.

Of the two optimization algorithms tested, *Global Response Search Method* (GRSM) and *Adaptive Response Search Method* (ARSM), the first resulted to be more robust when a global optimum is searched, while the second resulted to be more efficient. Regarding the curve matching setup, two response functions were tested: the integral of absolute difference between the experimental and the simulation values of the force-displacement curve and the integral of squared difference between the experimental and the simulation values of force-displacement curve, with the first one giving the lower difference the between simulated and the experimental curve.

The optimization led to good results with both modeling approaches as shown in Figure 30, with a difference between the simulated and experimental final displacement in both cases lower than 5%.

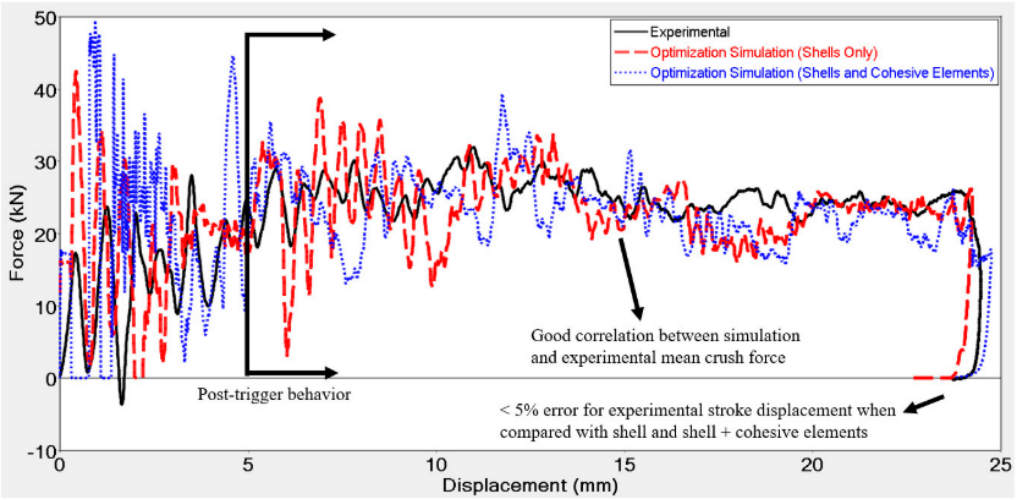


Figure 30: Experimental and numerical force-displacement curves from the crashworthiness test on flat sample after optimization for shells only and shells and cohesive elements models [98].

The model with cohesive elements also showed a damage visualization very similar to the one observed during experiments, with two layers bending on one side, one layer bending on the other side, and one layer being crashed as shown in Figure 31.

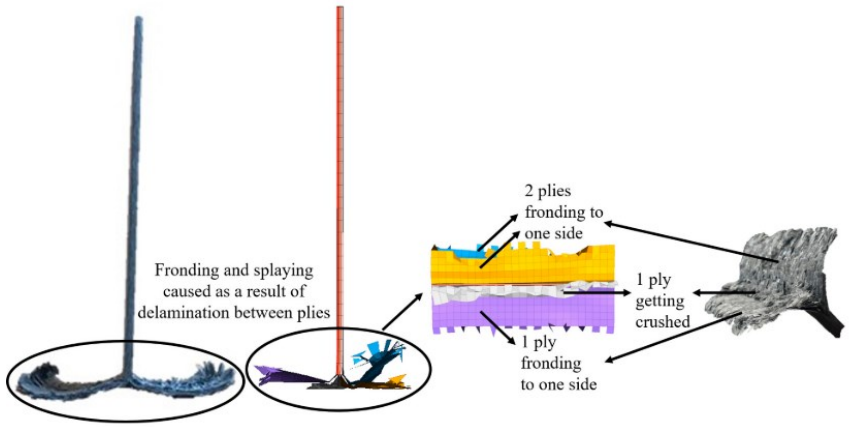


Figure 31: Failure mode from experiment and simulation of the coupon crash test with cohesive elements [98].

Using the optimized material card without any modification, a model of the crash test carried out on the impact attenuator in Figure 27 was built using the same modeling approaches previously described (same mesh size of 4 mm, element formulation and material and contact properties). The two failure modes of the macro-scale and meso-scale models are very different, with the first showing an unrealistic brittle behavior and the second more similar to the experimental failure, and able to predict the buckling failure of the flat walls (Figure 32).

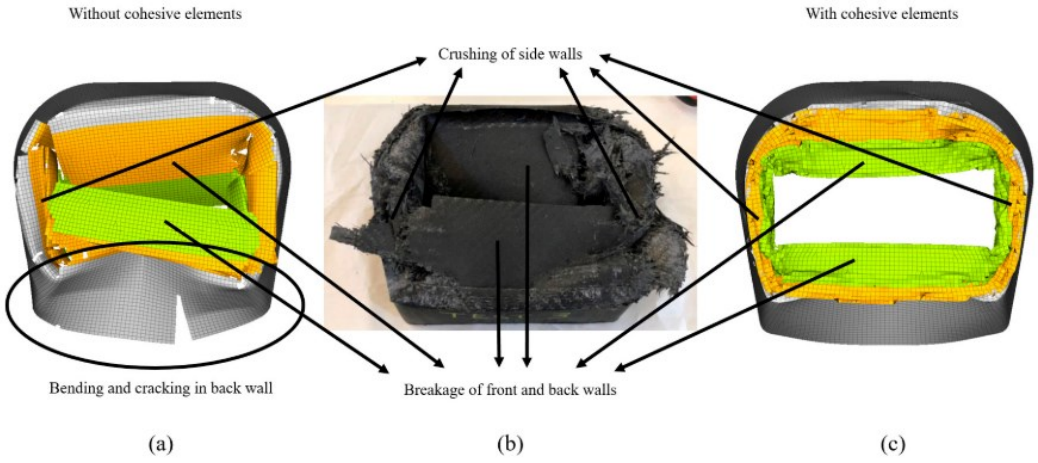


Figure 32: Failure mode of the crash test on the impact attenuator: (a) macro-scale single shell elements simulation, (b) experimental test, (c) meso-scale simulation with cohesive elements [98].

The difference in the final displacement of the impact mass around 5% considering the effect of some features of the experimental setup that were not taken into account in simulations [98]. The average crushing force for the three sections was predicted with good accuracy by the model without cohesive elements, while the model with cohesive elements overestimated the crash force of about 10% due to some non-realistic aspects of the failure process. Peaks are visible at the transition between parts having lower thickness and parts having higher thickness due to the sudden transition to a thicker part of the laminate (Figure 33).

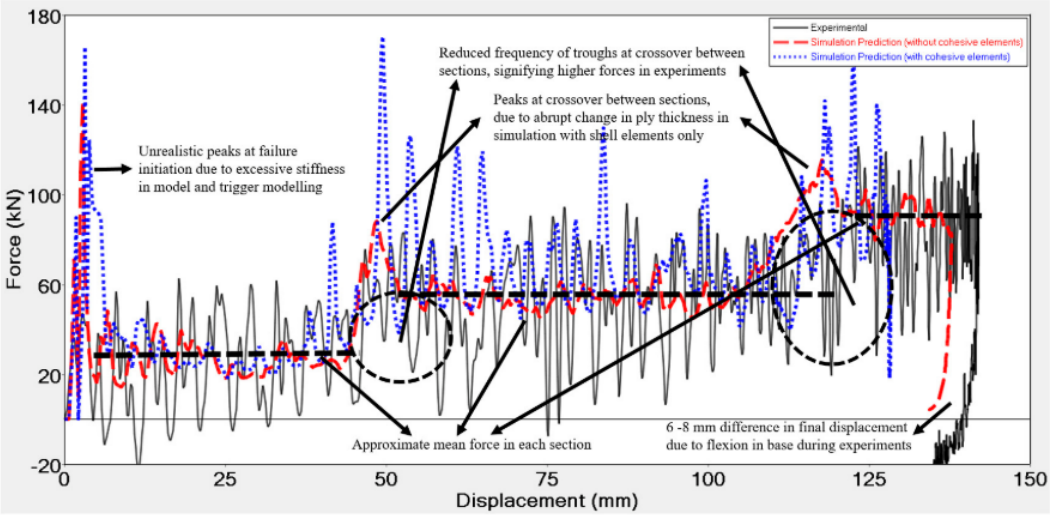


Figure 33: Force-displacement curves acquired during experimental crash tests and predicted through FEM modeling using the shells approach and the shells with cohesive elements approach [98].

Given the reasonably good results obtained with both modeling approaches and a runtime was 60 times higher for the meso-scale model, a macro-scale modeling approach can be sufficient for industrial purposes even if the accuracy in the prediction of the failure is lower.

# Chapter 3

# Design of a fixture for crashworthiness tests on flat samples

## 3.1 Problems related to the test of flat specimens

The core of the work presented here is the design of the testing fixture to perform in-plane crashworthiness tests on flat composite coupons. The first design of the fixture was mainly inspired by the previous fixtures presented in the literature, as described in section 2.4.1. The first experimental results pointed out several features of the fixture that could be improved, like the comfort of use, the repeatability of the results, the quality of the acquired signal. The main improvements developed during this project are described in this chapter.

The first step when starting the design of a new project is to write down a list of requirements based on the experience, on the customer's needs, on the literature or the state-of-the-art of the technology, on existing norms and standards. The main requirements for the developed testing fixture came from the review of the literature, from past experience of the research group on the crashworthiness of composites, and from some interviews performed to

international experts and potential users of the final product. The main requirements are listed below:

- Capability to perform crashworthiness tests avoiding buckling of the specimen and reducing to a minimum the probability of discarding the results due to wrong failure mode
- Flat specimens to minimize shape-related complexities and specimen cost
- Friction caused by sliding of the specimen against the anti-buckling device lower than 5% of the crash force
- Specimen thickness between 2 mm and 10 mm
- Capability to withstand forces up to 222 kN
- Low weight to be easily moved by hand
- Guarantee the visibility of the test and the failure mode from lateral and frontal view
- Fast and simple extraction of the tested specimen and positioning of the new specimen
- Avoid possible mistakes by the user in specimen positioning
- Simple cleaning and debris removal after test
- Testing temperatures between -70 °C and +150 °C

The testing fixture was designed as an accessory for the Instron 9450 drop tower family and have specific dimensions and features to be easily mounted in the testing chamber of the machine. To implement the requirements described here, some issues were found during the design and testing processes, that brought to the investigation and development of specific features described in this chapter.

### 3.1.1 Dynamics of the system

The first improvement of the testing fixture designed by Babaei and Garg [37, 96] and described in section 2.4.1 was aimed at improving the quality of the acquired force in order to have a more realistic force-displacement curve and a longer usable stroke to calculate the SEA. In the first design of the fixture, that was reproposing a concept published by Feraboli [36], the transmission of the load from the falling mass to the specimen happened through a steel plate having a weight of 3 kg guided by four columns (here called crashing plate), with the aim

of distributing the load from the impactor's head (a standard hemispherical head with diameter of 20 mm) to the specimen, minimizing the stress on the upper part of the specimen where it was supported by the anti-buckling columns to prevent any failure in that region.

This concept was not affecting the experimental force acquired by Feraboli but caused an extremely high level of vibration of the force signal when adopted by Babaei and Garg in impact tests, which was unwanted because due to the testing equipment and not to the real behavior of the material. After a first initial peak (Figure 34, blue dash-dot curve), the force rapidly fell to 0 N, thus indicating a loss of contact between the impact mass and the upper plate, then grows again to a lower peak and finally oscillates around a constant value reaching the condition of progressive crash of the material. The level of oscillations is still very high due to the bending deformation of the upper plate. Even if the acquired force curve was effective in giving some results in terms of average force and SEA (neglecting the parts most influenced by the first impact on the crashing plate), the peak force, CFE and level of oscillations were totally unrealistic.

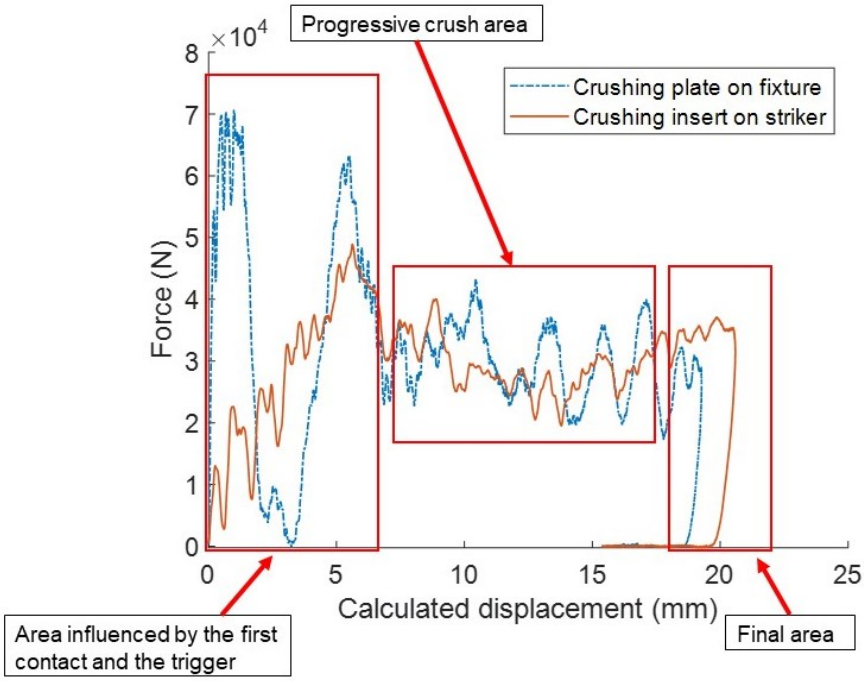


Figure 34: Force-displacement curves acquired during experimental crash tests with two different versions of the fixture. NEMA FR4 glass fiber/epoxy, thickness 3 mm, impact energy 600 J, impact mass 60.2 kg, impact velocity 4.46 m/s [18].

For this reason, the upper crashing plate was removed and the head of the impactor was substituted by a larger flat head with diameter of 50 mm, covering in this way 50% of the available upper area of the specimen [18]. The difference in the testing setup is shown in Figure 35 with the description of the main features of the two testing setups.

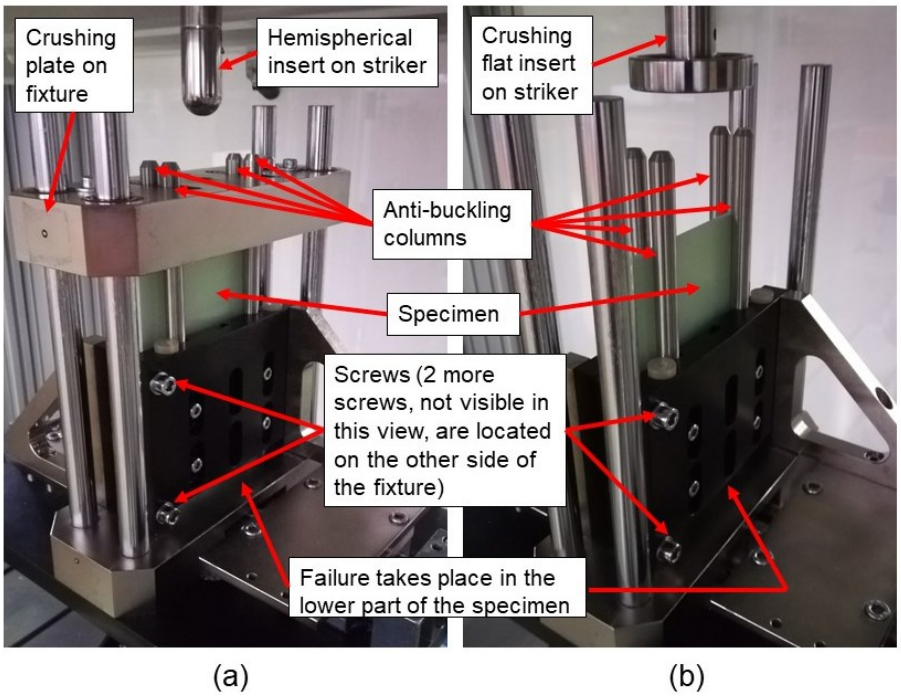


Figure 35: a) First version of the fixture for in-plane crashworthiness tests on flat composite specimens; b) new version of the fixture without upper crashing plate and striker with crashing flat insert [18].

The novel testing setup strongly reduced the vibrations in the signal and eliminated completely the inertial peak followed by loss of contact due to the impact against the upper crashing plate. Despite some low-amplitude oscillations that can still be due to vibrations in the testing equipment acquired by the load cell, the real trend of the force imposed by the specimen failure is now more clear (red continuous line in Figure 34), and the first 5 mm of the force-displacement curve show a linear increase of the force value caused by the progressive increase

of the cross section due the failure of the saw-tooth trigger geometry (Figure 19). The force trend is not perfectly constant, and this is due to the usual variability of the mechanical properties of the material, that can be seen similarly in quasi-static tests (Figure 35). With the new testing setup, oscillations of the force curve are partially due to some vibrations in the testing equipment, but strongly due to changes in the failure mode happening during the test as well, and then visible in quasi-static tests (Figure 36).

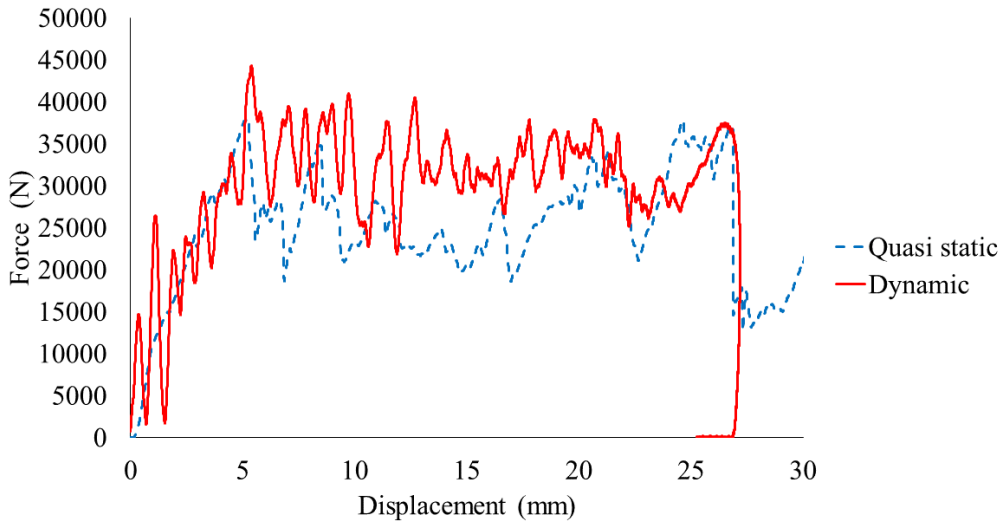


Figure 36: Comparison between a quasi-static (blue dashed line) and an impact (solid red line) crashworthiness test on a NEMA FR4 glass fiber/epoxy flat specimen with thickness 3 mm.

Some tests carried out on NEMA FR4 glass fiber/epoxy flat specimens with thickness 3 mm showed that the failure mode and energy absorption level of the material is not influenced by the new testing conditions [18]. The tests revealed the importance of the testing configuration when the peak force needs to be evaluated, and of the choice of a proper method to identify the part of the force-displacement curve for the calculation of SEA where progressive crash happens (i.e. the failure mode is constant) and the force level is not affected by external elements like the trigger (Figure 37).

a) b)

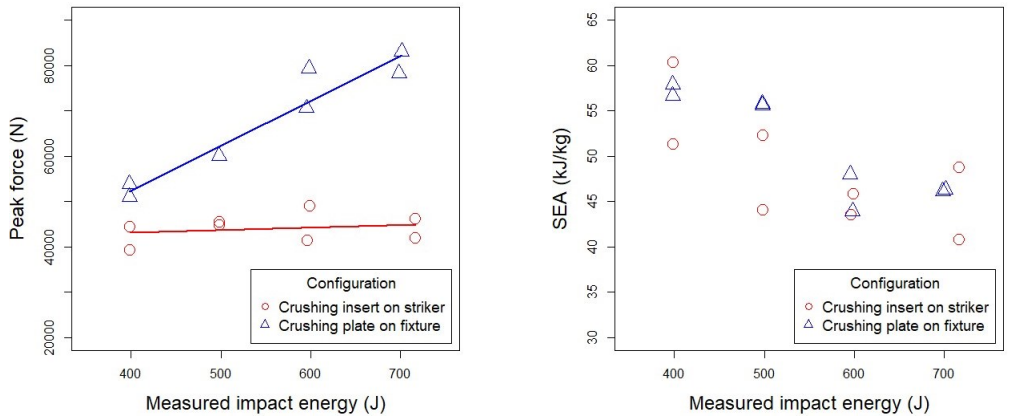


Figure 37: a) Peak force in the two testing configurations [18]; b) SEA in the two testing configurations with decreasing trend due to the choice of the part of the curve for SEA calculation (from 40% to 90% of the curve length), that with low impact energy is influenced by higher force because the crash failure is not completely developed [18].

In Figure 38, some frames acquired using a High-Speed Camera (HSC) during an in-plane crashworthiness test illustrate the different failure mode happening in different moments. This behavior, together with the effect of the failure mode on the energy absorption level [15], can explain the typical oscillations of force curves in quasi-static or dynamic crash tests.

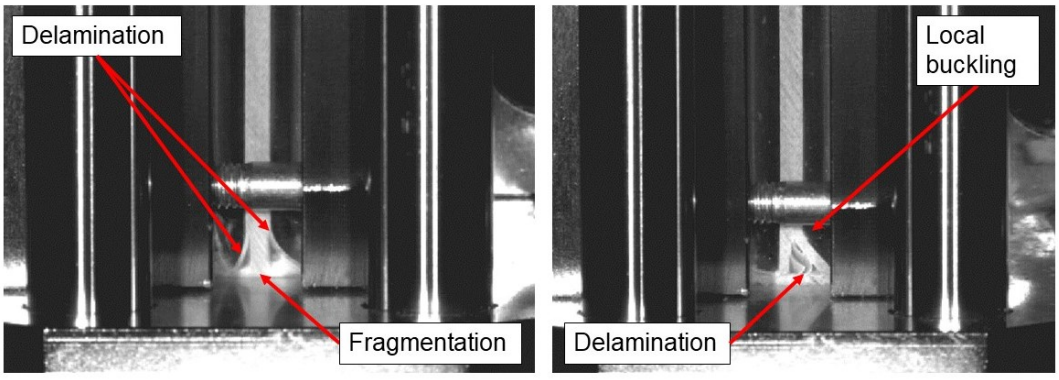


(a) (b)

Figure 38: Changes in the failure mode of the same test on a glass fiber/epoxy specimen in the high-speed video: a) initial part of the test, b) final part of the test [18].

### 3.1.2 Cutting effect and buckling of the specimen

The new fixture setup described at previous pages, that requires the direct impact of the dropped mass on the top of the specimen (Figure 39a), provided significant improvements in the quality of the acquired data, but a new problem regarding some unwanted failures on the top of the specimens raised. The testing procedure was designed to provide the measurement of a crash force when the failure is splaying (Figure 39b) and remains constant for a certain time.

a) b)

Figure 39: a) Detail of the contact area in the upper part of the specimen; b) typical splaying failure mode of a NEMA FR4 glass fiber/epoxy specimen after in-plane crashworthiness test.

Due to the reduction of the contact area between the insert on the striker and the upper part of the specimen, in the new version of the fixture the stress grows to a level close to the compression resistance of the material causing in some tests local or complete failure like in the specimen (Figure 40). This kind of failure is generally considered not acceptable as consists of a mixed failure mode (splaying in the center, tearing at the edges of the impactor), even if some authors have proposed a method to separate the effect of tearing and splaying in terms of absorbed energy [70, 72].

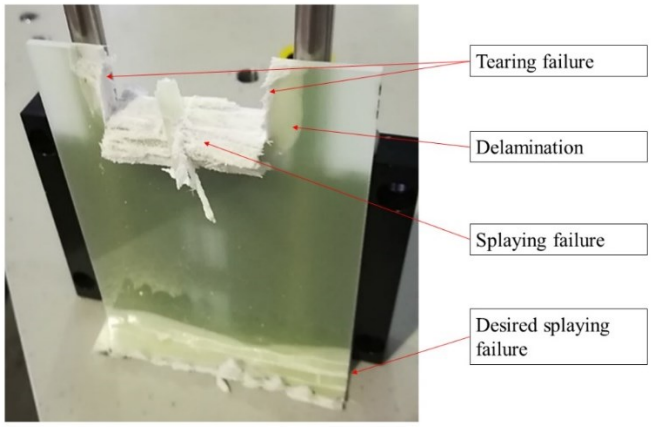


Figure 40: Undesired failure on the top of a NEMA FR4 glass fiber/epoxy specimen due to excessive stress in the upper area after in-plane crashworthiness test.

The collapse in the upper part of the specimen usually starts with a damage close to the edges of the impactor due to a stress concentration (Figure 41a) and later propagates until the complete failure (Figure 41b, Figure 40).

a)

b)

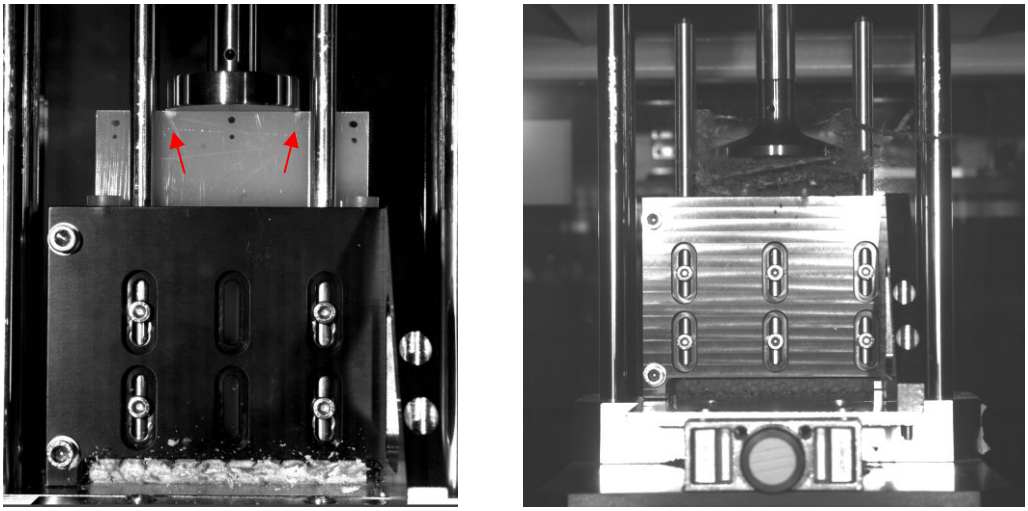

Figure 41: a) Initial damage caused by stress concentration at the edges of the flat disk impactor on a NEMA FR4 glass fiber/epoxy, where delamination is easily visible thank to the change in color from green to white; b) unwanted failure on the top of a carbon fiber/epoxy specimen.

The stress concentration was investigated by means of a static FEM simulation in Ansys (Figure 42), that pointed out that, at the peak force measured during crashworthiness tests, the stress reaches critical values higher than the compression resistance of the material as indicated by the Inverse Reverse Factor IRF (defined in Ansys as the ratio between maximum stress and resistance of the material) higher than 1 in some elements.

a) b)

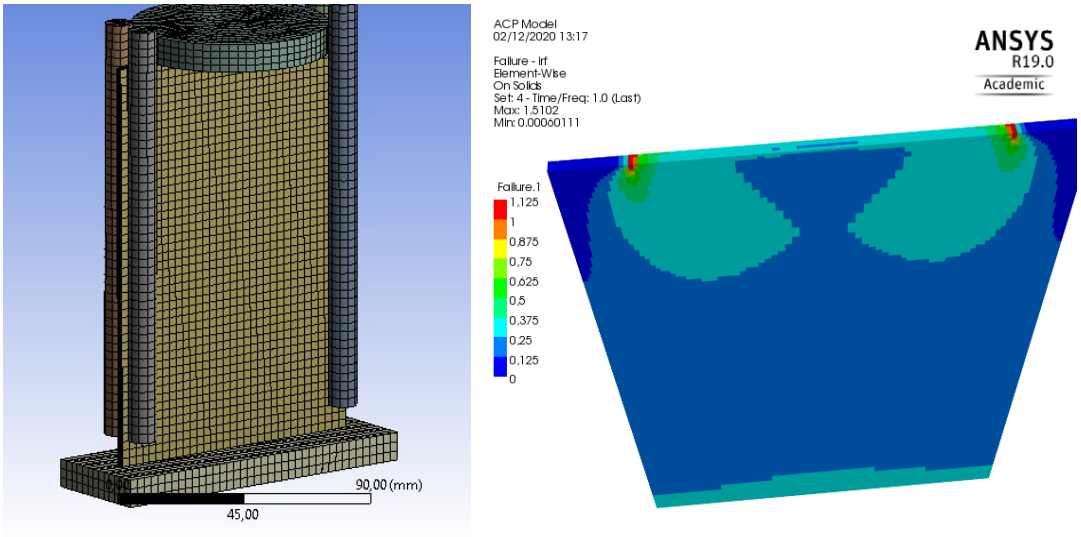


Figure 42: a) Static FEM model for the evaluation of the stress distribution in the contact area; b) Distribution of the IRF, defined as the ratio between the maximum stress and the resistance of the material (if higher than 1 the material is damaged).

To reduce the average and peak stress in the contact area, a larger flat insert with diameter increased from 50 mm to 70 mm was employed. To allow this improvement the fixture needed to be modified to avoid interference with the anti-buckling columns that were moved towards the lateral edges of the fixture. If this reduced the frequency of failures in the contact area, the columns were no longer in the optimal position to avoid the buckling of the specimen, as was predicted during the first design of the fixture [96]. For this reason, a central column (shorter to avoid interference with the impactor) was added.

This solution was useful to reduce the average stress on the upper part of the specimen (and partially the peaks as well), but the flat geometry of the impactor was always responsible for a stress concentration at its two edges caused by the *cutting* effect due to the sudden passage from an area loaded by high compression stresses to another unloaded one. To reduce this effect, some FEM simulations showed that the stress peaks are reduced if the surface of the impactor is not flat but has a slight curvature (Figure 43, Figure 44). What is interesting from Figure 43 and Figure 44 is that an optimum condition with a curvature radius of about 5 m (for NEMA FR4 3 mm specimens) was found; for higher values the failure happens for *cutting* due to stress concentration at the edges of the impactor, while for lower values the failure happens in the middle because of the lower contact area.

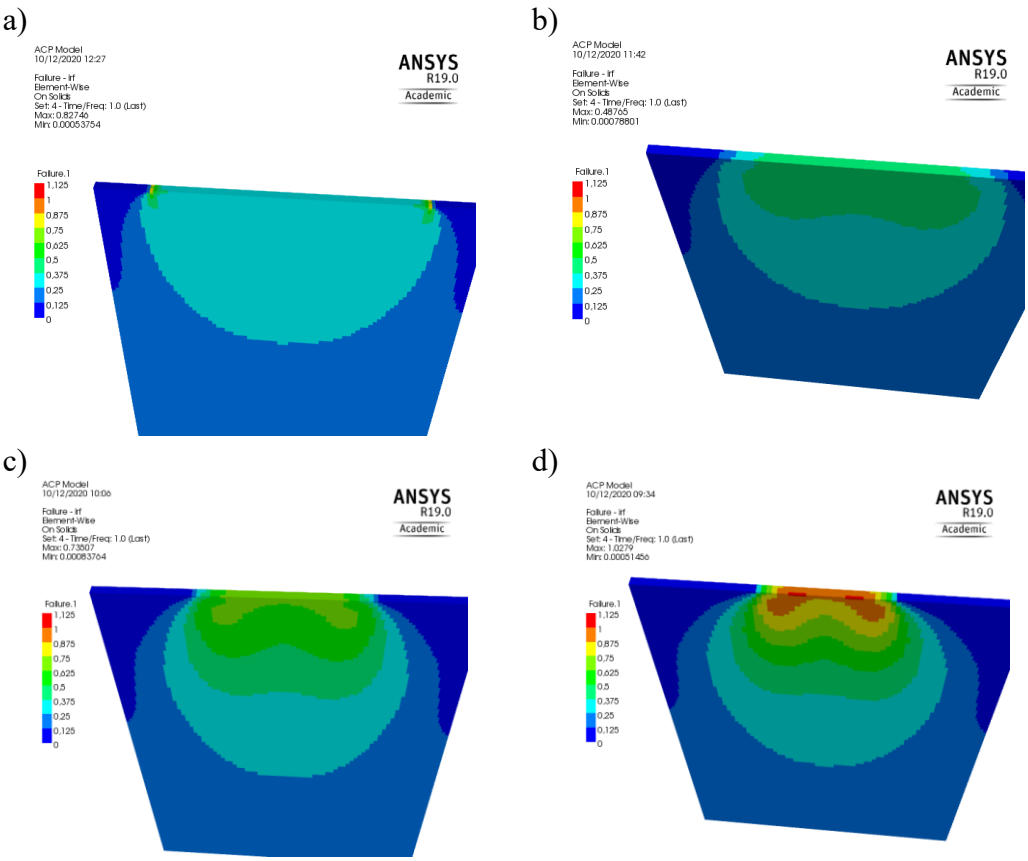


Figure 43: Damage (IRF) distribution in the contact area with impactors having different curvature radii: a) 20 m, b) 5 m, c) 2 m, d) 1 m for a NEMA FR4 glass/epoxy specimen with thickness of 3 mm.

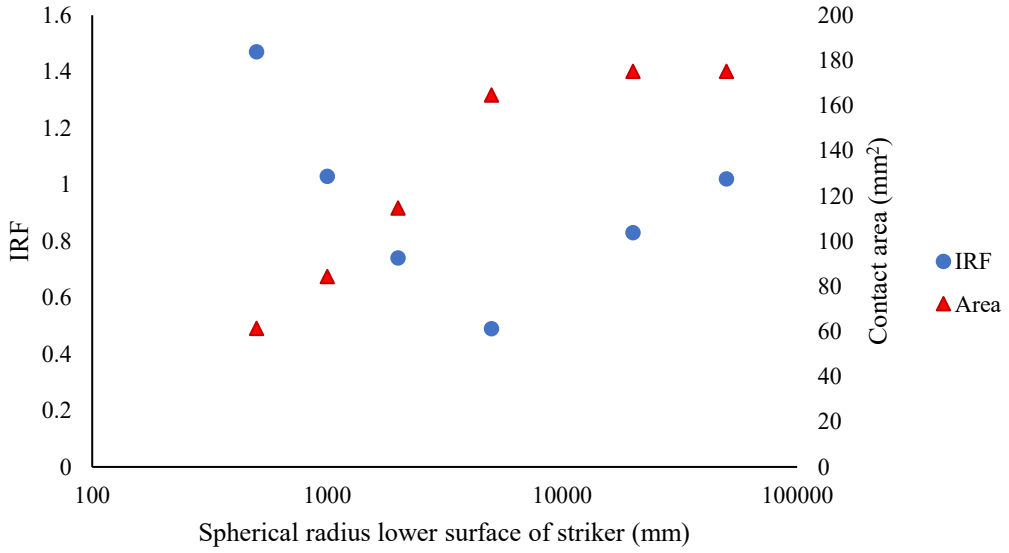


Figure 44: IRF and contact area trends in various simulations of the contact between impactors having different curvature radii for a NEMA FR4 glass/epoxy specimen with thickness of 3 mm; the lower damage index is found with a radius of 5 m.

This behavior was deeply investigated from a numerical and experimental point of view by the MS student Riccardo Destefanis in his thesis [105]. A detailed model of the failure was built and verified in some experiments, then the optimal radius was found for different materials, that need different optimal radii for stress concentration reduction depending on the thickness and the elastic properties of the material. After having found the optimal values for a wide range of materials, the radius capable of minimizing the stress on the wider range of materials was chosen and implemented on the testing fixture.

Another issue strictly connected to the necessity of having a stable splaying failure mode is the buckling of the specimen. As described in previous page, after a first version with two anti-buckling columns located on each side of the specimen, a third column was added to prevent buckling when the distance between the columns was increased to have a larger impactor. During DIC (Digital Image Correlation) observations carried out in [105] to validate the numerical model, some buckling failure were observed in the area not constrained by the central column (Figure 45).

a) b)

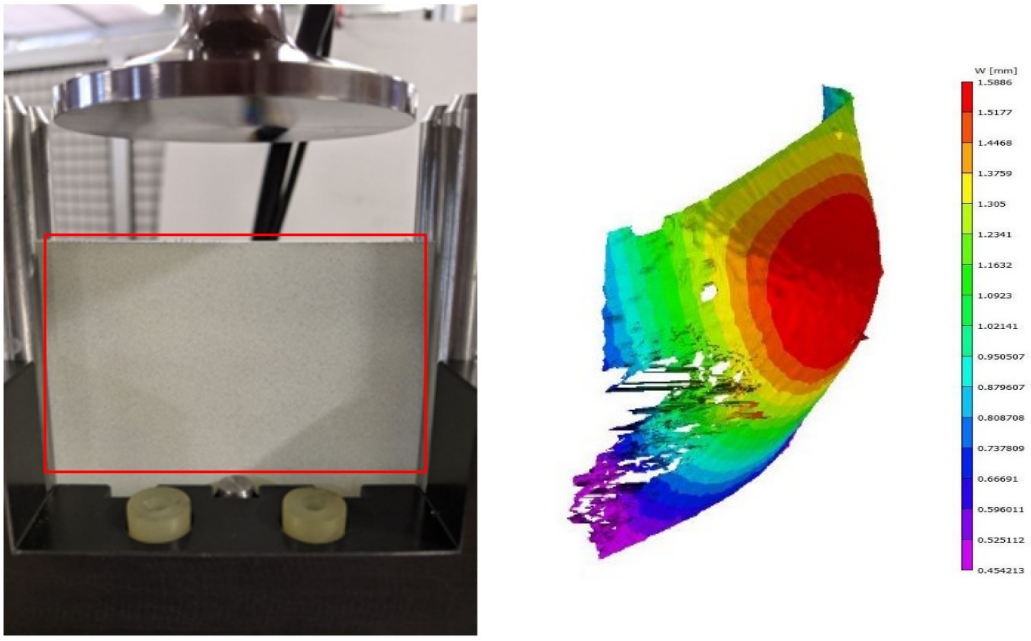


Figure 45: a) Area of the specimen where the 3D DIC was used to detect buckling [105]; b) out-of-plane displacement detected using DIC during a compression test showing buckling of the specimen in the central area, where the support of the anti-buckling columns is missing [105].

Several trials showed that the unwanted failures are more typical of some materials than others; in particular, being due to buckling in some parts of the composite plate, the unwanted failures typically happened on specimens with low thickness and elastic modulus. For this reason, a stiffness index was defined as

$$S = Et, \tag{5}$$

where E is the elastic modulus and t the thickness of the laminate. The performed tests indicated that specimens with a stiffness index lower than 100 were critical for the first versions of the testing fixture and could cause unwanted failures on the top of the specimens, sometimes only in few cases, sometimes in all the tested samples.

The observation of the buckling in the upper part of the specimen pointed out the necessity of adding a support in the part of the specimen remained unsupported, with the problem of interference with the impactor during the progression of the test. The only way to overcome the problem was to add a support able to move away when touched by the impactor; an effective solution was to design a central column with same height of the specimen that slides down with it when pushed by the impactor and that maintains the ability to prevent lateral deflections of the specimen (Figure 46a).

After the good results obtained with the sliding column, a last improvement was the reduction of the specimen width from 100 mm to 50 mm to completely cover the width of the specimen and avoid any problems related to stress concentrations in the upper part of the specimen, as now 100% of the upper surface of the specimen is in contact with the flat impactor (Figure 46b).

a) b)

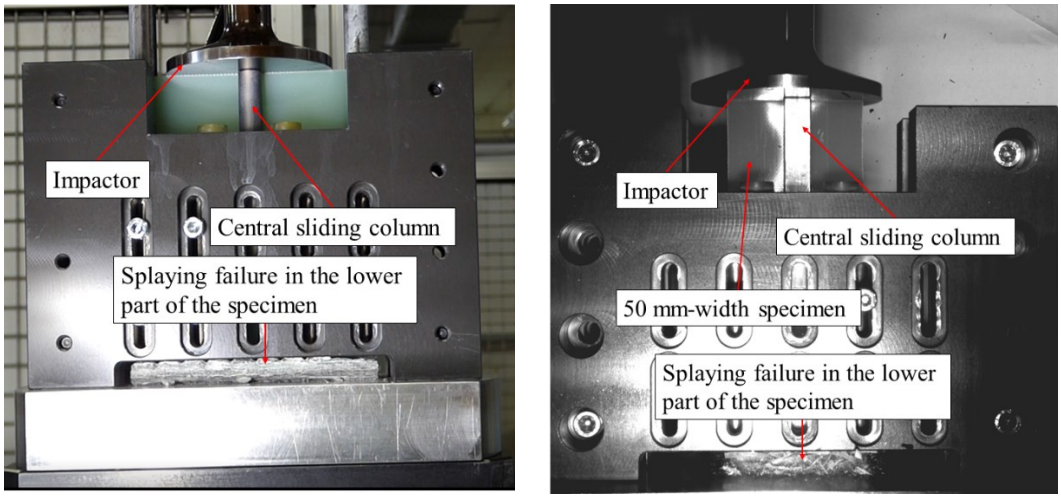


Figure 46: a) Fixture with central sliding column and specimen with original dimensions (150 mm x 100 mm); b) specimen with central sliding column and smaller specimen (150 mm x 50 mm).

With the smaller specimen a single column proved effective to sustain the specimen in the upper part and avoid buckling. The two long lateral columns that were supporting the full height of the specimen in previous versions were shortened and sustained only the lower part of the specimen, while the effectiveness of the central sliding column was improved choosing a squared section providing more adhesion with the specimen and stability.

The effectiveness of this testing setup, that has been implemented in the final prototype of the fixture, have been proven by testing several material samples with low thickness including glass and carbon fibers and both thermoset and thermoplastic laminates. The material with the lowest successfully tested stiffness index (S=24) was a NEMA FR4 glass/epoxy laminate with thickness of 1 mm, reaching a value which is half of the desired requirement (minimum thickness of 2 mm).

### 3.1.3 Clamping system and friction force

The experience gained during the tests of the first versions of the fixture pointed out the importance of the supporting structure not only to avoid the buckling of the specimen, but also to obtain a stable and repeatable failure mode, necessary to get consistent results. After some modifications not reported here for conciseness, the final design consisted of a stiff structure surrounding the specimen and connected to the base of the drop tower testing machine, and the specimen clamped between two plates with a controlled clamping force. One of the two plates is fixed in position, while the second one slides to clamp the specimen allowing to accommodate laminates with different thicknesses without changing any component of the fixture. The position of the full structure can be moved to maintain the centering respect to the falling mass and avoid non-completely axial loads on the striker that could cause errors in the acquired force or damages to the load cell.

One of the main themes of discussion on crashworthiness tests on flat specimens requiring an anti-buckling fixture is the friction due to the sliding between the specimen and the supporting columns. This friction is responsible of a part of the energy absorption that needs to be minimized to avoid a non-realistic overestimation of the energy absorption characteristics of the material. The two

possibilities to address this issue are reducing the clamping force to the minimum able to avoid the buckling of the specimen and reducing the friction coefficient to the lowest value possible. While some authors [36, 57] have decided to reduce the friction using knifes instead of circular columns (Paragraph 2.2.3), for this fixture the chosen strategy was to use circular columns made of different materials to find the most effective. Some results of these studies have been published in some publications summarized in the following.

The first study to evaluate the effect of friction in the test was performed with crash tests on a laminate made of four layers of Microtex GG630 carbon fiber fabric coated with E3-150 epoxy resin with content 37% in volume, whose mechanical characteristics have been previously tested (Table 1). Crash tests were performed with clamping forces equal to 0.8 kN, 4 kN and 8 kN, imposed by screws fastened with controlled torque. The testing setup was involving the impactor with flat disk with diameter of 70 mm and three stainless steel columns supporting each side of the specimen (with the central one having lower lenght to avoid interference with the impactor). The results showed a non-negligible increase in the SEA (1 kJ/kg for every additional kN of clamping force); on the other hand, the good results obtained with a clamping force of 0.8 kN indicate the possibility of testing with minimal clamping forces reducing the overestimation of the SEA to less than 1 kJ/kg [106].

After this first result, a new testing configuration to directly measure the contribution of the sliding friction has been developed and used to compare the effect of different materials by means of sliding tests. The specimen is moved upwards and clamped with imposed clamping force, and the impact on its top makes it slide downwards without any failure (Figure 47a). In this way, only the friction force due to clamping is acquired by the load cell on the striker (Figure 47b). Tests were performed on a NEMA FR4 glass fiber/epoxy in dynamic conditions (impact velocity 1 m/s, impact energy 13 J, impact mass 26 kg, 8 kN clamping force, 90 kN load cell on the striker, sampling at 1 MHz). The average sliding force is calculated in the range of the force-displacement curve between 5 mm and 10 mm to neglect the oscillations due to the first contact with the specimen and the final force increase due to the transition to static friction when the velocity tends to zero.

a) b)

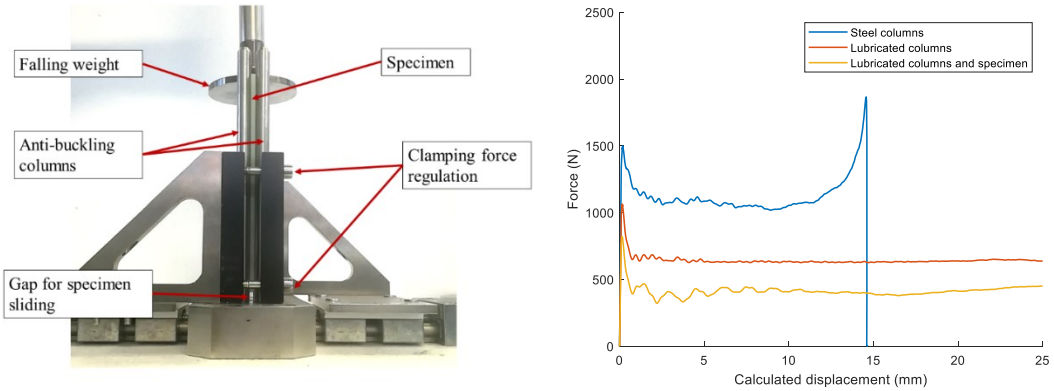


Figure 47: a) crashworthiness fixture with setup modified for slide tests for friction force evaluation [107]; b) filtered force-displacement curves acquired during slide tests of a NEMA FR4 glass/epoxy specimens and columns with three different tribological conditions (stainless steel surface, columns lubricated with the deposition of spray PTFE, both columns and specimens lubricated by PTFE) [107].

Friction tests reported in [107] compared three tribological conditions:

- stainless steel AISI 303 dry columns,
- application of a PTFE (Polytetrafluoroethylene, commercially known as Teflon) solid spray lubricant (CRC dry PTFE lube) on columns,
- application of a PTFE solid spray lubricant (CRC dry PTFE lube) on both columns and specimen.

Later some additional tests were performed to study the friction in other tribological conditions:

- PTFE industrial coating on steel columns,
- Nichel-PTFE industrial coating on steel columns,
- Dry CuSn12 bronze columns.

Considering the final results (Figure 48), the best result was obtained with the PTFE coating with an average friction force of 481 N, but after 50 tests the coating was visibly eroded, and an increase of the friction force was detected.

Given that the substitution of 6 supporting coated columns is a non-negligible cost that would be sustained by the final user of the fixture, this solution was discarded. Very similar slide forces were obtained with the application of spray PTFE on columns and specimen (502 N) and on columns only (583 N), but the observation that the lubricant layer is eroded after 4-5 cycles, and that the spray to be newly applied requires about 5-10 minutes drying before performing a new test make this solution adequate only in very critical cases (e.g. when the crash force of the specimen is very low and would be too influenced by friction). The best compromise was identified in the dry bronze columns solution, that is not subjected to erosion and causes a limited amount of friction (655 N in average).

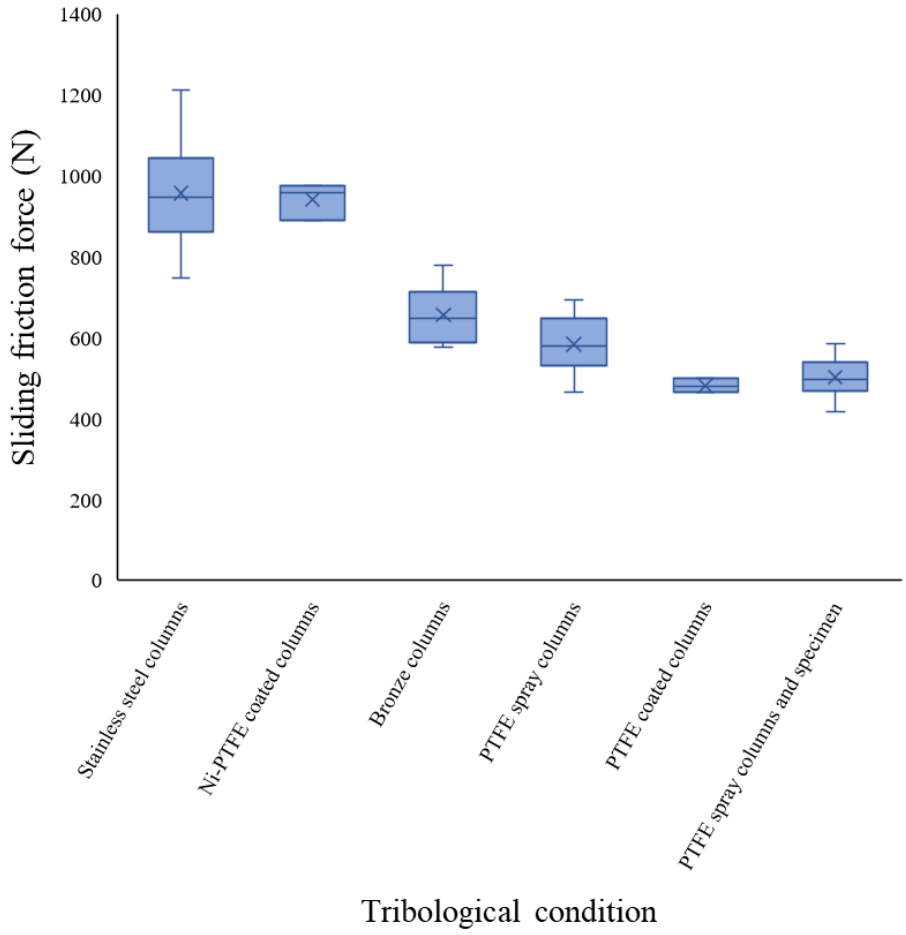


Figure 48: Results of slide friction tests in several tribological conditions.

From the acquired sliding force it is possible to calculate the friction coefficients in Table 5 following the approach proposed in literature [108]:

$$\mu = \frac{F_S}{2F_C} \quad (6)$$

Where $F_S$ is the slide force acquired, $F_C$ is the clamping force and the multiplying factor 2 is necessary to consider that the clamping force acts on both sides of the specimen.

**Table 5**: Results of slide tests for friction measurement

| | Average sliding force $F_S$ (N) | Friction coefficient $\mu$ |
|---|---|---|
| **Stainless steel columns** | 956.6 | 0.060 |
| **Ni-PTFE coated columns** | 940.9 | 0.059 |
| **Bronze columns** | 655.5 | 0.041 |
| **PTFE spray columns** | 583.0 | 0.036 |
| **PTFE coated columns** | 480.8 | 0.030 |
| **PTFE spray columns and specimen** | 502.0 | 0.031 |

Based on the experimental investigations reported in this paragraph, an innovative solution was implemented in the final design of the testing fixture. The anti-buckling columns were manufactured by bronze including the upper sliding column with squared section to avoid the need of consumable parts substitution and of application of lubricants. The clamping force was controlled including a handle able to limit the torque of the screw-driven mechanism that moves the clamping plate and applies the clamping force. The imposed clamping force was limited to 1 kN.

A final verification of the friction force was performed on the final fixture with same testing conditions described at previous pages and using the same

NEMA FR4 reinforced epoxy, giving an average force of 298 N. This value needs to be compared with the crash force measured during the test to estimate the overestimation caused by the sliding contact with the anti-buckling supports. Considering NEMA FR4 specimens, the average crash force measured is 14.1 kN, if the laminate has a thickness of 3 mm and 5.4 kN with thickness of 1 mm. The friction force corresponds then to 2.1% (thickness 3 mm) and 5.5% (thickness 1 mm) of the crash force, thus confirming that the friction becomes influent with low force values. Even if the friction force has been reduced as much as possible, in case of very low crash force a PTFE lubricant can be applied to further reduce the friction coefficient and a slide test can be performed to measure the friction force and subtract it from the crash force to have a more realistic crash force estimation.

### 3.1.4 Failure trigger

As anticipated in paragraph 2.1.3, the geometry of a crash box is designed to have a weaker part where failure starts and later propagates to the rest of the structure; several approaches have been proposed in the literature to get the same effect on material samples for crashworthiness tests. To find the optimal condition for the testing procedure described here, six different trigger geometries have been manufactured on GG630 carbon/epoxy laminates to find the most adequate for material characterization. Main goal of the trigger is promoting a stable splaying failure mode involving a small portion of the specimen to waste the lowest test stroke (and then useful data) possible. In the following pages the results published in [109] will be summarized. The six trigger geometries chosen for this study were called for simplicity using letters A to F:

- Trigger A (Figure 49a): machined saw-tooth trigger with depth 2.5 mm
- Trigger B (Figure 49b): machined saw-tooth trigger with depth 5 mm
- Trigger C (Figure 49c): machined saw-tooth trigger with depth 10 mm
- Trigger D (Figure 49d): two large triangles (with width of 50 mm) machined with depth 10 mm.
- Trigger E (Figure 49e): a 5 mm deep delamination in the mid plane of the laminate was created including a thin Polytetrafluoroethylene

(PTFE) layer during the layup process, that prevents the bonding between the second and the third layer.

- Trigger F (Figure 49f): the thickness of the laminate was reduced from four to two layers for a depth of 5 mm. In the trigger area, the first and fourth layers were removed to preserve the symmetry respect to the mid plane of the laminate.

Even if often used in the literature, steeples (chamfers) or other kinds of asymmetric triggers were not taken in consideration in the testing campaign because they could cause asymmetric splaying or bending instead of a splaying failure mode.

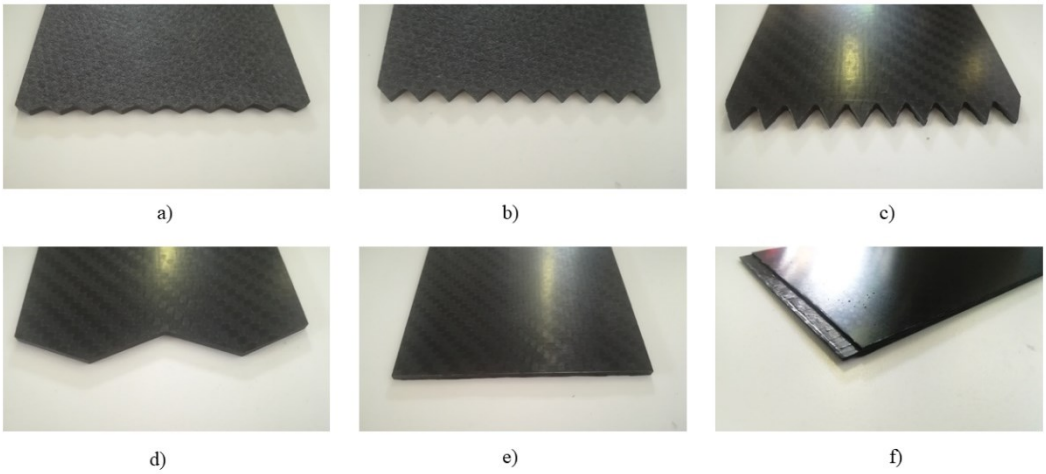


Figure 49: Failure trigger tested in [109]: a) triangular saw-tooth with depth of 2.5 mm; b) triangular saw- tooth with depth of 5 mm; c) triangular saw- tooth with depth of 10 mm; d) two large triangles with depth of 10 mm; e) internal notch created positioning a thin PTFE layer in the mid plane of the laminate for a depth of 5 mm; f) reduction of the thickness of the laminate from four to two layers for a depth of 5 mm.

The specimens in Figure 49 were all tested in quasi-static conditions (2 repeated tests) with an Instron 8801 hydraulic universal testing machine at Politecnico di Torino. The tests were run at constant speed (10 mm/min) acquiring the load by means of a load cell with maximum load of 100 kN, and the

displacement of the impactor by means of an LVDT sensor. To run these tests the fixture needed to be modified with some additional components that were clamped in the hydraulic grips of the testing machine. In addition, three repeated tests were performed in impact conditions with an impact energy of 800 J, an impact velocity of 7 m/s and a mass of 32.9 kg. The unsupported height was set to 5 mm in all the tests. Some examples of the acquired force-displacement curves in quasi-static conditions are plotted in Figure 50.

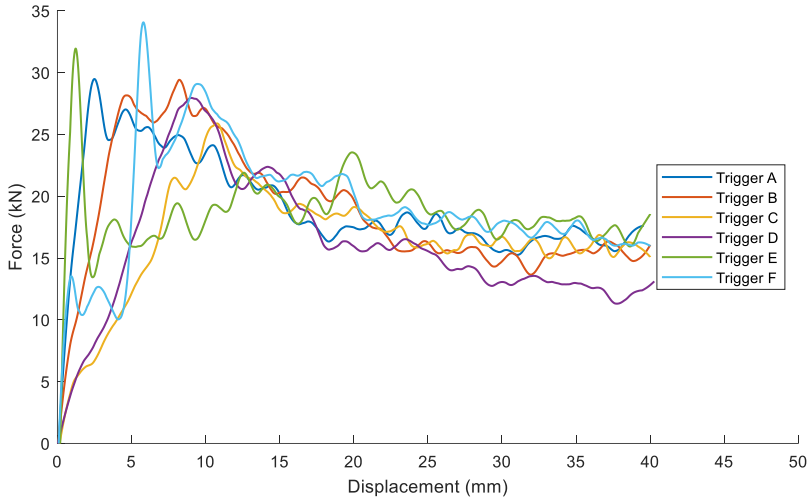


Figure 50: Typical filtered force-displacement curves acquired during quasi-static compression tests [109].

As a result, the general behavior is similar for all the trigger geometries. The first 10 mm of quasi-static force-displacement curves are strongly characterized by the trigger geometry and show the main effect of the triggers, that causes different trends in the rising of the force value from zero to a peak that corresponds to the transition from the trigger to the full cross-section of the specimens, and then to the initiation of the desired splaying failure. From about 10 mm to 20 mm the force reduces due to the development of the crash front to a failure mode that remains constants after 20 mm. Curves acquired during the impact tests are instead plotted in Figure 51.

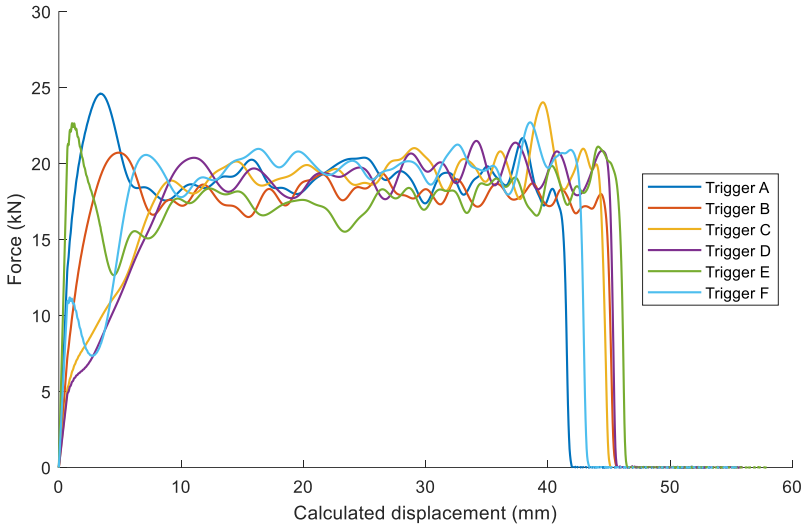


Figure 51: Typical filtered force-displacement curves acquired during impact compression tests [109].

Dynamic curves are similar to quasi-static ones in the first 10 mm, then tend to stabilize more rapidly around the steady state force value, probably because the crash front formation is facilitated by high strain rate and vibrations induced by the impact. After 10 mm, the steady crash condition is achieved, and the curve progresses horizontally until the impact energy is completely absorbed.

Observing Figure 50 and Figure 51 it is possible to get the result that the failure trigger affects only the first 10 mm of the curves, while for higher displacements the crash force and failure mode are well comparable. In details:

- Specimens having saw-tooth machined trigger (A, B, C) showed a linear increase of the force value up to the peak that corresponds to the initiation of the failure on the full cross section. The slope is inversely proportional to the depth of the trigger.
- Specimen D had a behavior very similar to C because consists of larger triangles with same depth.
- Trigger E consists of an artificially created internal delamination that causes the initial splaying of the laminate; since 100% of the cross section of the specimen is loaded at the first contact with the impactor, this causes a high peak of force that instantaneously drops

when the two half parts of the specimen bend in opposite directions due to the artificial internal delamination. After the two laminae are completely bended, the typical splaying failure starts, and the crash force is at the same level as the other tests.

- Trigger F presents a two-steps curve, with the first step ranging from 0 mm to 5 mm where the 2-layers part of the laminate is crashing, and the second step corresponding to the initiation of the failure on the 4-layers part and progresses constantly up to the end of the curve.

The observation of the peak force and SEA measured during the tests showed a strong effect of the testing condition on the peak force, with higher values measured in impact tests because of the high frequency vibrations generated during the impact that sum to the crash force originated by the material (Figure 52a). This effect is amplified by the trigger geometries E and F, that do not present a smooth increase of the cross section like in saw-tooth triggers: this causes a taller initial peak and more oscillation in dynamic force curves. The higher depth of the saw-tooth trigger reduces the force peak, but a longer part of the crash curve needs to be discarded for steady crash analysis.

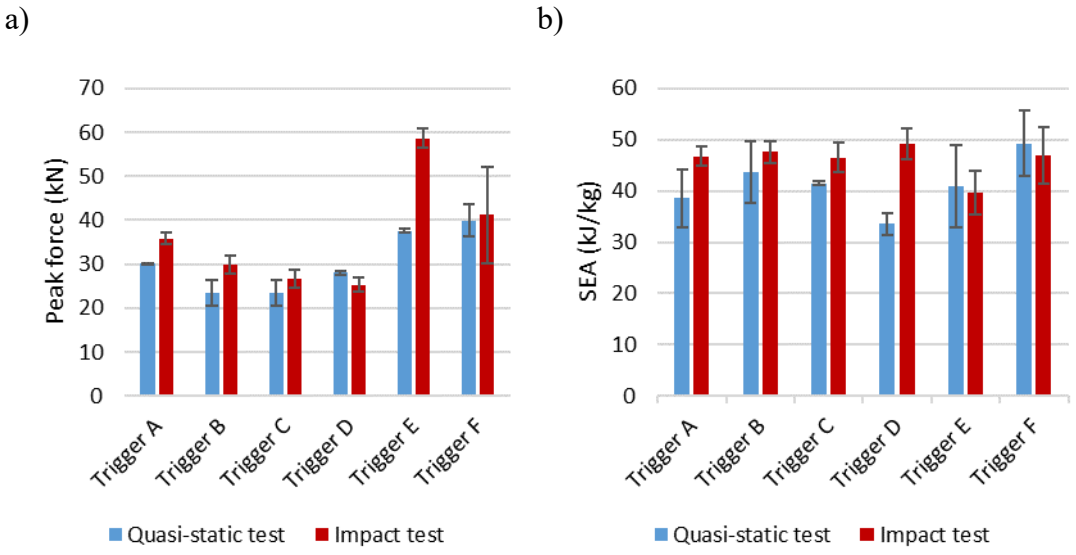


Figure 52: a) Peak force measured during quasi-static and impact crashworthiness tests on flat specimens with different failure triggers [109]; b) SEA measured during quasi-static and impact crashworthiness tests on flat specimens with different failure triggers [109].

The SEA was calculated in an interval of the force-displacement curve comprised between 20 mm and 40 mm to focus on the steady crash and neglect the first part inevitably affected by the trigger. This is necessary because the objective of the test is to provide a characterization of the crash behavior of the material, and then must not be influenced by the trigger geometry. Even if the displacement corresponding to the failure of the trigger is neglected, an influence of the trigger geometry on the failure development and on the energy absorbing characteristics during the progressive splaying crash cannot be excluded a priori, and this consideration led to the activity presented in this section. As plotted in Figure 52b, it is necessary to distinguish between the quasi-static and impact (dynamic) tests: in dynamic tests the SEA is comparable in all the specimens except trigger E, that causes a lower energy-absorbing failure mode probably due to the artificial internal delamination that causes a failure mode where energy is mainly absorbed by the delamination in the middle of the laminate and the external layer results less fractured. Results of quasi-static tests are more influenced by scattering and by the low number of repeated tests (only 2 repetitions were performed). Triggers A, B, C and E gave similar SEA in quasi static tests, that resulted lower than respective dynamic tests. Lower SEA was obtained with trigger D in quasi static conditions, with a strong difference from the dynamic condition that gave very high SEA. Trigger F showed instead high SEA both in quasi static and dynamic conditions. These differences are not easily explained and will be probably clearer if investigated with a higher number of tests.

In conclusion, test results showed that, the smoother is the transition from the first contact with the impactor to the failure of the full cross section of the specimen, the lower is the peak force. This means that the triangular triggers with depth 10 mm (C and D) are probably the most suited for crashworthiness tests because the lower initial peak reduces the probability of obtaining an unwanted failure on the top of the specimen caused by an excessive force on the upper part of the specimen (see paragraph 3.1.2.). Furthermore, a lower peak force causes also lower vibration on the force data during impact tests. On the other end, a 10 mm-deep trigger means that at least 10 mm of the force-displacement curves need to be neglected for the calculation of SEA, and this is a lot considering that the maximum usable stroke of the test allowed by the fixture in its final design is 40 mm and can be even lower in case of low-energy impacts. For this reason, a better compromise between the lower peak force and the longest usable stroke is the

saw-tooth trigger with depth of 5 mm, that was chosen for the following tests. A saw-tooth machined trigger is also cheaper and simpler to be manufactured, as the specimen only requires to be cut by water-jet or milling from a larger plate without the inclusion of an additional internal layer (trigger F) or producing a thickness reduction (trigger G). The final detailed geometry of the flat specimen is in Figure 53.

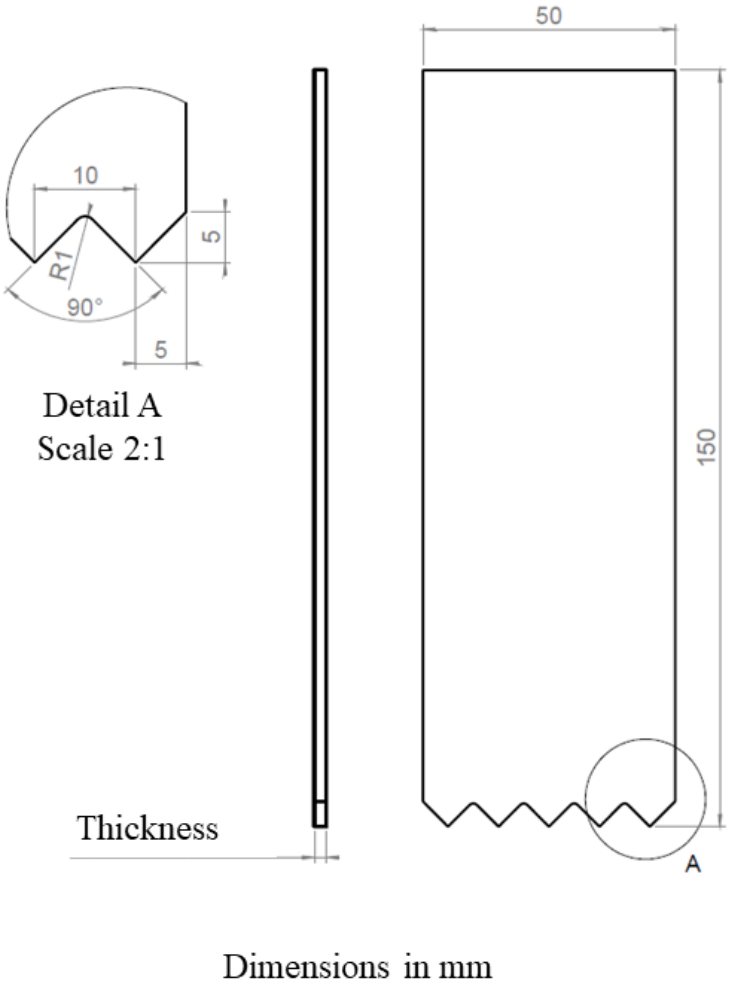


Figure 53: Drawing of the geometry of the flat specimen for in-plane crashworthiness characterization of composites developed in this work.

### 3.1.5 Failure modes

In chapter 2, the main studies carried out on the failure modes of composites in crash conditions have been summarized. As a general rule, fibers cracking absorbs more energy than matrix failure, and more fragments are produced more energy is absorbed by the failure. Several failure modes can take place in the same material depending on the constraint conditions, yielding the general conclusion that the geometry of the structure influences the level of energy absorption achieved in the crash test. Given the importance of the failure mode on the energy absorption of composites, the failure mode is an important parameter to be studied through a standard testing procedure.

The first step was to include in the design a window to allow the observation of the failure from a lateral view of the specimen using a camera. This allows to observe the evolution of the failure in time during the test, e.g. as shown in Figure 54, that represent a typical situation observed in carbon/epoxy samples. Most of the tested samples showed this kind of behavior, but some exceptions can be found if defects are present in the material or in some non-standard testing conditions. Several failures have been observed during various tests, allowing to identify the connection between failure mode and force signal.

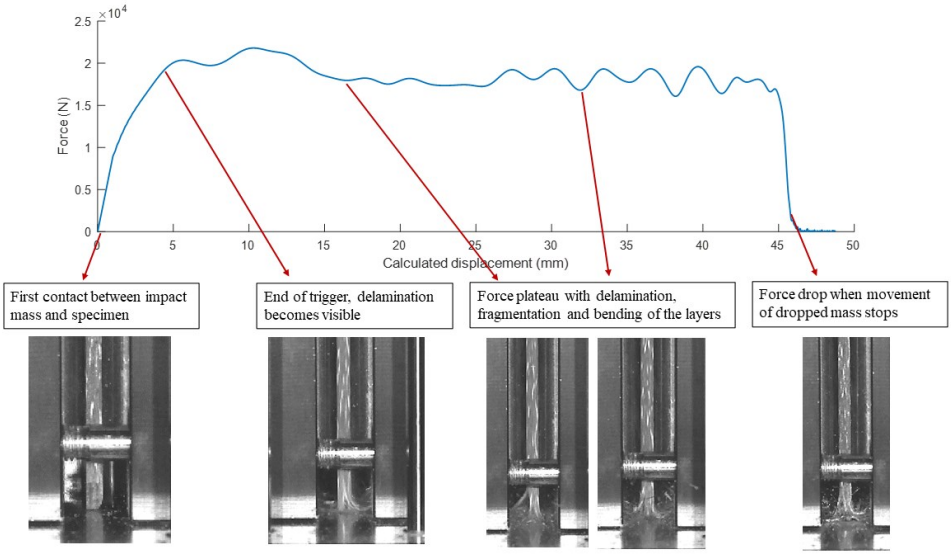


Figure 54: Filtered force-displacement curve and failure mode observed during the crash test on a 4-layers GG630 carbon-epoxy laminate (impact energy 800 J, impact velocity 7 m/s, mass 32.9 kg) [107].

In the test shown in Figure 55 the crash force reaches the typical value of a GG630 carbon/epoxy laminates in the first 20 mm of the curve, then it reduces because of the formation of a crack in the mid-plane that induces bending of the foils with lower fragmentation and consequently lower energy absorption. As a final step, the force reduces further due to the crack growth. This behavior could be due to the presence of defects in the internal areas of the material, and the results may be discarded because the average force used to calculate the SEA is reduced due to the change in the failure mode.

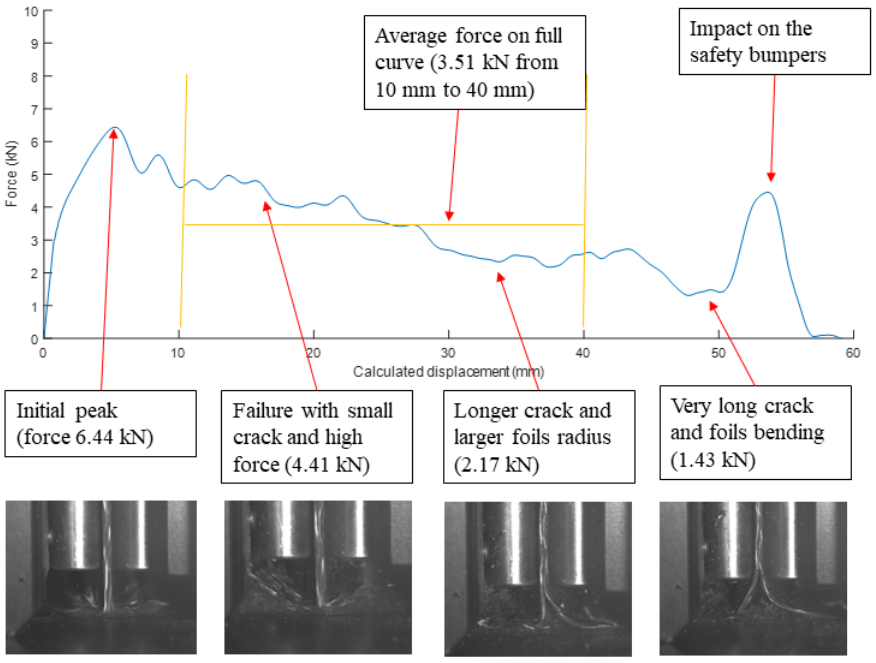


Figure 55: Filtered force-displacement curve and failure mode observed during the crash test on a 2-layers GG630 carbon/epoxy with unusual changes in the failure mode; a long crack with elastic bending of the foils caused a strong decrease of the crash force.

Similar behavior can be observed in Figure 56 where a lower level of crash force is measured when a delamination grows in the mid plane of the laminate. The lower energy absorption is due to the lower fragmentation of the two foils when they bend with a large curvature radius.

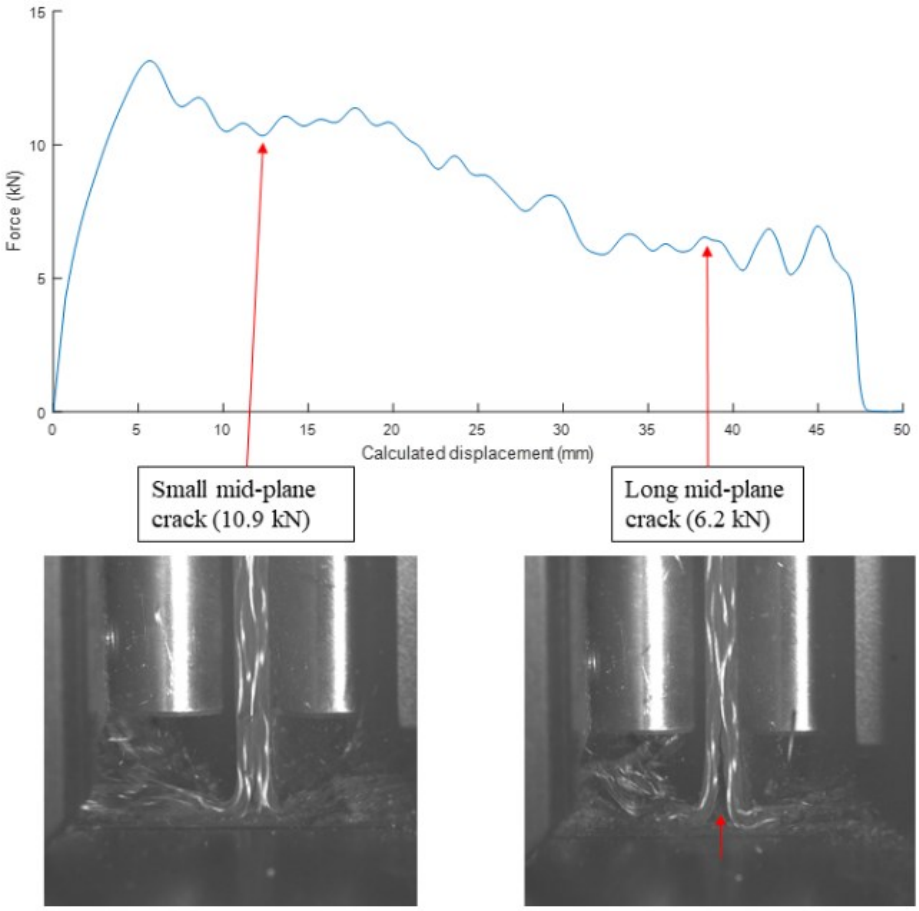


Figure 56: Filtered force-displacement curve and failure mode observed during the crash test on a 4-layers GG630 carbon/epoxy with unusual change in the failure mode; initially the mid-plane crack is small and the force is higher, for displacement higher than 25 mm the mid-plane crack is longer and the force is lower.

The way the specimen is constrained is another factor that can cause changes in the failure mode. In Figure 57, the 4-layers Microtex VV770 glass twill E9-150 epoxy specimen bended on one side due to the low thickness (2.4 mm) combined with an unsupported height of 20 mm; therefore, the force lowered from 13.8 kN to 4 kN.

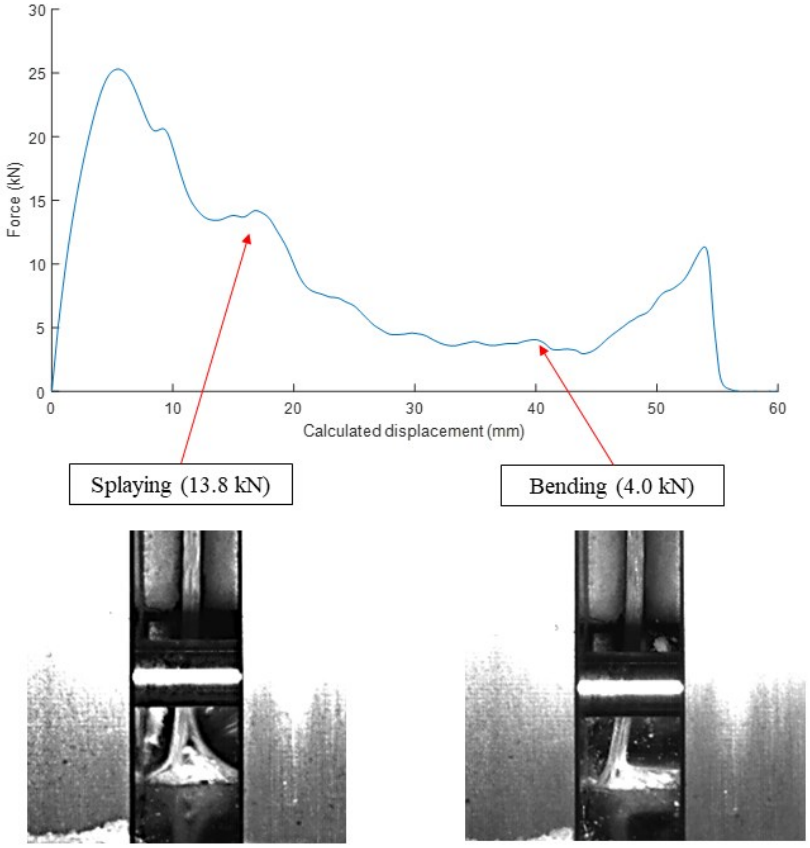


Figure 57: Filtered force-displacement curve and failure mode observed during the crash test on a 4 layers VV770 glass-epoxy specimen that bended laterally because of the low thickness and tall unsupported height.

These results show how the testing setup can tolerate different failure modes and acquire the respective consequences on the measured force and SEA. These differences can be caused by the material itself or induced by the constraints applied to the specimens. The first versions of the fixture allowed to change the unsupported height from zero to 20 mm to study its effect on failure mode and SEA.

**Table 6**: Mechanical properties of Microtex VV770T-32 carbon/epoxy laminate from datasheet supplied by the producer (only the density was measured by the author)

| Property | Value | Standard |
|---|---|---|
| **Density** | 1.83 kg/dm$^3$ | Measured by the author |
| **Tensile modulus** | 23.0 GPa | ISO 527:1997 |
| **Tensile strength** | 450.1 MPa | ISO 527:1997 |
| **Compressive modulus** | 25.1 GPa | ASTM D6441:14 |
| **Compressive strength** | 473.9 MPa | ASTM D6441:14 |
| **Shear modulus** | 3.5 GPa | ISO 6031:2015 |
| **Shear strength** | 99.5 MPa | ISO 6031:2015 |
| **Poisson's ratio** | 0.13 | ISO 527:1997 |

Some experimental tests carried out on GG630 carbon/epoxy and VV770 glass/epoxy specimens (mechanical properties in Table 6) with different thicknesses indicate that better results are obtained with unsupported height between 5 mm and 10 mm, where there are not important changes in the failure modes or in the SEA as reported in Figure 58. A lower height causes instead an over-constraining of the specimen, that can cause tearing if the laminate is very thick because of the difficult flow of the crashed material under the columns.

a) b)

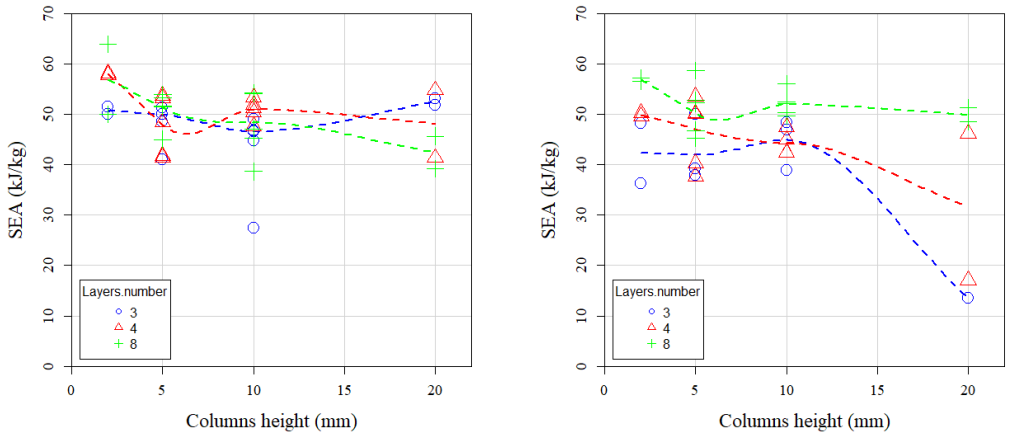


Figure 58: a) SEA of GG630 carbon/epoxy laminates with different thicknesses as a function of the unsupported height; b) SEA of VV770 glass/epoxy laminates with different thicknesses as a function of the unsupported height.

With 20 mm unsupported height some specimens tended to bend, but this does not happen in all the specimens; the scatter of results then tends to increase. These observations, together with the negligible differences found changing the unsupported height between 5 mm and 10 mm led to fix this value to 7.5 mm in the final version of the fixture. This value can be changed in specific studies, if needed, building some special columns able to guarantee the desired unsupported height.

As anticipated in paragraph 2.1.2, in the literature the macroscopic categories in which the failure modes are divided are splaying, tearing, fragmentation and buckling. While buckling is something generally unwanted on a crash box because of the low level of energy absorption, and fragmentation is something happening during the crash of many materials and difficult to isolate from the other failure modes, splaying and tearing are the easiest to be found and identified in crash tests. The fixture described here was mainly designed to test the splaying failure mode, but the possibility to obtain a tearing failure mode was implemented with a solution proposed by the company Engenuity [64]. Reducing to zero the unsupported height of some columns means adding some obstacles to the flow of

the crashed material, that results forced in specific directions. In this way, the presence of the obstacles can cause tearing of the laminate in some points.

Some trials with different constraint conditions have been performed on NEMA FR4 specimens with thickness 3 mm and the results are schematized in Figure 59. All the tests were performed with an impact energy of 800 J, a mass of 60.4 kg and an impact velocity of 5.2 m/s. The constraint conditions a) consist of 5 supporting columns on each side of the specimens all leaving an unsupported height of 10 mm. The other constraint conditions are the same, with the difference that the anti-buckling columns are moved down to 0 mm (i.e. do not allow the flow of crashed material under them) where it is indicated by the red circles. Figure 59 clearly shows how the SEA increases from 51 kJ/kg in the splaying mode a) to 60 kJ/kg in the configuration b), which constrains the laminate to bend in right direction, and c) and d), which cause some tearing. Even higher SEA is achieved with setup e), while the maximum has been achieved in configuration f) the causes 5 tears in the laminate and a SEA of 65 kJ/kg, an increase of 30% respect to the SEA in splaying mode.

Thanks to the interesting results obtained from these tests, the final version of the testing fixture allows to use some special columns with 0 mm unsupported height to test the tearing failure mode. The results obtained are compared in Chapter 4 to those obtained testing the same material with different coupon geometries to observe the change of the SEA.

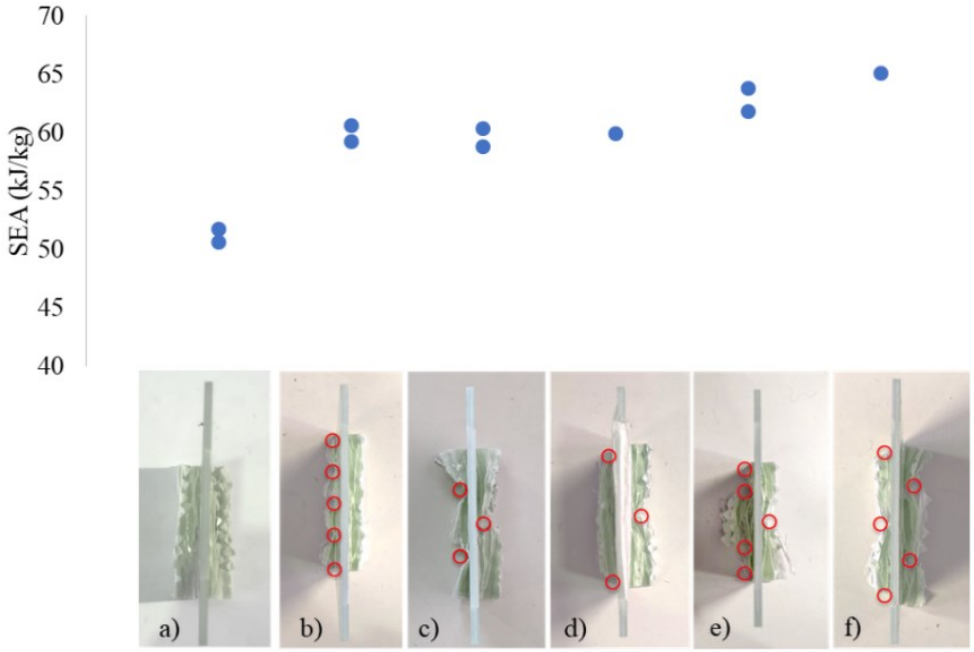


Figure 59: Effect of the constraint conditions on the SEA of a NEMA FR4 laminate; the red circles indicate the presence of a column with unsupported height equal to 0 mm.

### 3.1.6 Specific Energy Absorption calculation

A critical aspect of a standard procedure to calculate the SEA of the composite is to use a unique and shared approach to calculate this result. This is not immediate because several aspects need to be defined:

- The part of the force-displacement curve for the calculation of the average force needs to be identified, neglecting the initial part where the material is weakened by the failure trigger and the last part where the failure tends to stop because of the deceleration of the impact mass
- The dimensions of the specimens are not regular, so the procedure for measuring the specimen before the test needs to be decided (how many repeated measurements, with what instrument?)
- The mass of the specimen needs to be measured to calculate the density of the material

- Is it enough to measure some samples from a batch of specimens or is it necessary to measure and weight every single specimen before the test?

These aspects were investigated by the student Enio Colonna in his Ms' thesis [110], and the main achievement are summarized in the following. A preliminary review of the available literature on crashworthiness tests for material characterization pointed out that details on the approach followed to identify the part of the force-displacement curve to be considered for SEA calculation are usually not given. The simplest approach would be to divide the total absorbed energy (i.e. the area of the force-displacement curve) by the mass of crush material, but this does not allow to neglect the trigger area (where the material is intentionally weakened) and the final part where the failure is stopping because the kinetic energy of the mass is almost completely consumed. The typical approach consists of fixing a displacement range where the average force is calculated [17], but this could not be adequate if curves of different length are compared (e.g. if two materials with different SEA are tested with same impact energy); furthermore, an objective reason to choose the extremes of the range should be found. Another approach consists of deciding the extremes observing the impact curve to neglect the non-acceptable parts but it is obviously non-robust because different operators would choose different values based on their experience. A different approach to analyze curves with different lengths can neglect the initial and final parts defined as a percentage of the total time of the test, as required for example for the calculation of the fracture energy in the wedge peel impact test standard ISO 11343 [111]. A similar approach was applied considering a percentage of the total displacement of the test, with some drawbacks reported in [18]: if the percentages are not chosen correctly, some portions that should be neglected were instead considered in some curves.

In [110], these different approaches were applied to a set of eleven tests on a NEMA FR4 glass/epoxy laminate with thickness 3 mm. The specimens were all tested under the same impact conditions (energy 800 J, mass 60.39 kg, velocity 5.15 m/s), and should ideally give the same SEA result, despite some scattering due to the intrinsic variability of the material properties or other uncontrolled external factors. For this reason, the algorithm that minimizes the scatter of results on this set of tests can be considered the best for a testing standard. Some Matlab scripts were prepared to calculate the SEA in the desired range of the force-displacement curve according to the following algorithms:

a) Starting and final point set in each test by the user
b) Full curve considered
c) Fixed starting and final point applied to the whole set of curves
d) Starting and final points defined as a percentage of the total displacement of the test
e) Variable displacements algorithm as described below.

The variable displacements algorithm e) was originally developed after studying the previous methods, trying to combine the advantages of each of them. The result is a complex algorithm that looks for the stable crash of the material trying to minimize the part of curve to be neglected applying the following steps, also represented in a sample curve in Figure 60:

1. Filtering of the curve by applying a bandstop filter from 1 kHz to 40 kHz to hide the natural frequencies of the load cell of the striker and 700 points smoothing to have a regular signal (suited for a sampling frequency of 1 MHz)
2. Identification of the peak force and its position in the curve
3. Identification of the initial point of the curve starting from the peak position and decreasing the time until the force becomes zero
4. Identification of the final point of the curve starting from the peak position and increasing the time until the force becomes zero
5. Calculation of the variable *force limit* as 50% of the force value in the midpoint of the curve.
6. Identification of the starting point for SEA calculation with an iteration that starts from a displacement equal to the trigger depth and terminates when the *force limit* is reached, plus a margin of 1.5 mm to neglect the typical reduction of crash force after the peak caused by the end of the trigger and start of the failure on the full cross section of the specimen.
7. Identification of the final point as the point after which the force falls under the *force limit*, further reduced of a margin of 1.5 mm
8. If some points of the curve obtained in this way have force lower than the force limit, some unwanted phenomena could have happened at the end of the test, so the final point is further reduced until the force grows again over the *force limit*.
9. If the final point obtained in this way is higher than 40 mm, the final point is automatically set to 40 mm because after this point some

decelerators positioned on the fixture start to operate to slow down the impact mass and avoid damages to the fixture.

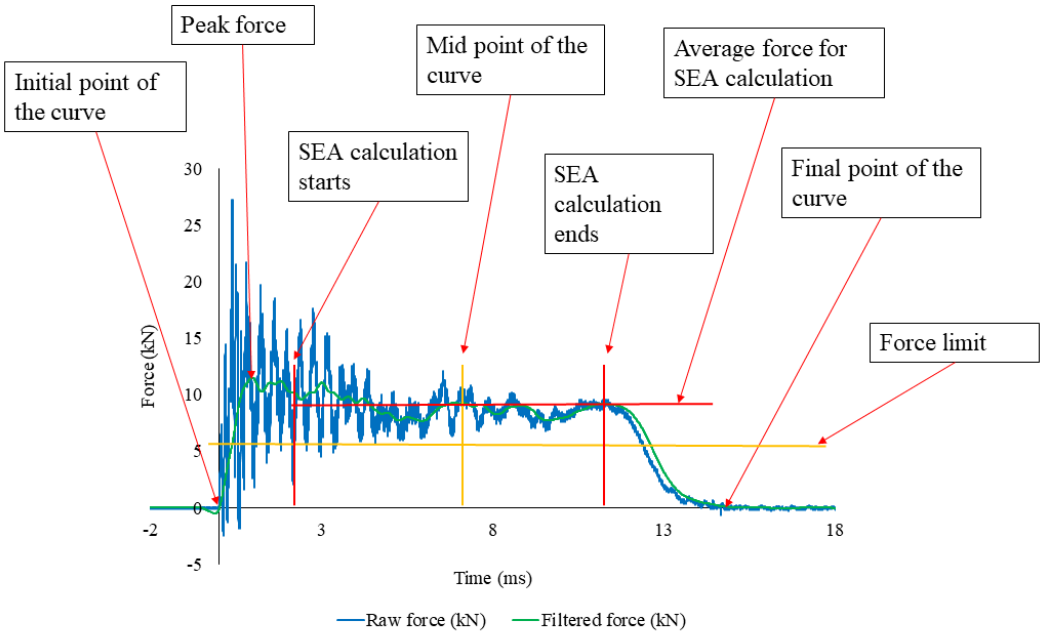


Figure 60: Critical points of the curve identified by the variable displacement algorithm.

This algorithm was applied to the cited set of curves, and the same was done with the other algorithms called with letters b) to d), while a) was considered not acceptable for a standard because the interval is subjectively decided by the operator. The results are summarized in Table 7, where it is possible to see that considering the full curve gives a lower SEA because it is affected by the portion of material weakened by the trigger, that needs to be neglected. The other calculation procedures are consistent in terms of average SEA result, with the variable displacement algorithm showing the lower scattering, and thus resulting the most effective for the calculation of SEA under the hypothesis that the calculation method should reduce as much as possible its contribution to the scattering of the results. The calculation method d), based on a percentage portion of the curve length, presents a low standard deviation, slightly higher than the

variable displacements algorithm, and could then be another good candidate for a standard because of the simpler implementation.

**Table 7**: Calculation of the average SEA on a set of specimens applying different methods.

| | Average SEA (kJ/kg) | Standard deviation of SEA (kJ/kg) |
|---|---|---|
| **b) Full curve** | 48.29 | 3.94 |
| **c) Fixed starting and final points** | 51.70 | 3.54 |
| **d) Fixed percentage of the curve length** | 51.33 | 3.29 |
| **e) Variable displacement algorithm** | 51.28 | 3.26 |

A second theme that needs to be discussed for the definition of a standard is on the method for the measurement of the specimens. In this work the typical approach followed required to measure for each tested specimen:

- the length of the specimen in two points
- the width of the specimen in two points
- the thickness of the specimen in four points
- the mass of the specimen

Four measurements of the thickness are required because it is the most influent dimension for the calculation of the density. The dimensions are taken using a digital caliper with resolution of 0.01 mm, which is significantly lower than the irregularities of the surfaces of composite specimens, and a scale with resolution of 0.001 g. From these results it is possible to calculate the cross section $A$ and the density of the material $\rho$ required for the calculation of SEA with Equation 1, considering the reduction of volume caused by the saw-tooth trigger (10 triangles having base of 10 mm and height of 5 mm). The experience gained during this work pointed out the necessity of measuring each specimen, because the actual dimensions can be very different from the nominal ones due to the typically large tolerance that can be achieved during composite curing and machining. To answer the question if it is necessary to measure each single

specimen, or the average dimensions of some specimens extracted from the batch is enough to have a good result, both the methods have been applied to the tests described in this paragraph [110]. The SEA has been calculated in each specimen considering its actual dimensions and the average dimensions of the full set; 70% of the curves showed a difference between the two results lower than 1%, and just one curve showed a difference higher than 2%. For this reason, the error committed using the average dimensions measured on the set can be considered acceptable for large sets of samples that would need a lot of time for specimen measurement, even if the results are obviously more accurate by considering the actual dimensions of each specimen.

## 3.2 Final version of the testing fixture

The final paragraph of this chapter presents the final design of the testing fixture for crashworthiness tests on composite flat laminates, that comes out from all the studies described in the previous pages. The dimensions of the specimens have been reported in Figure 53, with the thickness that can range from 2 mm to 10 mm, which was considered sufficient to cover the range of thicknesses used for crashworthiness applications. To maintain a perfect centering respect to the axle of the falling mass, the upper part of the fixture can be moved horizontally to compensate the displacement of the midplane of the specimen when the thickness changes; some reference marks were added for this reason. The design consists of a shell structure with a door on the left (Figure 61) to easily insert and remove the specimen that acts also as one of the clamping plates, and another clamping plate on the right (not visible because inside the shell) that slides from right to left to clamp the specimen with a clamping force limited to 1 kN by the controlled-torque handle on the right to avoid excessive friction force. An experimental investigation performed on this version of the testing fixture with the same method described in paragraph 3.1.3 estimated 300 N average friction force for a NEMA FR4 glass/epoxy specimen sliding after being clamped in the fixture, which can be considered sufficiently low.

The experience gained through the tests described in chapter 3.1.5 allowed to design the device to make it able to test the composite laminate in several

conditions. Substituting some of the supporting columns with similar ones properly modified it is possible to trigger different failure modes like tearing, bending or local buckling. Special attention is dedicated to the tearing test (see test results in 4.1.2), as it showed to give a good representation of the increase of SEA that can be achieved when moving from a splaying failure mode to a tearing failure mode.

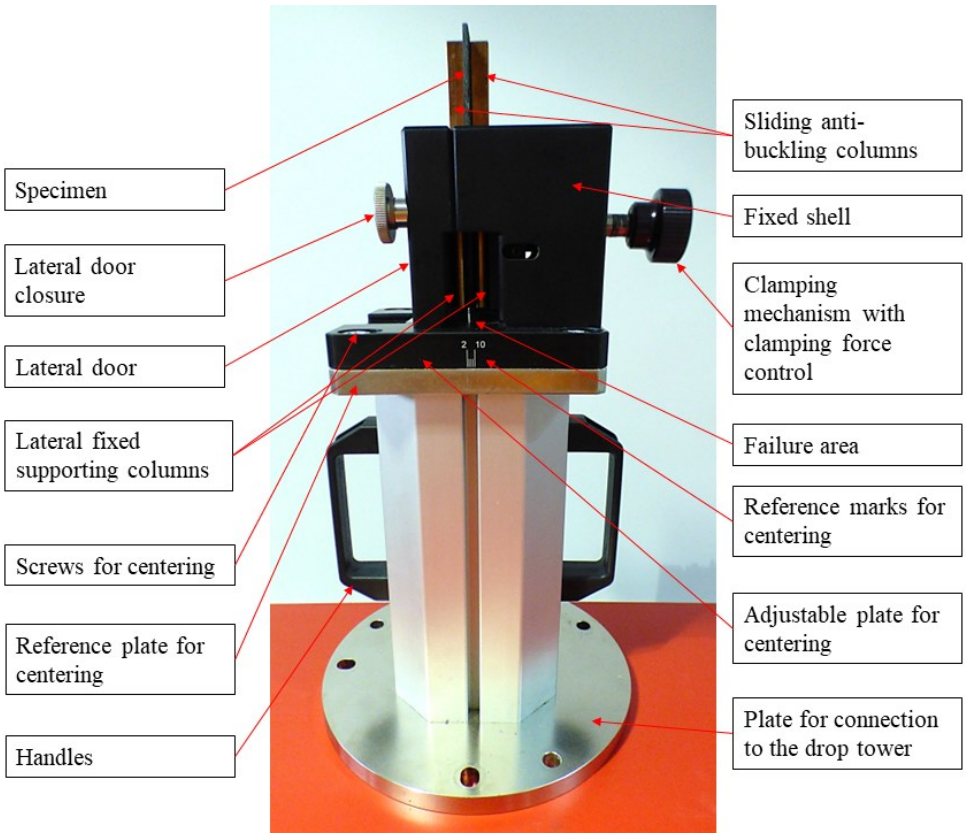


Figure 61: Final version of the fixture for crashworthiness tests on composites.

The procedure for the substitution of the tested specimen with a new one is simple, as described in Figure 62. Rotating the handle on the right side the specimen is unclamped and the upper sliding columns automatically return in the correct position for testing; then it is possible to rotate the handle on the left side and open the door to remove the specimen. After the debris and powders are

removed to get again a clean crash surface, the specimen can be positioned and the door closed, carefully fastening the handle on the left. Then the specimen can be clamped rotating the handle with limited torque on the right side; now the setup is ready for the test.

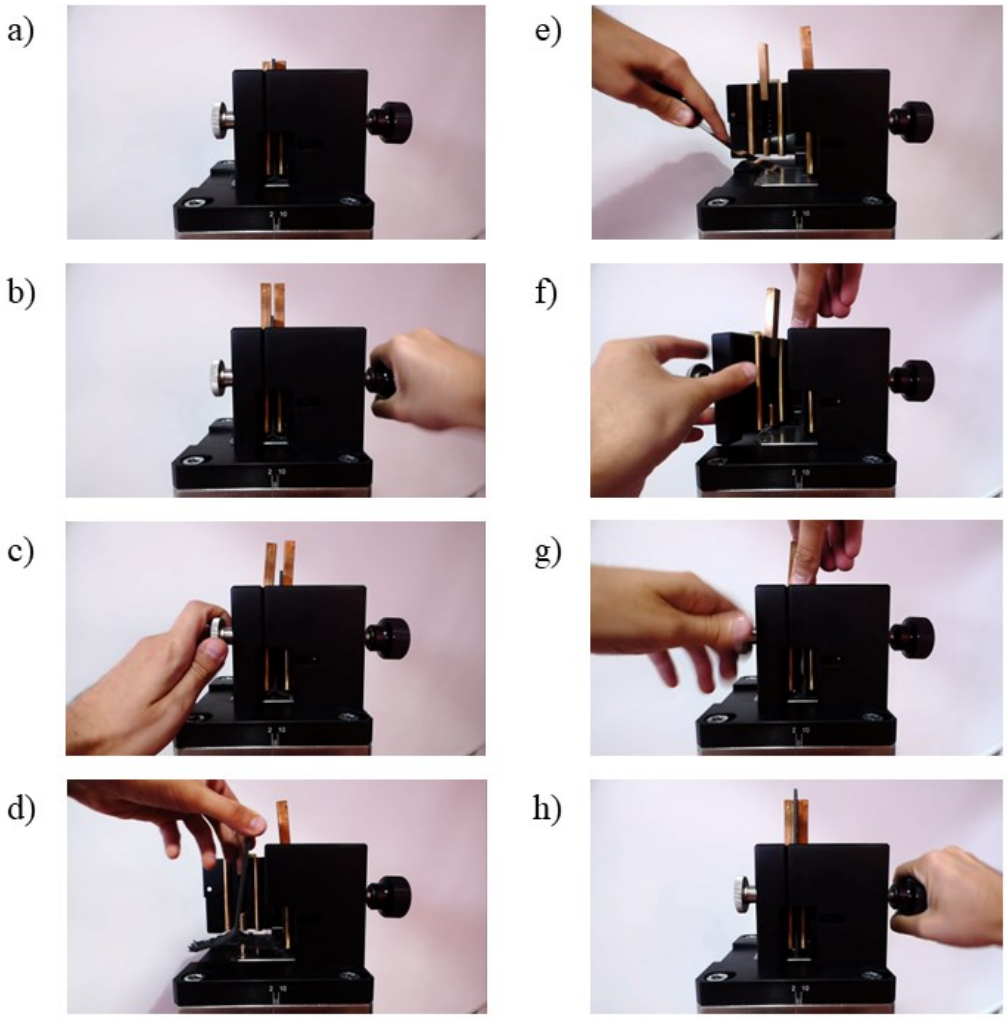


Figure 62: Procedure for removing a tested specimen and clamping a new one: a) fixture after the end of the test; b) unclamping the specimen rotating the handle on the right; c) opening the door on the left side; d) extraction of the specimen; e) removal of the debris and powders; f) positioning a new specimen and door closing; g) fastening the door using the handle on the left side; h) clamping the specimen using the torque-limited handle on the right side.

The specimen is supported by three bronze columns on each side, with the lateral ones shorter to avoid interference with the impactor falling from the top and the central one divided in a fixed part at the bottom and a sliding part on the top that can be pushed down by the impactor. A flat insert with minimum diameter of 60 mm should be used to assure the full covering of the upper part of the specimen, that is positioned with the trigger in the lower part, where failure takes place. Three of the six fixed anti-buckling columns can be substituted with longer ones to test in tearing configuration generating two tears in the laminate. A window on one side of the specimen allows a good visual and lightning of the failure process during the test (Figure 63).

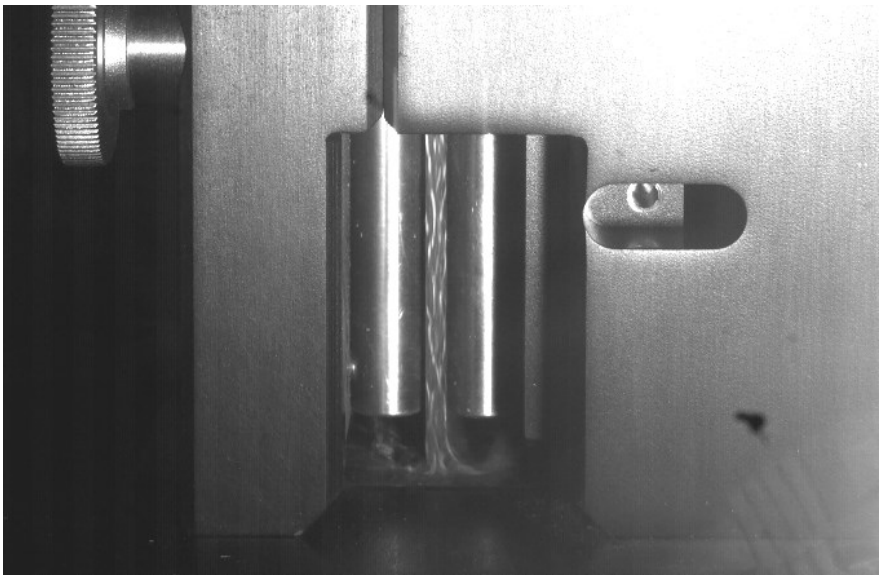

Figure 63: Failure of a 4-layers GG630 carbon/epoxy laminate observed with a Photron FASTCAM Mini AX 200 high-speed camera during a crashworthiness test.

The observation of the failure mode is a fundamental part of the testing procedure, as it allows to observe and identify the failure mechanisms obtaining important information on the crash behavior of the material. The failure mode can be correlated to the force-displacement curve and the SEA values measured as described through some examples in Paragraph 3.1.5.

# Chapter 4

# Experimental results

## 4.1 Use of the fixture in the mechanical characterization of a material

The testing procedure described in Chapter 3 is intended as a part of the process of mechanical characterization of a composite material. The SEA or SCS of the material can be included in a material database useful for material selection. What cannot be neglected is the influence of the geometry and of the failure mode on the energy absorption level, as described in Chapter 2. This is one of the main reasons why a standard test to assess the crashworthiness of composites is today not available and cannot be neglected in the present work. The fixture has been designed to apply two different constraint conditions to the specimen, performing a tearing test or a splaying test, and the results have been compared to those obtained on a self-supporting specimen proposed by Feraboli [52]. A Microtex GG630T-37 carbon fiber-epoxy prepreg (manufacturing process described in Section 2.4.2) was used to manufacture specimens for standard characterization, flat specimens for crashworthiness tests and waved specimens to represent the element level of the building block approach. A component was also manufactured and tested as described in Section 2.4.2. In this chapter, the results obtained on the different coupon tests are outlined for the selected material. The results obtained with different materials and the influence of other parameters like the impact velocity and testing temperatures are also presented in Paragraph 4.2.

### 4.1.1 Standard material characterization

The first step to build a mechanical properties database for the GG630T-37 carbon/epoxy material was to perform tensile, compression, shear and flexural tests following the international ASTM standards as described in Paragraph 2.4.2. The obtained properties (Table 1) are useful for the design of a new crash box and should be used to build the material card in an FEM software. Given the known effect of the strain rate on the mechanical properties of polymers [42] and composites [43], future work could be aimed at investigating the possibility to report the results of mechanical tests at higher strain rate, to get closer to the conditions achieved during real crashes. After the static mechanical properties of the material were found, a specific crashworthiness test was performed to evaluate the energy absorption capability of the material during compression failure.

### 4.1.2 Crashworthiness tests on flat specimens

The crashworthiness of the selected material was tested using flat specimens and the final version of the fixture described in this work (Paragraph 3.2). The laminate, made of four layers having all orientation 0°, was cut in specimens having the dimensions reported in Figure 53. Impact compression tests were carried out on a Instron 9450 drop tower equipped with a striker with strain-gauge load cell with maximum force of 90 kN, and the force was sampled at a frequency of 1 MHz. Equation 5 was used to calculate the displacement of the dropped mass, that corresponds to the crashed length of the specimen. The SEA was calculated according to the Equation 2, and the part of the curve where the average force is calculated was identified using the variable displacement algorithm described in Paragraph 3.1.6. The tests were performed with an impact energy of 400 J, a mass of 15.75 kg and an impact velocity of 7.1 m/s. The failure modes obtained with the splaying test and the tearing test are reported in Figure 64, where it is possible to see that delamination is the main failure mechanism in splaying tests and fibers failure with laminate cutting is the main failure mechanism in tearing tests.

a) b)

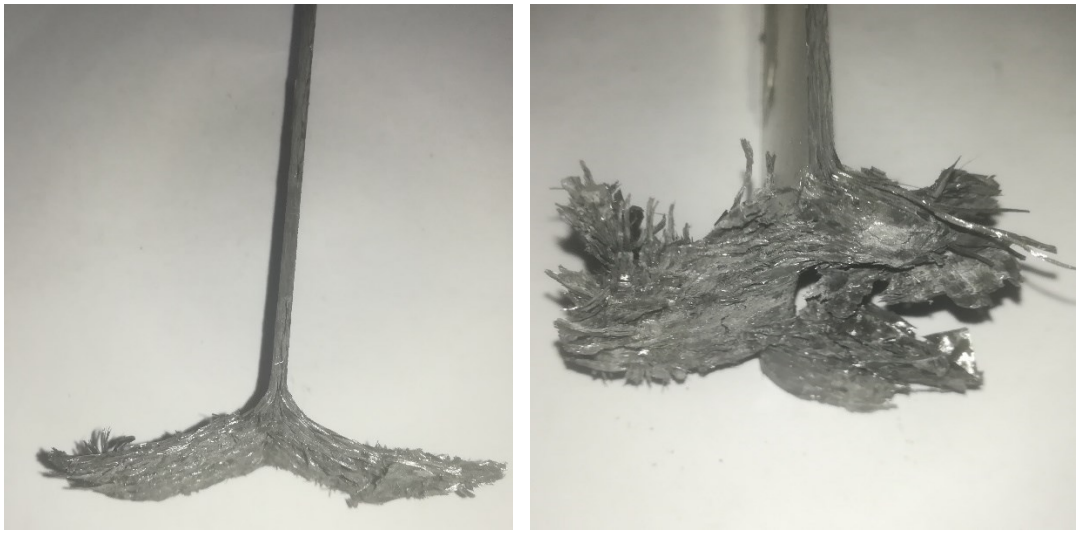

Figure 64: a) Failure mode obtained from a splaying test on a carbon/epoxy specimen, consisting of two large foils; b) Failure mode obtained from a tearing test on a carbon/epoxy specimen, consisting of three foils (one on the left, two on the right) generated by the additional constraints.

The acquired force signal (blue curve in Figure 65) is subjected to high noise due to the impact against the specimen and the sliding columns, that excites the axial modes of vibration of the load cell, that has natural frequencies below 40 kHz. To avoid this effect and obtain a filtered curve, a band stop filter between 1 kHz and 40 kHz was applied to the force signal together with 700 smoothing points, that clean the force signal obtaining the red curve in Figure 65 [110]. Even if the SEA was always calculated on the raw force, it has been verified that the results like SEA, SCS or average force do not change if the filtered curve is used instead of the unfiltered one. This is inevitably not true for peak force and CFE, as the peak force is directly modified depending on the choice of the filter. These values are not realistic even in the case of the unfiltered curve because the peak force is overestimated because of the oscillating component of the signal. A more realistic value of the peak force given by the material would be obtained from a quasi-static test, neglecting the effect of the higher strain rate achieved during impact tests.

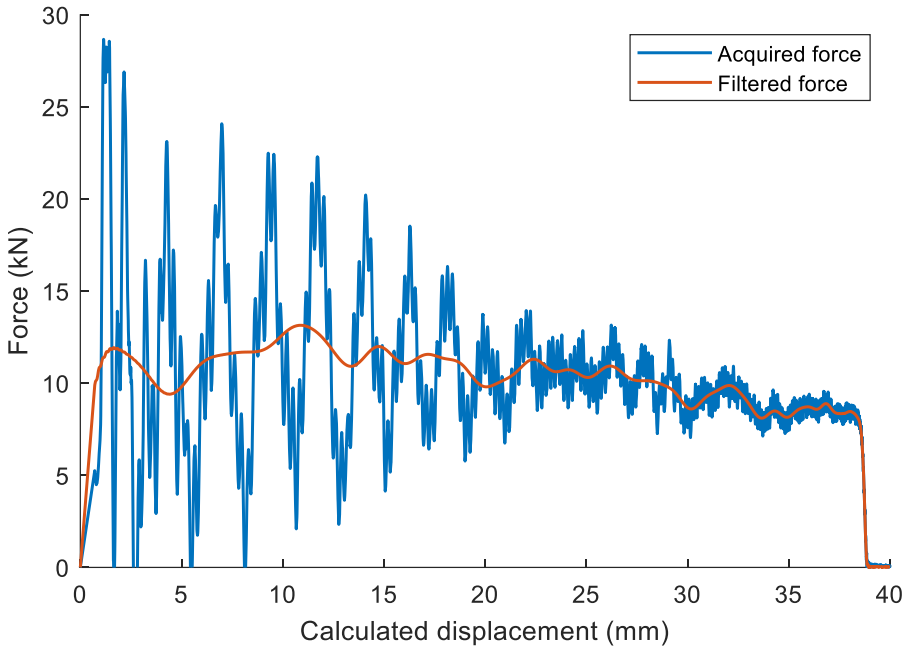


Figure 65: Force-displacement curve (blue) acquired during a splaying test, with high noise caused by the contact with the sliding columns on the fixture. The effect can be reduced applying a filter obtaining the red curve.

The filtered force-displacement curves obtained during the splaying tests can be observed in Figure 66. It should be noted that the realistic values of the curve are those comprised between 0 mm and 40 mm, as after 40 mm of test the drop tower bumpers start operating to decelerate the dropped mass absorbing a part of the kinetic energy; this means that, even if the force values are still realistic because the brakes act on the mass carrier and not on the load cell, the actual force applied to the dropped mass is higher and consequently the displacement values are no more accurate. The force peak visible in curves B and E is due to the impact of the impactor's head on the rubber bumpers positioned on the support, that act as final brakes for the dropped mass. Before calculating the SEA of the material, two observations can be done looking at the curves in Figure 66.

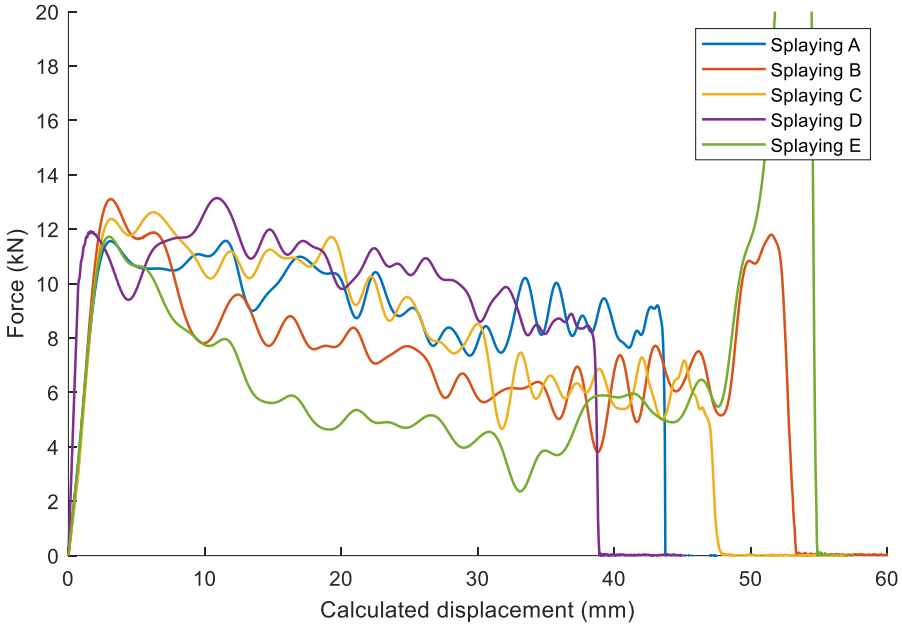


Figure 66: Filtered force-displacement curves obtained from the splaying tests on GG630T carbon/epoxy samples.

The first observation is that all the curves present a decreasing trend in the force value with the increase of the displacement, in some curves more pronounced than in other. The reason of this behavior can be explained observing the high-speed videos recorded during the test, that can be correlated to the force trend. Figure 67 shows as an example test D in various instants, with a long crack that grows vertically in the midplane of the specimen during the test. The presence of a crack reduces the crash force because the two laminae tend to bend with a large radius and a lower level of fragmentation than what is usually achieved with a small curvature. The reason of the growth of the crack could be related to the formation of a debris wedge as reported in the literature [16, 66, 112]. The debris wedge is made of pulverized material that remains constrained between the two foils and facilitates the delamination in the midplane of the specimen. The accumulation of debris grows during the test, and this could explain the progressive growth of the crack in Figure 67.

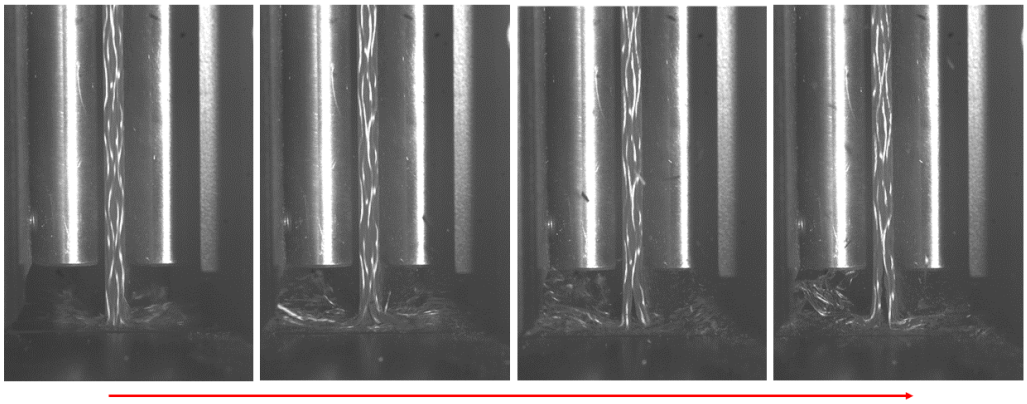

Figure 67: Growth of a crack during the splaying test on carbon/epoxy specimen D, from left to right.

A second observation is related to the scattering of the curves, which is not negligible and appears increasing with the test stroke. Some scattering in the results is usual when testing composites due to the complex structure and the several defects that can be present, and this effect is even more evident in crashworthiness tests because of the different (sometimes even coexisting) failure modes. The scattering of force-displacement curves can be correlated to the shape of the crashed specimen in Figure 68, as previously found on the same material [106]. The shape of the crashed specimen can change in different tests, showing higher or lower level of fragmentation of the two foils or a wider or narrower opening angle. The reason of this variability is still under investigation, even though the most probable explanation is that it could be due to internal defects of the material. This hypothesis should be confirmed in the future by performing some tests after having employed nondestructive techniques to assess the possible presence of defects in the material or using special specimens with artificially created defects with known position and extension, which is out of the scopes of the present work.

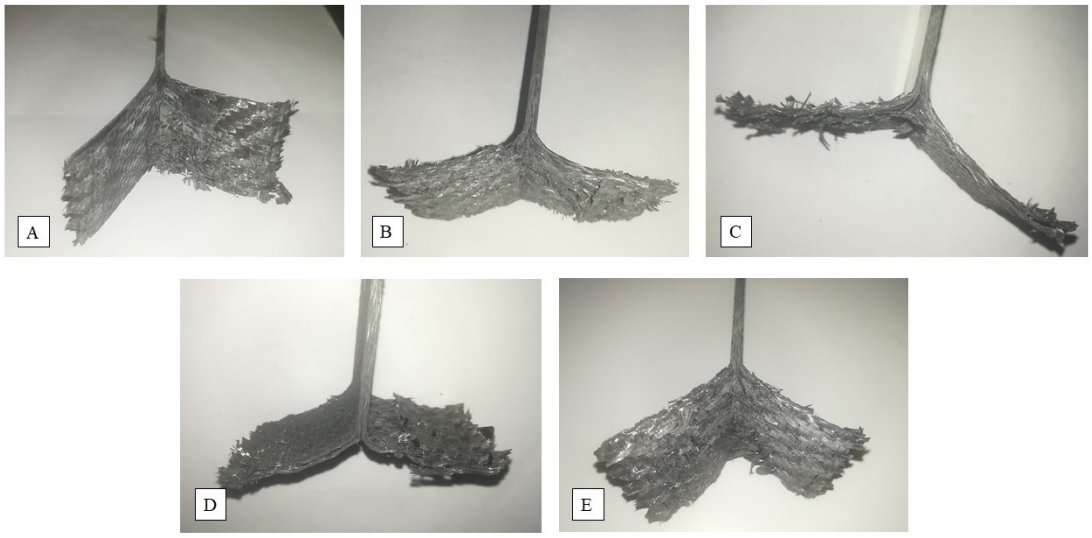


Figure 68: Splaying failure mode found on carbon/epoxy flat specimen after crashworthiness test.

In the specimens used for this work, some macrographs (Figure 69) only showed the presence of some superficial porosity, probably not able to influence the crash failure of the specimen.

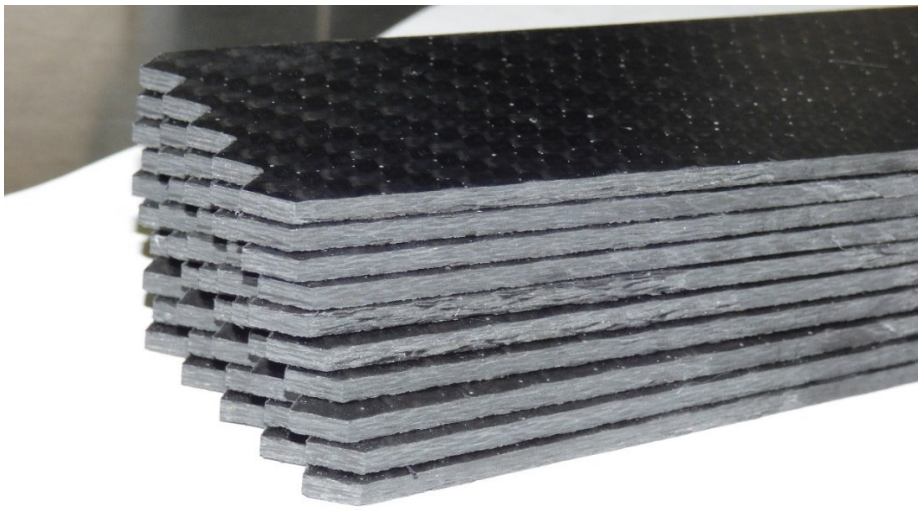

Figure 69: High resolution picture taken to observe the superficial porosity which is probably not influent on the test results and the thickness where internal defects are not visible; some black stripes in some specimens are burrs due to the cutting process.

Some small internal delamination was visible observing the thickness using a microscope (Figure 70), but it was not possible to understand if that defects extend internally or are superficial defects generated by the cutting process.

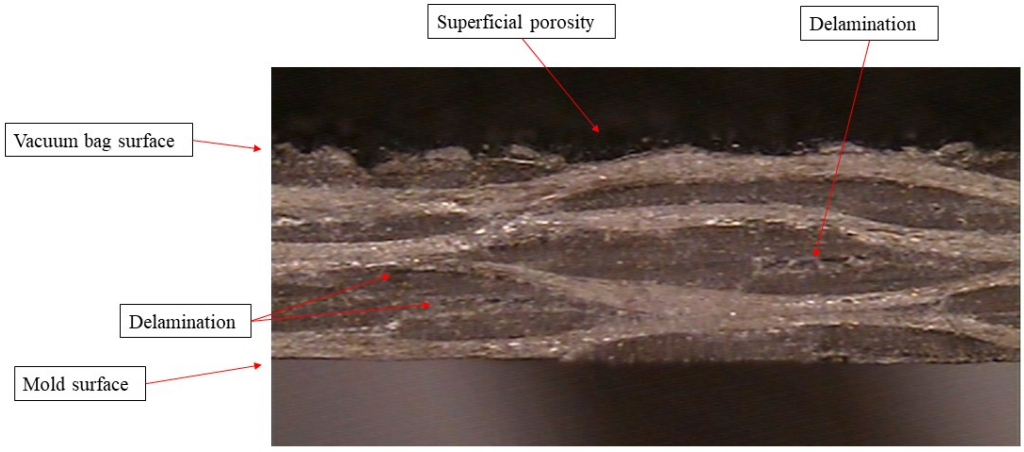


Figure 70: Thickness side of a GG630T carbon/epoxy four layers specimen observed using a microscope.

Another reason of the scattering and oscillations in the force curve is the complex failure mechanism taking place in a relatively simple test as a splaying test. If from the macroscopic point of view the splaying failure can be described as a delamination in the mid plane of the laminate with formation of two fronds, when the failed material is observed using a microscope (Figure 71) the failure appears a complex mixture of delamination, fibers breaking and pull-out, matrix debonding and fragmentation. All this failure mechanisms alternate in the failed material and during the test, probably causing the characteristic oscillations of the acquired force.

a) b)

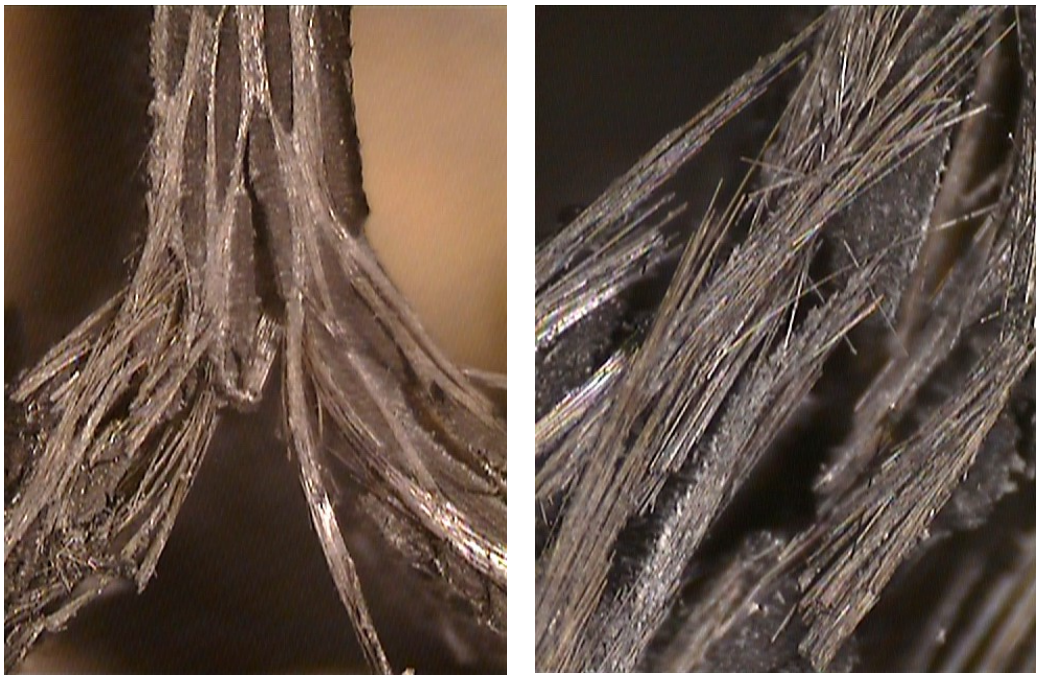

Figure 71: a) Failure mode obtained from a splaying test on a carbon/epoxy specimen, consisting of two large foils; b) Failure mode obtained from a tearing test on a carbon/epoxy specimen, consisting of three foils (one on the left, two on the right) generated by the additional constraints.

Results of tearing tests (Figure 72) are very different because of the different failure mode, that causes higher energy absorption as expected, with average forces of about 12.6 kN, significantly higher than in splaying tests (8.4 kN). Therefore, the curves are shorter because the same initial kinetic energy is dissipated in a lower displacement due to the higher crash force. From Figure 72 it is possible to see that the scattering of curves is lower, and the decreasing trend of splaying tests is not present.

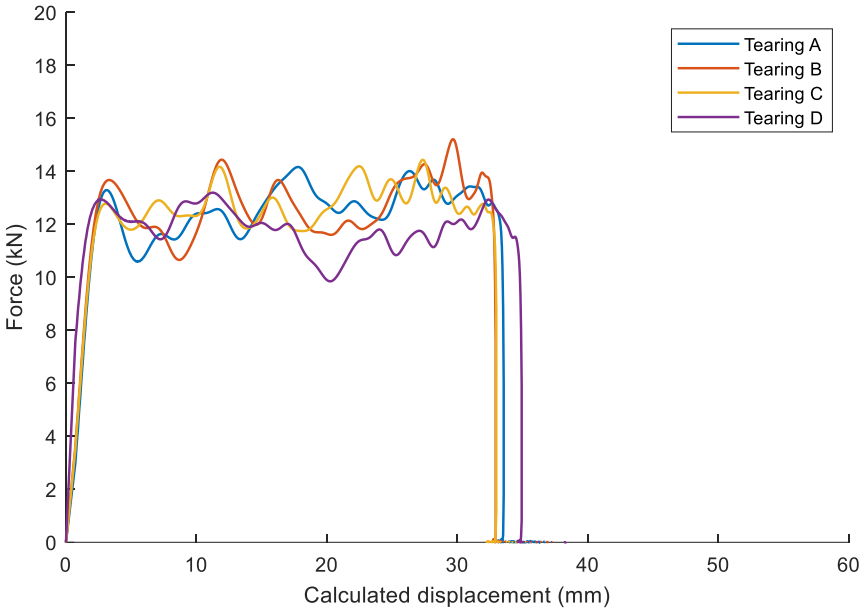


Figure 72: Filtered force-displacement curves obtained from the tearing tests on GG630T carbon/epoxy samples.

These effects are explained by the different kinds of tests that impose some constraints in the failure area forcing a different failure mode to take place (Figure 73). Forcing the material to fail always in the same way reduces the scattering of the force signal, and the constraint prevent the formation of the mid-plane delamination seen in the splaying tests and the formation of the debris wedge; for this reason, no decreasing trend of the force-displacement curve is visible.

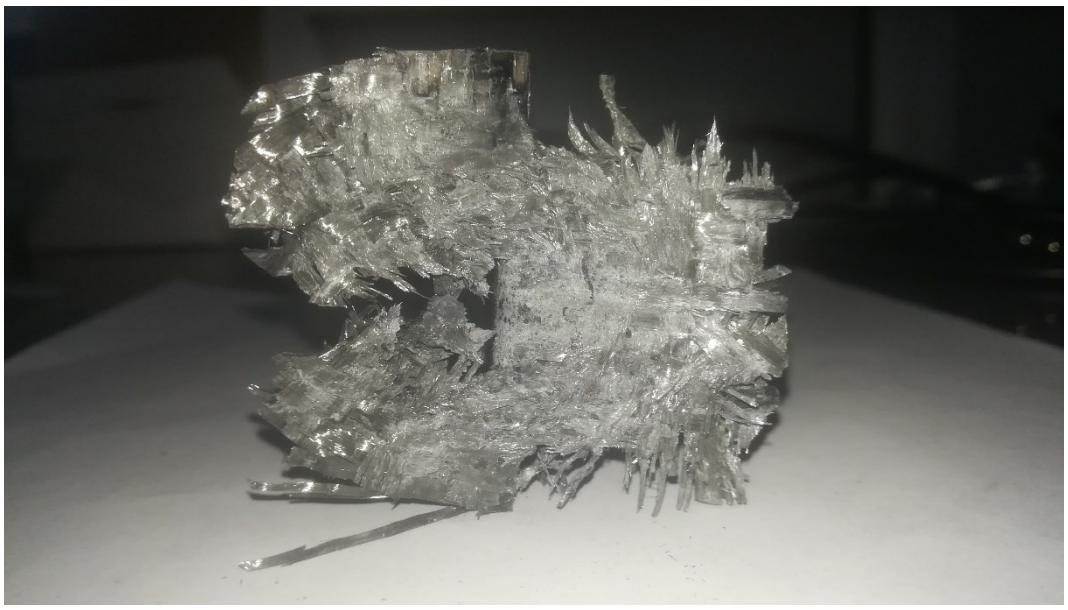

Figure 73: GG630T carbon/epoxy specimen after tearing test seen from bottom, with two foils on the left and one foil on the right.

The failure is then characterized by two tears and by the bending of the obtained three foils (Figure 73). Inside the foils, delamination and fragmentation can take place as showed in Figure 74, representing then a complex fracture mode close to typical failures of real structures. The failure mode is similar in all the tests as reported in Figure 75.

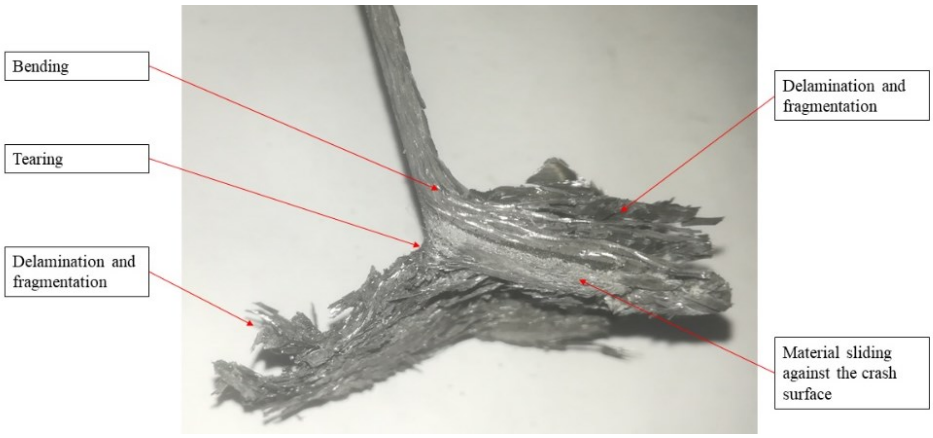


Figure 74: lateral view of a GG630T carbon/epoxy specimen after tearing test.

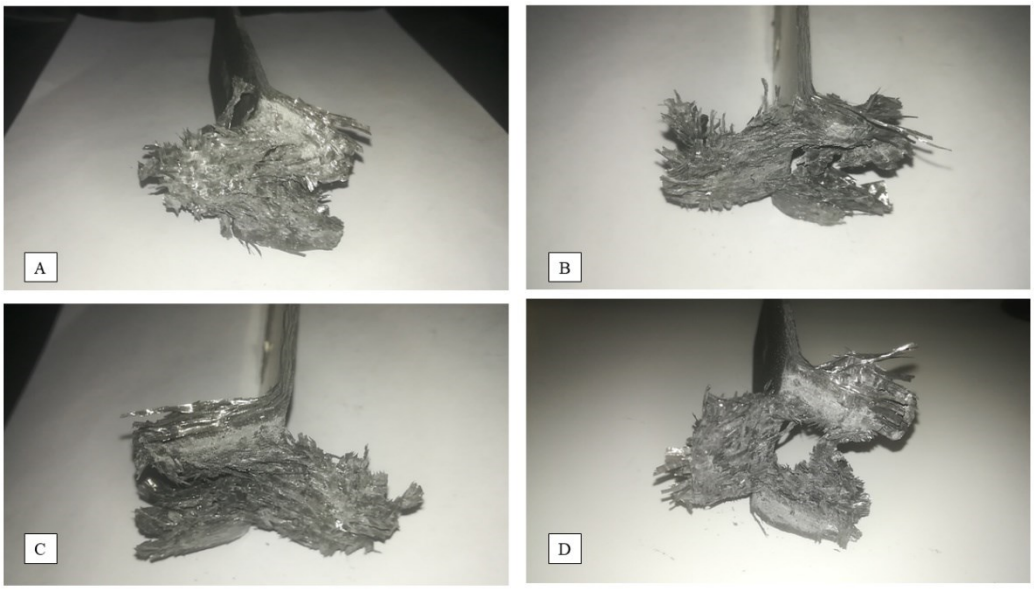


Figure 75: Tearing failures found on carbon/epoxy specimens after tearing test, all having similar aspect.

The tearing test causes higher crash force than the splaying test because the fiber breaking failure mechanism becomes predominant in the two areas where tearing takes place. This test can then give a quantitative information on the increment of energy absorption that can be achieved when the laminate tears instead of bending or splaying. This result is not enough to describe all the possible failures that can be obtained during the crash test on a real component but it is an useful result for material characterization as it describes the energy absorption level of another failure mode. The effect on the SEA and SCS is described in Paragraph 4.2.3 to compare the result with a waved specimen that simulates the element level of the building block approach. Furthermore, the tearing test is a good benchmark for validating or optimizing a numerical model, as described for example in Chapter 5.

### 4.1.3 Crashworthiness tests on waved specimens

The half-circle specimen proposed by Feraboli in [52] was chosen to represent the element level of the building block approach for its curvature, that makes it similar to crash box elements or subfloor structures employed in aerospace for

impact energy absorption [15]. Another advantage is that it can be tested standing alone without the use of a testing fixture and that its manufacturing process is simpler than closed section specimens. On the other hand, the flat specimen remains the cheapest and simpler specimen to be manufactured.

Specimens with the cross section in Figure 76 were produced using the same layup and process used for the flat specimens described in Section 2.4.2: four layers oriented with 0° respect to the testing direction positioned on a half mold covered by a vacuum bag before the autoclave curing. The mold was designed to produce specimens having a cross section with midplane corresponding to the geometry proposed by Feraboli in [52]. The thickness grew instead from 2 mm to 2.5 mm due to the different material used. A possible trigger mechanism for this specimen would be a chamfer trigger, but a saw-tooth trigger was preferred to have the same triggering mechanism as in the flat specimen. Given the waved geometry of the specimen that makes an automatic cut difficult, the saw tooth was cut manually.

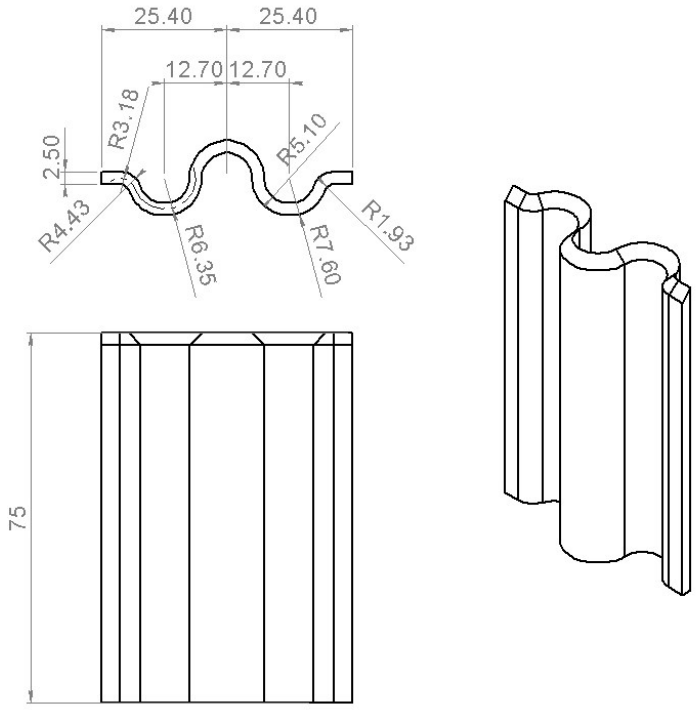


Figure 76: Geometry of the waved specimens used for crashworthiness tests, adapted from [52] to have a nominal thickness of 2.5 mm that corresponds to four layers of the Microtex GG630T prepreg.

A fixture was designed to clamp the waved specimen, keep it centered respect to the axis of the falling mass and avoid its possible movements during the impact test. The specimen lays with the lower surface on a horizontal plate and is clamped in its lower part, leaving 62 mm of unclamped height for crash, as visible in Figure 77, taken after the test.

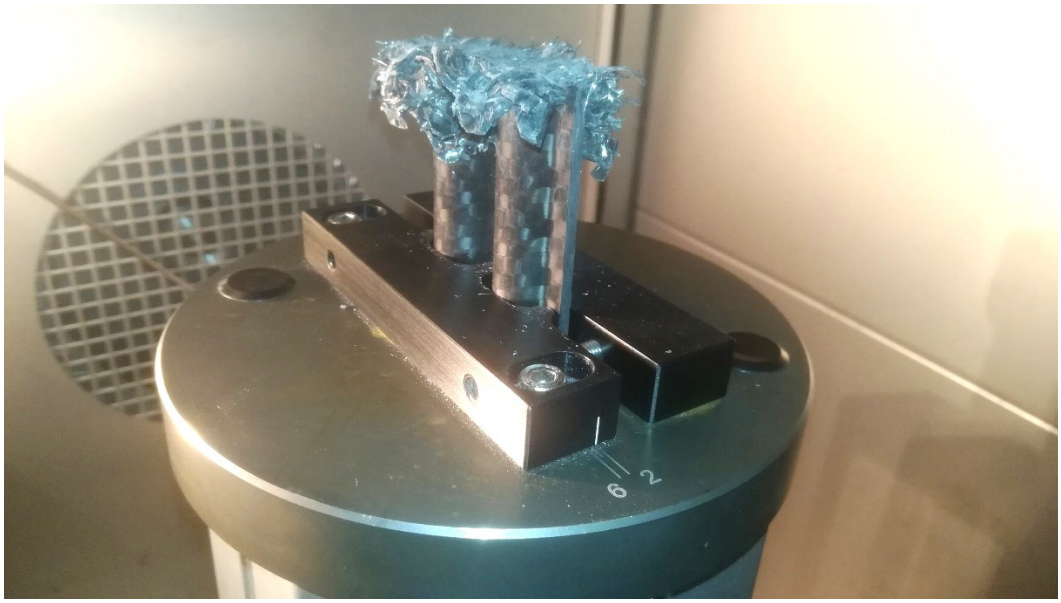


Figure 77: Carbon fiber/epoxy waved specimen clamped on the testing fixture in the drop tower testing chamber after crashworthiness test.

The impactor gets directly in contact with the upper part of the specimen, where failure takes place (Figure 78). The force was acquired using the same instruments used for the tests on flat specimens and the SEA was calculated adopting the same approach, using Equation 2 instead of Equation 1 to avoid the measurement of the cross section of the waved specimens, that is a difficult process potentially capable to generate non-negligible errors.

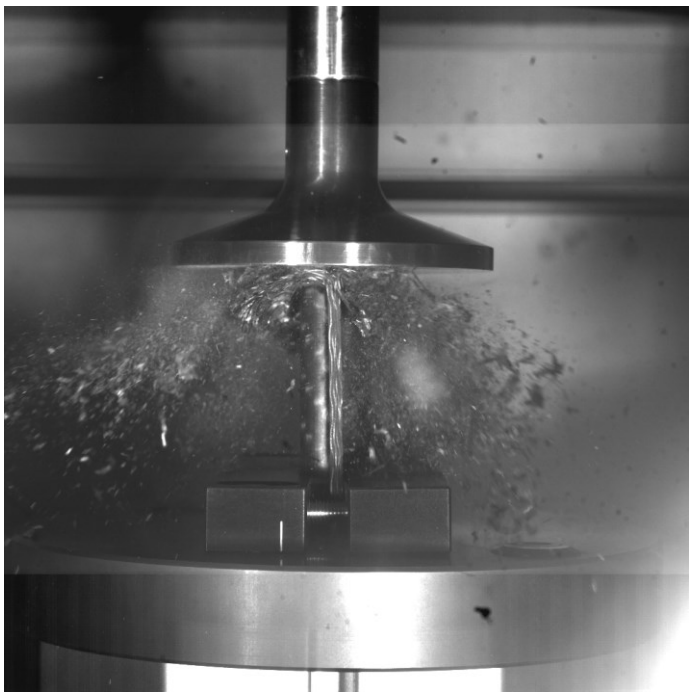

Figure 78: Frame from the high-speed video recorded during the crashworthiness tests on carbon/epoxy waved specimens.

The filtered force-displacement curves acquired are plotted in Figure 79, where it is possible to observe the smooth increase of the force value up to a displacement of about 5 mm, corresponding to the depth of the failure trigger. The force than stabilizes around a constant value that allows to calculate the SEA. It can be noticed that given the ability of the specimen to stand and crush correctly without the need of an anti-buckling fixture, this structure can be considered a good representation of an element in the building block approach and a valid geometry to be used to build a crash absorber with good effectiveness thanks to the low peak forces.

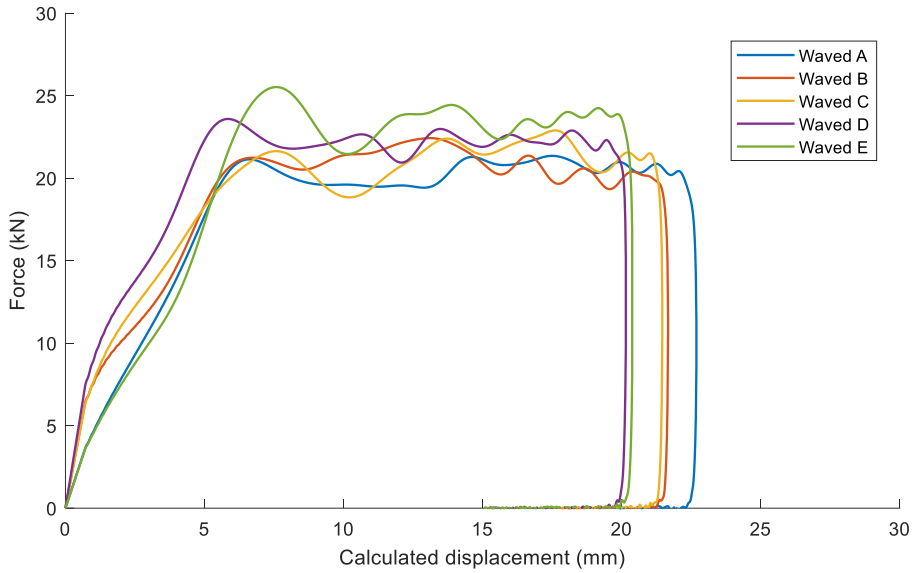


Figure 79: Filtered force-displacement curves acquired during crashworthiness tests on waved specimens.

The failure mode is the same in all the specimens, as shown in Figure 80. It consists of a mixture of delamination, fibers fracturing and fragmentation. The fibers fracturing is mainly concentrated in the half-circles areas, where the curvature triggers their failure, while from the lateral side of the specimen it is possible to understand how in the mid plane of the specimen splaying always tends to happen (Figure 78). The high level of fragmentation and fibers breaking is the probable explanation of the crash forces recorded, that range between 20 kN and 24 kN, and SEA as described in the following.

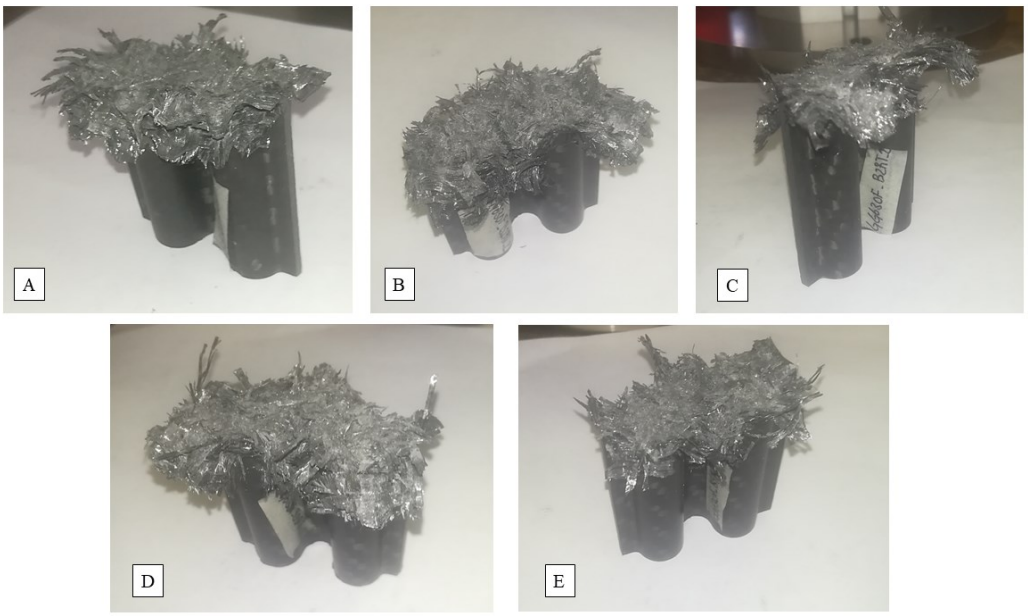


Figure 80: Failure mode of waved carbon/epoxy specimens after crashworthiness tests.

The test results can be compared to those obtained with the other two tests carried out on flat specimens (splaying and tearing tests). Given that the material, the stacking sequence and the production process were the same for both flat and waved specimens, and that the tests were all carried out in the same impact conditions (impact velocity 7.1 m/s, impact mass 15.75 kg, impact energy 400 J), it is possible to state that the results are only influenced by the testing condition (i.e. splaying test, tearing test or waved specimen test). The SEA values measured in the splaying and tearing tests on flat specimens and on the waved specimens have been plotted in Figure 81, where the splaying test gives the lower SEA because mainly consists of delamination and matrix fragmentation, in agreement with the literature that classifies the splaying failure mode as less efficient than tearing [15]. The other extreme is represented by the waved specimens proposed by Feraboli, that showed very high SEA thanks to the failure mechanism involving a lot of fiber fracturing. The SEA obtained from tearing tests falls in the middle, and this is due to the constraints that cause more fiber tearing than in the splaying tests, but not enough to reach the values obtained from waved specimens.

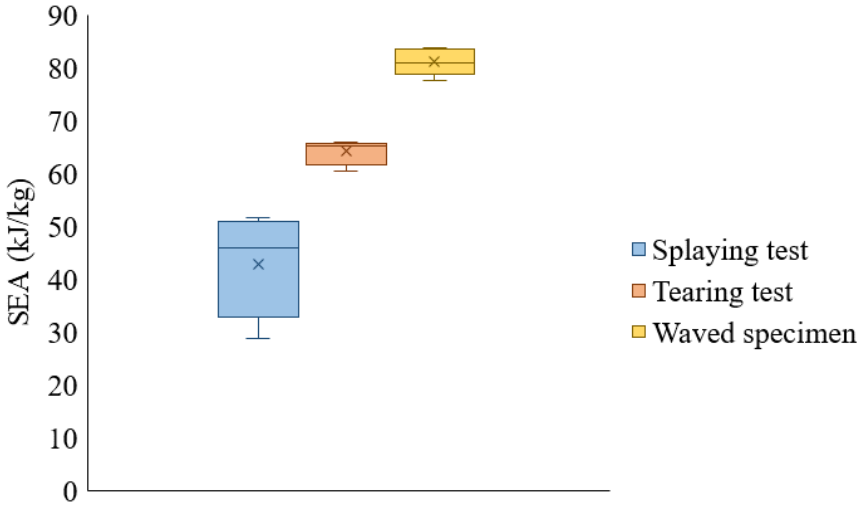


Figure 81: SEA calculated from crashworthiness tests on carbon/epoxy specimens from the splaying and tearing tests carried out on flat specimens and on the waved specimens.

The interpretation of these results within the framework of the characterization of the four layers GG630T-37 carbon/epoxy laminate is something not easy as it cannot immediately be extended to the design of a new crash box. The real product will probably have a geometry that differs from the tested samples, and the well-known effect of the geometry on the failure mode and consequently on the energy absorption will probably cause the crash box to have an SEA that differs from that of the tested coupons. The only way to obtain a prediction of the energy absorption level of a newly designed crash absorber requires the use of FEM modeling: if some models using the same material cards and modeling approaches can give a good prediction of the behavior of the material in the three tests, that require high flexibility in reproducing the different failure modes, that would be probably a model able to predict the behavior of a new complex structure like a newly designed crash box. Some investigation on this topic have been performed using the LS-Dyna explicit code and the results are presented in Chapter 5.

Another possible interpretation of the SEA results in the different tests would be to consider the splaying tests and the waved specimens tests as two extremes of a linear behavior where the SEA depends on the performed test and the tearing

test falling in the middle of the two behaviors. However, what can be drawn both from the literature and the experience gained during this work is that the two tests are not respectively the minimum and maximum level of energy absorption provided by the material: buckling is usually a failure mode that absorbs less energy than splaying [15], and the waved geometry proposed by Feraboli is totally conventional, and a change in its shape or curvature radius can cause changes in the SEA [52]. Same conclusion can be drawn for the tearing test; changing the position of the constraints, a different number of tears of the laminate can be generated, with consequent variation in the energy absorption level.

In conclusion, while the three presented tests appear to be useful to describe different behaviors of the material, a numerical approach based on the use of the test results to calibrate the non-physical coefficients of the material card is probably the best way to deal with the prediction of the behavior of a new product.

Another information obtained from the plot in Figure 81 is the higher scattering of splaying test results compared to the tearing test and the waved specimen test. This effect is probably due to the higher sensitivity of the splaying test to the internal defects of the matrix, that results reduced in tearing and waved specimen tests where the main responsible of the energy absorption is the fiber failure. If this conclusion will be confirmed in future by dedicated experimental investigations, the splaying test could be a good candidate to easily assess the presence of internal defects in the laminate.

### 4.1.4 Crashworthiness tests on a full-scale component

The SEA values obtained testing coupons and elements presented in the previous sections can be compared to those obtained on the impact attenuator described in Section 2.4.2. The attenuator showed a lower level of energy absorption than all the other results obtained on flat and waved specimens (Figure 82).

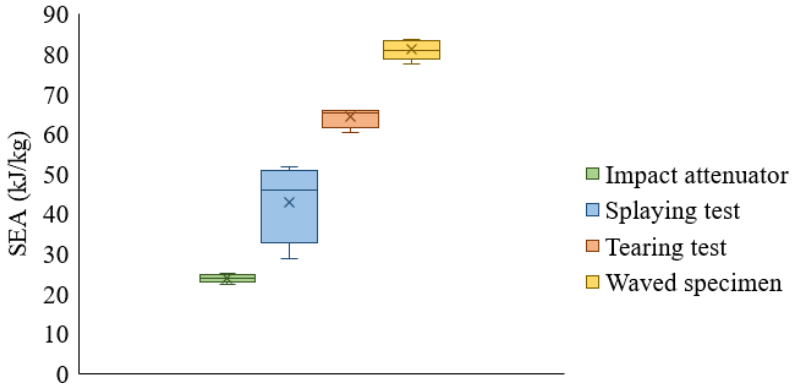


Figure 82: SEA calculated from crashworthiness tests on carbon/epoxy specimens and components.

This is easily explained by the observation of the failed component, that shows a complex coexistence of different failure modes as shown in Figure 83, with wide undamaged areas due to the presence of flat walls that tended to buckle instead of splay. This effect is also amplified by the tapered geometry of the walls. The described behavior results in a low level of energy absorbed for most of the component, that causes the low global SEA.

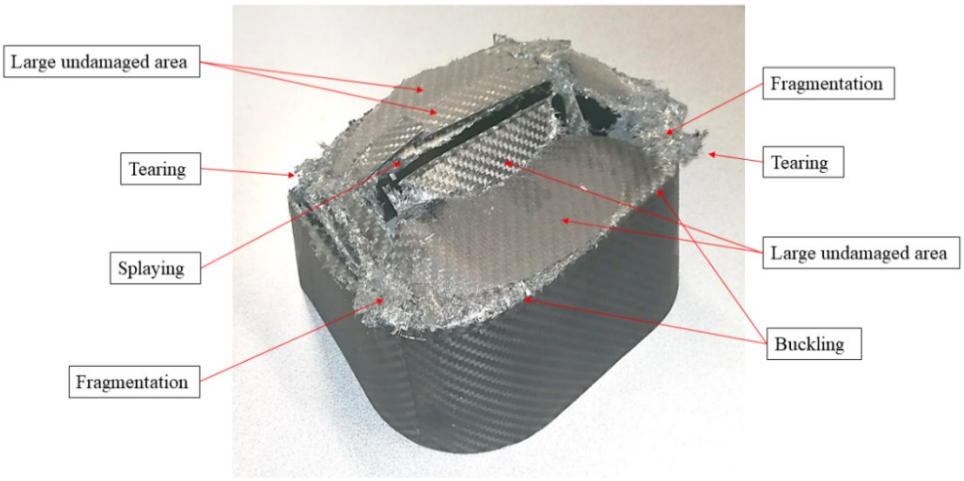


Figure 83: Failure of a full-scale carbon/epoxy impact attenuator after crashworthiness test, with several coexisting failure modes.

Tearing and fragmentation, generally known as the most efficient failure modes of composites, mainly occur at the four corners, where the curvature causes fibers rupture. The attenuator could then be further optimized changing its geometry to achieve better efficiency and lower weight or higher energy absorption. The final results of the investigation are reported in Table 8.

**Table 8**: Summary of crashworthiness tests on GG630T-37 carbon/epoxy.

| | **Average SEA (kJ/kg)** | **Standard deviation of SEA (kJ/kg)** | **Coefficient of variation** |
|---|---|---|---|
| **Impact attenuator** | 23.8 | 1.0 | 4.3% |
| **Splaying test** | 42.7 | 9.6 | 22.6% |
| **Tearing test** | 64.2 | 2.6 | 4.0% |
| **Waved specimen** | 81.0 | 2.5 | 3.1% |

Table 8 shows the low scatter of the SEA measured on the impact attenuator, with low values of coefficient of variation (i.e. the ratio between standard deviation and average) comparable to those measured in waved specimen tests and tearing tests. This result indicates a good uniformity in the behavior of the four impact attenuators tested under impact load. The splaying test is the only one showing a coefficient of variation higher than 5% (i.e. 23%), confirming the necessity of further investigation to understand if this behavior could be due to internal defects.

## 4.2 Effect of the testing conditions on the crashworthiness of composites

The presented testing procedure aims not only at characterizing the material, but also to study its behavior under various conditions like different laminate thicknesses, testing temperatures or impact velocities. The effects of these factors have been studied on various materials and some results are summarized in the

following pages. All the studies were carried out on the GG630T-37 carbon-epoxy prepreg to complete the characterization of this material, while some tests with different laminate thicknesses were carried out on a VV770 glass/epoxy prepreg and NEMA FR4 carbon/epoxy plates.

Some of the tests presented in this section were carried out in different moments during the development of the project, and some changes in the testing setup are highlighted. Anyway, all the results appear to be consistent, and this proves that the various modifications implemented on the fixture have not influenced the test results.

### 4.2.1 Effect of laminate thickness

Several laminates made of GG630T-37 carbon-epoxy twill prepreg oriented 0° were manufactured and tested in splaying configuration in two different phases with two different versions of the fixture: some 3-layers, 4-layers and 8-layers thick laminates were tested with the older version of the fixture that requires 100 mm-wide specimens, while 2-layers and 4 layers laminates were tested with the last version of the fixture that requires 50 mm wide specimens. From the box plot in Figure 84 no significant difference appears in the average values and scatter, thus suggesting that the thickness of the laminate is not influent on the SEA. The comparison between the 4-layers tests with 50 mm and 100 mm wide specimens confirms the absence of unwanted effects on the testing results due to the different width of the specimens or to the different testing fixture.

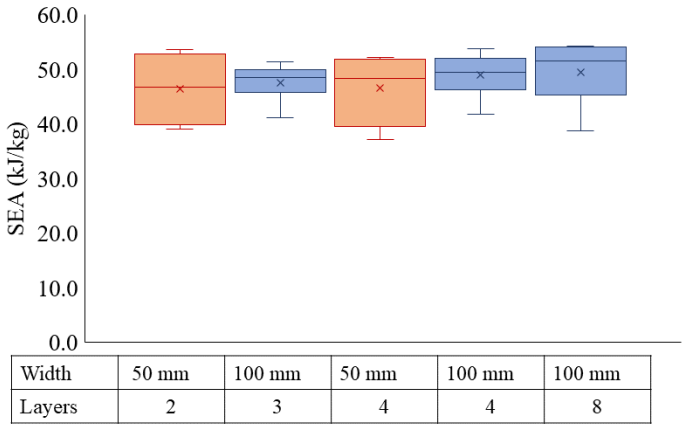


Figure 84: SEA of carbon/epoxy laminates having different thicknesses and widths.

The result is consistent with the failure modes observed after the test, as shown in Figure 85. All the specimens splayed in a similar way independently from their width or the fixture used, with various levels of fragmentation of the foils that contribute to the scatter of SEA values, regardless of the thickness. The two-layers laminate showed, due to the low thickness, sometimes asymmetrical splaying with one foil more fragmented than the other (Figure 85a), while the three-layers laminate showed two asymmetric foils due to the central layers that flows on one side (Figure 85a). The specimens having four and eight layers showed instead symmetric foils.

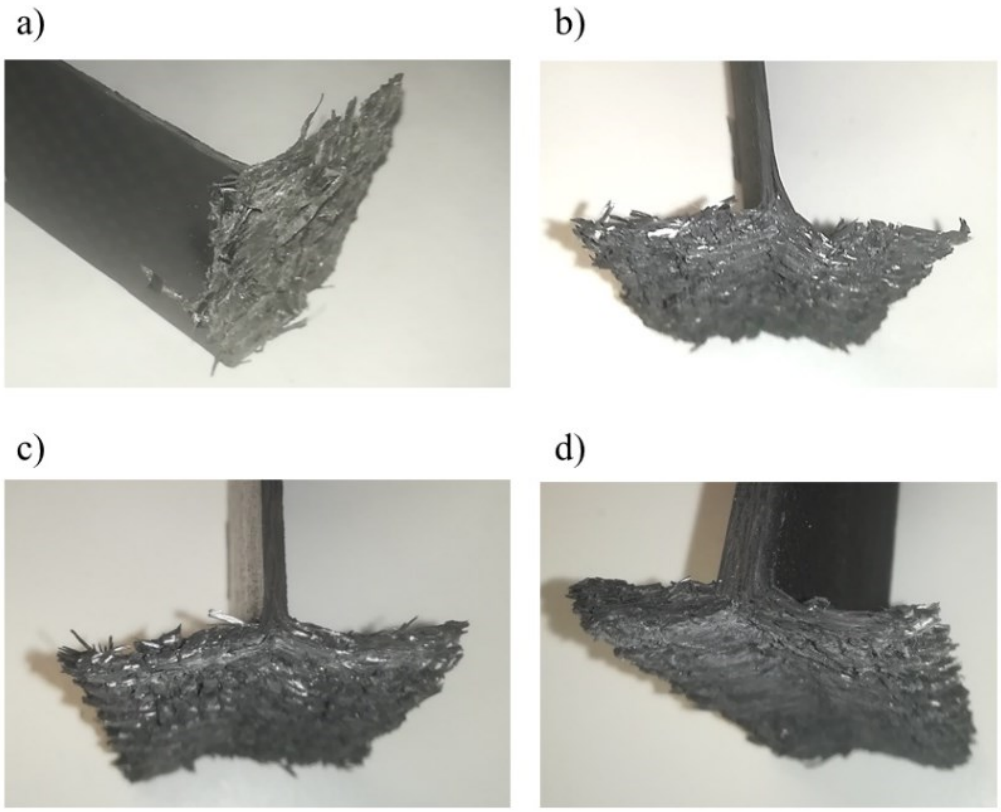


Figure 85: splaying failure modes of carbon/epoxy laminates with different thicknesses: a) 2 layers; b) 3 layers; c) 4 layers; d) 8 layers.

A similar investigation was carried out on NEMA FR4 glass/epoxy laminates of different thicknesses ranging from 1 mm to 10 mm. Tests were performed on the old and new versions of the testing fixture and on 50 mm and 100 mm wide specimens. Some differences in the SEA values were detected, but no trend appears clear from the plot in Figure 86. Given the nature of the material, that is commercially available in ready-to-cut plates, the variation of SEA is probably due to batch-to-batch variability, that during preliminary studies, not reported here, was found even on batches of plates with same thickness bought in different periods.

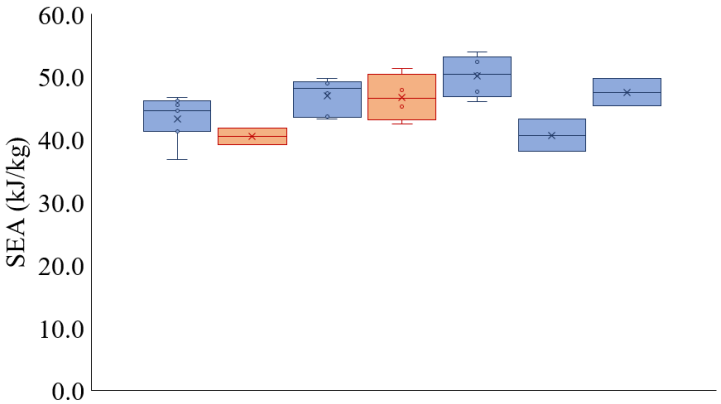


| Fixture | Old | New | Old | New | Old | Old | Old |
|---|---|---|---|---|---|---|---|
| Width | 50 | 50 | 50 | 50 | 100 | 100 | 100 |
| Thickness | 1 | 1 | 3 | 3 | 3 | 5 | 10 |

Figure 86: SEA of NEMA FR4 laminates having different thicknesses.

The old and the new fixtures can be compared with the tests of laminates with thickness of 1 mm and 3 mm. The results on 3 mm-thick specimens are well comparable, while slightly higher difference is visible on 1 mm thickness, even if the results still fall in the same range.

The failure mode of all NEMA FR4 carbon/epoxy specimens consists of the formation of two foils and in some cases a delamination growing vertically close to the midplane of the laminate (Figure 87).

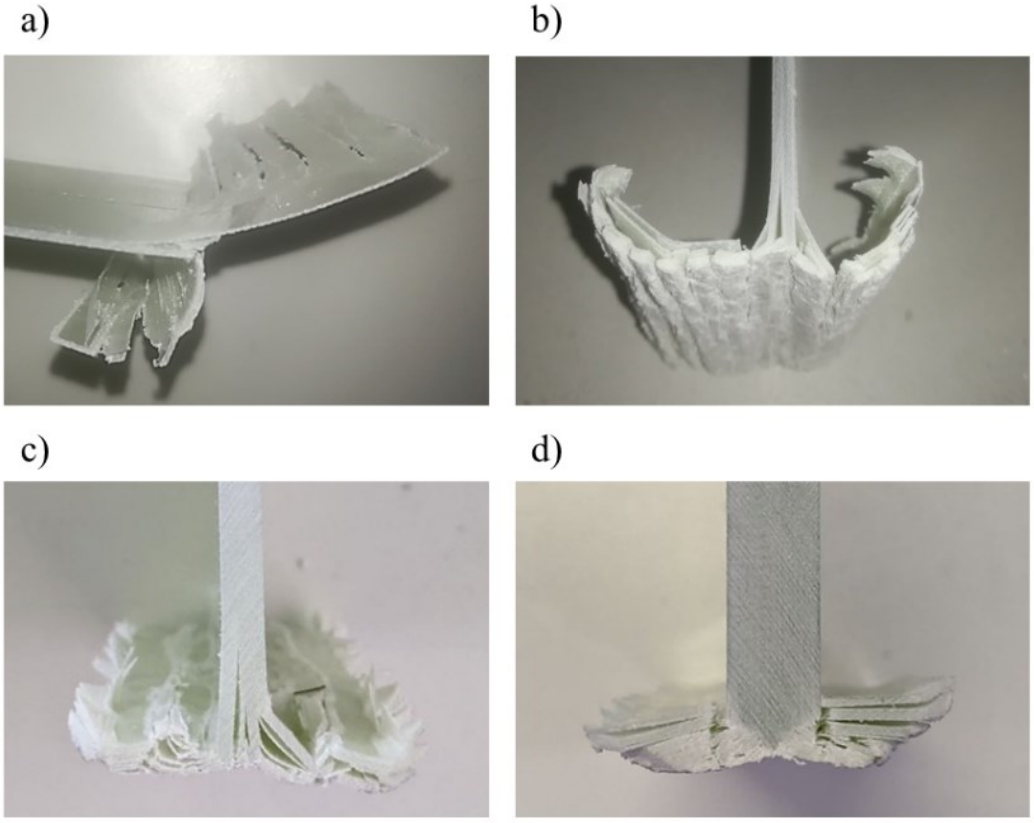


Figure 87: Failure mode of NEMA FR4 laminates having different thicknesses: a) 1 mm, b) 3 mm, c) 5 mm, d) 10 mm.

Similar tests were carried out on a Microtex VV770T-32 glass/epoxy prepreg in laminates consisting of 3 layers, 4 layers and 8 layers (mechanical properties in Table 6). SEA increased with the laminate thickness, probably due to the higher stiffness of the thicker specimens compared to the thinner ones. This effect is typical of this material, as similar result was not obtained on GG630 carbon/epoxy or NEMA FR4 glass/epoxy materials. The increase of SEA is visible in Figure 88 and confirmed by a linear regression returning a p-value of 0.2%, even if the scatter is quite wide ($R^2$ value 0.34).

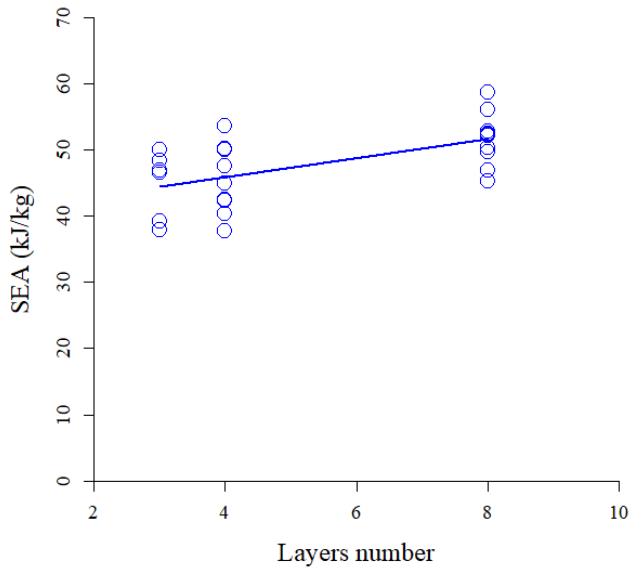


Figure 88: SEA of VV770 glass/epoxy specimens as a function of the number of layers of the laminate.

The splaying failure mode (Figure 89) found after test is similar to those obtained with the carbon/epoxy specimens.

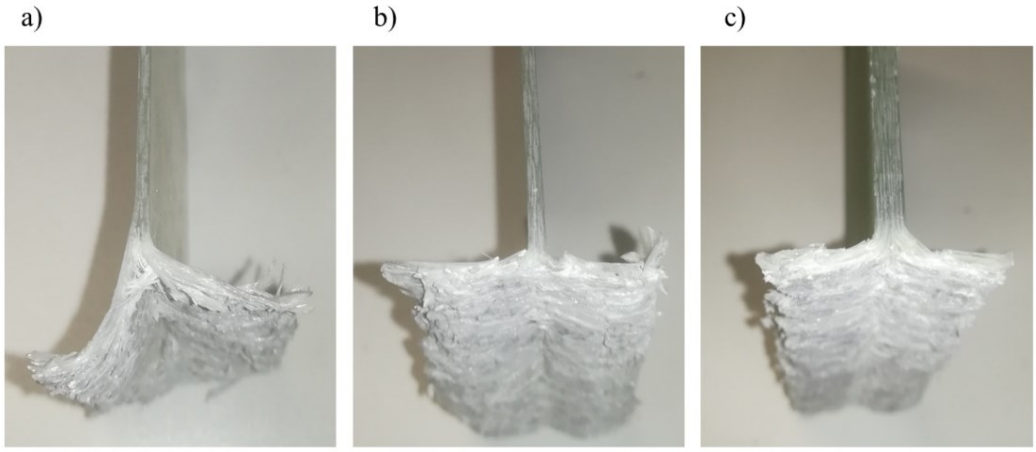


Figure 89: Failure mode of VV770 glass/epoxy specimens after splaying test: a) 3 layers specimen, b) 4 layers specimen, c) 8 layers specimen.

The possibility to test different laminate thicknesses using the same setup allows then to identify different trends in different materials. This information is useful during the design of a crash box because different parts of the structure can have different thickness.

### 4.2.2 Effect of impact velocity

Strain rate is one of the most interesting parameters when dealing with impact testing, and this is particularly true when polymers are involved like in composites. In this work the effect of the strain rate was studied by means of tests at different impact velocities, and impact tests compared to quasi-static tests performed with a modified fixture using an Instron 8801 hydraulic universal machine in the laboratories of Politecnico di Torino (Figure 90).

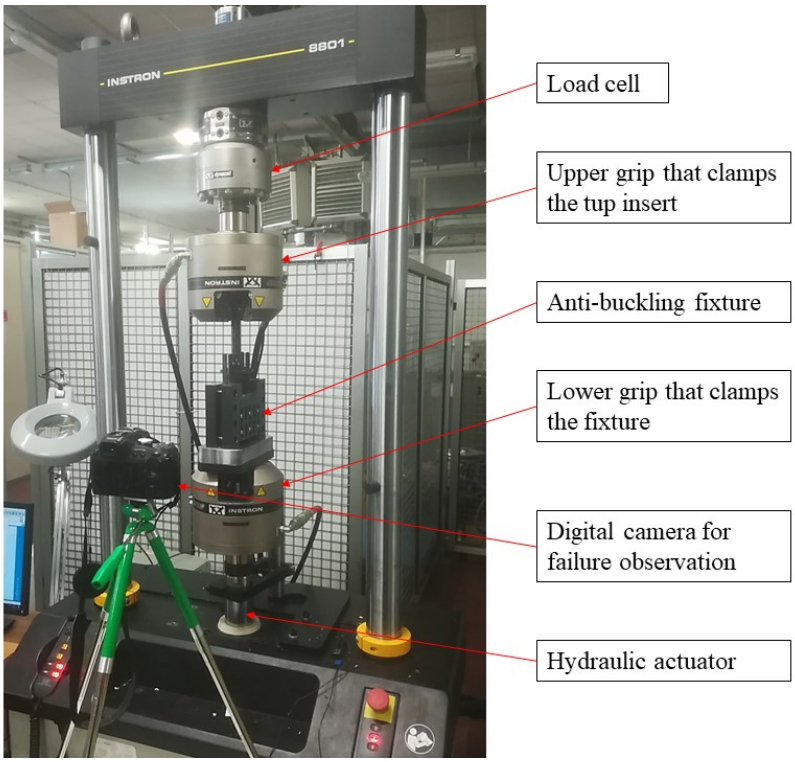


Figure 90: Test setup modified for quasi-static tests.

Two different testing campaigns were carried out using flat specimens made of GG630T carbon/epoxy prepreg. The first campaign was published in [106] and consisted of impact tests carried out at 5 m/s, 7 m/s and 10 m/s in splaying conditions. No effect of the impact velocity on the SEA was detected during those tests, as visible in Figure 91a.

A second testing campaign focused on the effect of the failure trigger on the SEA [109] found analogue SEA results in impact conditions with 7 m/s impact velocity (47 kJ/kg in average, which is not far from the 44 kJ/kg calculated in the previous investigation on another batch of material [106]), and lower SEA (41 kJ/kg) in quasi-static compression tests carried out at a constant speed of 100 mm/min. Both quasi-static and impact tests were affected by high SEA scatter, but an analysis of variance test showed a significant effect of the testing condition (p-value 0.6%, test results summarized in Figure 91b).

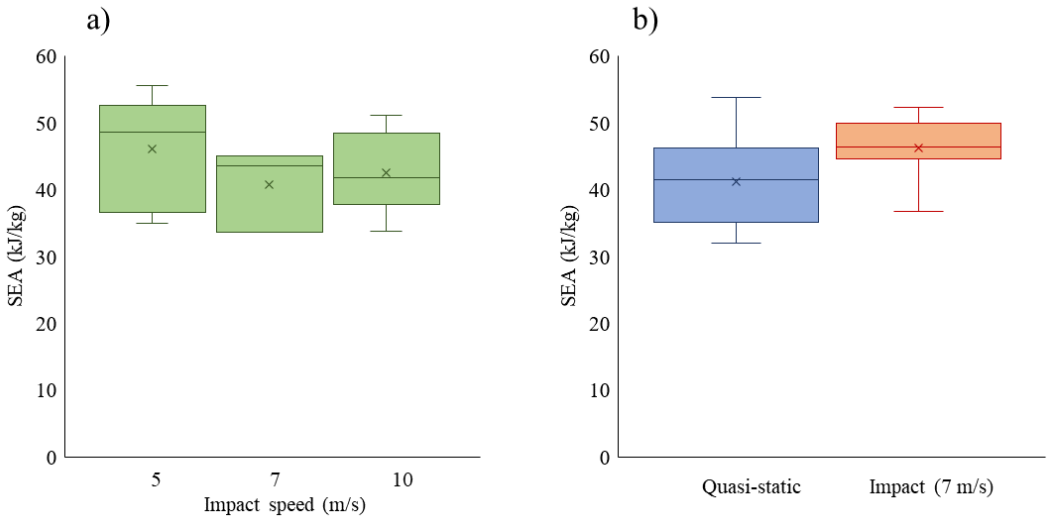


Figure 91: a) SEA of carbon/epoxy specimens as a function of the impact velocity obtained from impact tests [106]; b) SEA of carbon/epoxy specimens in quasi-static and impact crashworthiness tests [109].

To study the effect of the impact speed on a different material and geometry, some tubular specimens were tested in quasi-static conditions at a constant speed of 100 mm/min and in impact conditions at a velocity of 5 m/s and 9 m/s. The tubular specimens were cut from longer tubes made of glass 0°/90° fabric in epoxy resin known with the commercial name of NEMA G10. The material is similar to NEMA FR4 and is used for similar applications, even if FR4 is commercially available in flat plates while G10 is available in tubes. The tubes had an external diameter of 30 mm, a wall thickness of 1 mm and a height of 150 mm to be clamped in the same fixture used for tests on flat specimens. A chamfer lathed on one of the sides acted as failure trigger. The specimens showed a mixed failure mode as reported in Figure 92a, consisting of splaying with some material flowing inside the tube and some material flowing externally, with tearing in some points. The tests showed a decreasing trend of the SEA with higher impact velocity, as highlighted in Figure 92b.

a) b)

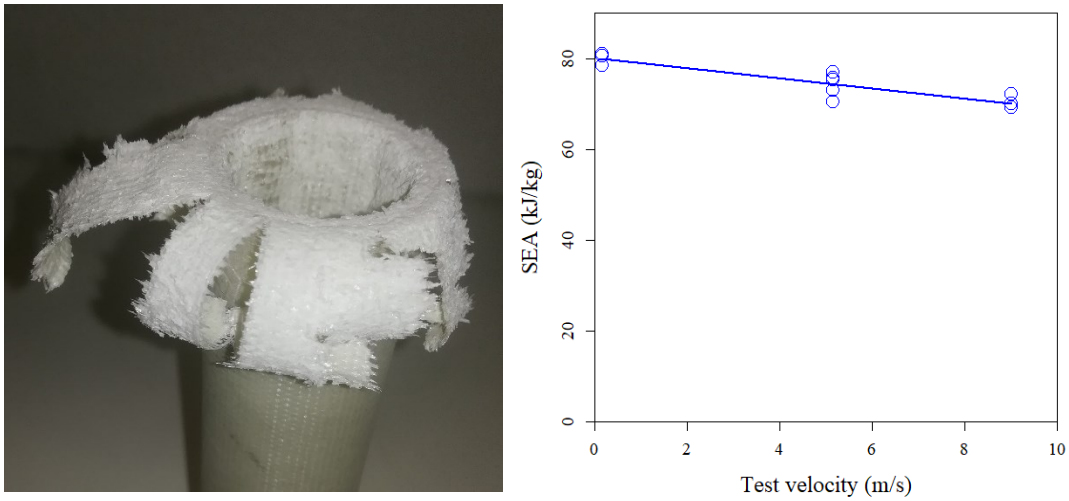


Figure 92: Failure mode of SEA of G10 glass/epoxy specimens and SEA as a function of the test velocity.

The two materials (carbon/epoxy flat specimens and glass/epoxy tubular specimens) showed two different trends of the SEA as a function of the test velocity. Explaining this effect is not easy and requires deeper investigation in future works on different materials. A similar increase of SEA at higher test velocity has been obtained by Thornton et al. on glass/epoxy and carbon/epoxy tubes [113] and more recently by Barnett et al. on short fiber carbon/epoxy [24]. It can be due to an increase in the strength of the matrix, as it is found experimentally in epoxies [42]. The decrease observed on the glass/epoxy tubes is something more difficult to explain, probably due to the complex fracture behavior of composites which is influenced by the different specimen geometry as well. Decreasing trends with increased testing velocity were found on Polyester composites [113]. The observed trends certainly require further deeper studies but confirm the usefulness of the proposed testing procedure to observe strain-rate dependent behaviors.

### 4.2.3 Effect of the testing temperature

The characterization of the GG630T-37 carbon/epoxy laminate was completed with tests at high and low temperature to assess the effect of the environmental conditions on the crash process and material properties. Tests were carried out in the thermostatic chamber of an Instron 9450 drop tower at room temperature (23 °C), -40 °C and 80 °C, that are typical testing temperature adopted in the automotive field to represent the possible conditions found by the material during operation. Flat specimens were tested in splaying and tearing failure mode, and the same tests were carried out on waved specimens as well. The impact energy in all the tests was 400 J, the dropped mass 15.75 kg, and the impact velocity 7 m/s.

The SEA plotted in Figure 93 indicates mild effects of the testing temperature on test results. No trend is visible in tearing tests (blue box plots), while a decrease of the SEA of waved specimens was found at high temperature (green box plots). Flat specimens (red box plots) tested at room temperature showed high scatter, that was lower at high temperature (with similar average SEA) and at low temperature, where a decrease of the average SEA was found.

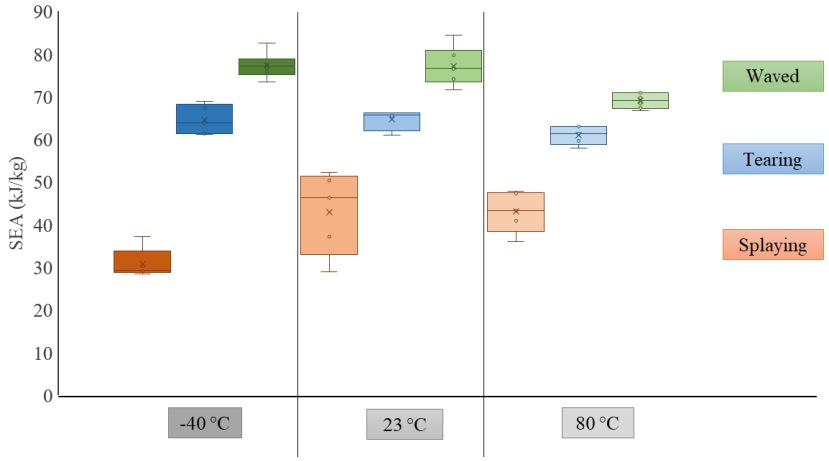


Figure 93: SEA of GG630 carbon/epoxy at different testing temperature: flat specimens in splaying and tearing conditions and tests on waved specimens.

The failure modes (Figure 94, Figure 95 and Figure 96) look similar regardless of the testing temperature, with some exceptions described in the following.

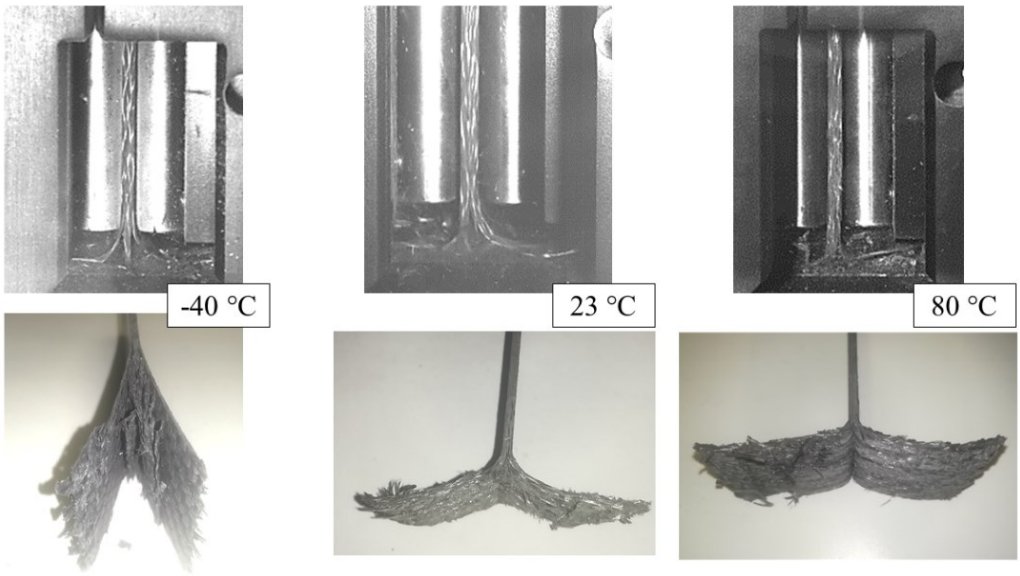


Figure 94: Failure modes of flat carbon/epoxy specimens during and after splaying test at different temperatures.

The decrease of the SEA at low temperature in splaying tests is probably explained by the embrittlement of the matrix, that causes a different failure mode as shown in Figure 94. The lower SEA of waved specimens at high temperature could be due instead to a softening behavior because the temperature gets close to the glass transition temperature of the matrix (135 °C) or to changes in the interaction between matrix and fibers triggered by the high temperature.

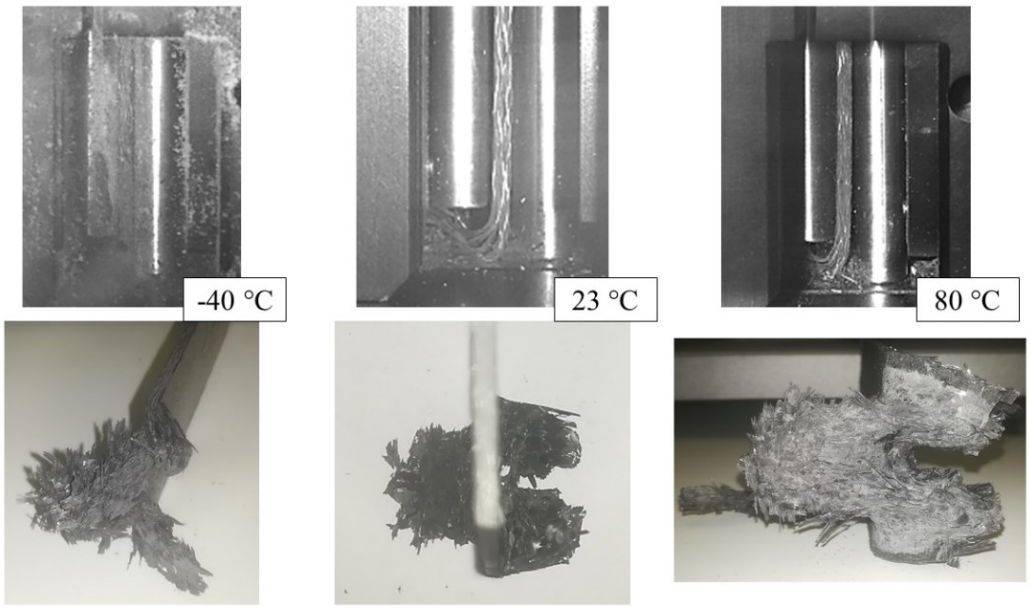


Figure 95: Failure modes of flat carbon/epoxy specimens during and after tearing test at different temperatures.

These hypotheses require necessarily further investigations to be confirmed because the failure mode does not show visible changes at different temperatures (Figure 96) and this effect seems to be only typical of waved specimens, while matrix-related or interface-related behaviors would be expected to give some effects in the splaying test, that mainly involves delamination.

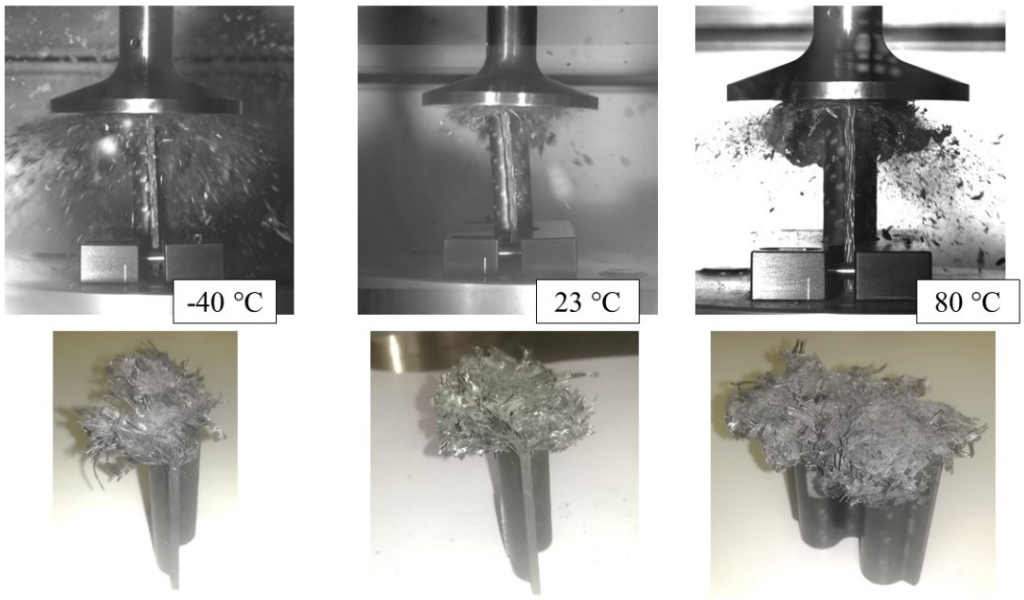


Figure 96: Failure modes of flat carbon/epoxy specimens during and after splaying test at different temperatures.

Similar trends showing the best performances at room temperature and a decrease of SEA at higher or lower temperature in epoxy-based composites can be found in the literature [24, 113]. Interesting work for the future will be the study of the behavior of other materials, both thermosets and thermoplastics, at different temperatures, or tests performed at temperatures higher than the glass transition temperature.

# Chapter 5

# Numerical modeling

## 5.1 Modeling approach

Last step in this research project is the evaluation of the usefulness of the experimental results to tune the material cards of FEM codes and evaluate their predictive capabilities, that would strongly reduce the cost and time of development of new crash box composite structures. Between the available explicit FEM codes able to simulate crashes and composites, LS-Dyna was chosen because of the high number of material models and algorithms available, that is witnessed by a wide literature [74]. The LS-Opt optimizer was employed to work with LS-Dyna keyword files and run sensitivity analyses on the material models, Design of Experiment (DOE) analyses, and curve matching optimizations. The steps of the research path can be summarized as follows:

- realization of a model reproducing the splaying test carried out on the developed fixture and use it for the identification of the unknown parameters of the material card related to the delamination failure dominated by the matrix,
- realization of a model reproducing the tearing test carried out on the developed fixture and use it for the identification of the unknown parameters of the material card related to fiber failure,

- verification of the validity of the identified parameters by using them to predict the failure of the waved specimen, characterized by a more complex geometry and different SEA.

Crash simulation of composites are generally recognized as a complex matter to deal with, and this was confirmed by this work that gave only preliminary results that deserve to be further investigated in future works. Due to the high number of parameters available in LS-Dyna, only the most important steps of the research are summarized in the following, together with the final setup of the model. Due to the simultaneous development of the experimental setup and the numerical models, the latter does not reproduce the final version of the fixture, but the previous one designed for 100 mm-wide specimens and impactor for direct contact with the specimen (Section 3.1.1). The material under investigation is the same GG630T-37 carbon/epoxy laminate characterized by experiments in Section 4.

## 5.2 Simulation of the crashworthiness test on flat specimens

The planned research required to optimize the simulation parameters based on the results of experimental tests on flat coupons. The first model built for this work reproduced the splaying test, by modeling the specimen with a single layer of shell elements. Several investigations on mesh, element formulations, contact parameters and material parameters were carried out on this model and are reported in Section 5.2.1. While capable to reproduce the experimental force-displacement curve, the single shell layer model was not able to reproduce the delamination that happens during the splaying test, and showed wrong behavior in tearing tests without the increase of the SEA found during the experiments; for this reason, a new model consisting of two shell element layers bonded by cohesive elements was prepared (Section 5.2.2).

Then some studies on the parameter identification in LS-Opt were performed to find the most effective way to set up the optimization for a material with unknown properties as described in Section 5.2.3. Finally, the predictive capabilities of the model were tested in Section 5.3.

Two experimental tests (a splaying test and a tearing test) on a four layers GG630T laminate were taken as reference to build the numerical models. Both tests were conducted on 100 mm-wide flat specimens with an impact energy of 800 J, an impact velocity of 7 m/s and a dropped mass of about 33 kg. Both specimens had a 5 mm-deep saw tooth trigger that needs to be taken in account in the numerical model to correctly reproduce the initial force peak. The curves were filtered as described in section 3.1.6 to simplify the operation of the curve matching algorithms and are reported in Figure 97.

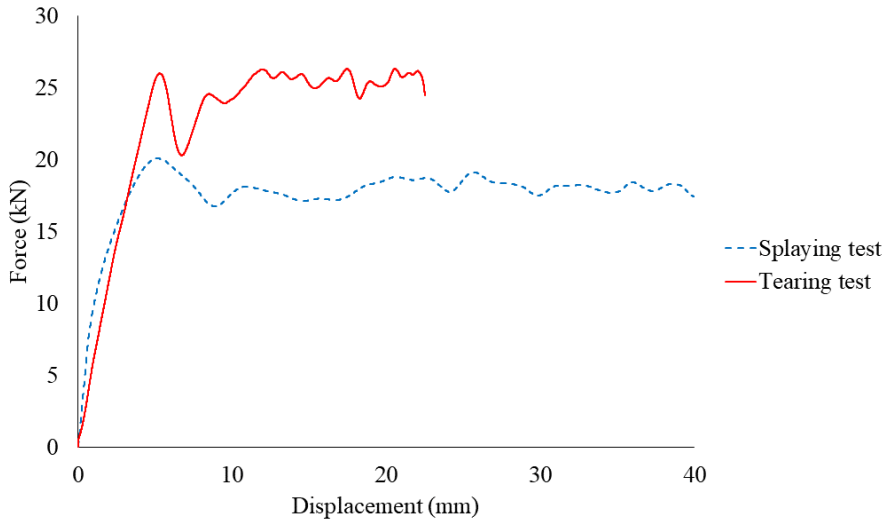


Figure 97: Experimental curves used as target for the realization of the FEM models.

## 5.2.1 Single shell element model

The first approach adopted to simulate the splaying test on the carbon/epoxy laminate was to model a single layer of shell elements. The PART_COMPOSITE card in LS-Dyna allowed to model the laminate as four layers (0.625 mm thickness each, total thickness 2.5 mm), and for each one the software uses an integration point. As the laminate was made of four 0° layers, the model was set accordingly. Element formulation 16 (fully integrated shell element) and 8 (Belytschko-Leviathan shell) were used in the first trials as explained in the following.

The impactor was modeled as a single layer of shell elements made of steel with a thickness of 2 mm, fully integrated formulation and elastic material model MAT001. The material properties of steel were attributed to the part. This solution was required to have an effective contact with the specimen and avoid non-realistic failures in the upper part of the specimen that were not happening during experiments. The impact dropped mass was modeled as a concentrated mass in the central node of the impactor. The anti-buckling columns were modeled using rigid material (MAT020), while the lower crash plate (the surface against which the specimen fails) was modeled as a rigid wall with a friction coefficient of 0.06. A CONTACT_AUTOMATIC_SINGLE_SURFACE was set to reproduce contacts between specimen, anti-buckling columns and impactor. The dynamic friction coefficient was set to 0.06 as found during the experiments (Section 3.1.3, stainless steel columns), and the static friction coefficient was estimated as the double of the static one and set to 0.12. The simulation setup is shown in Figure 98.

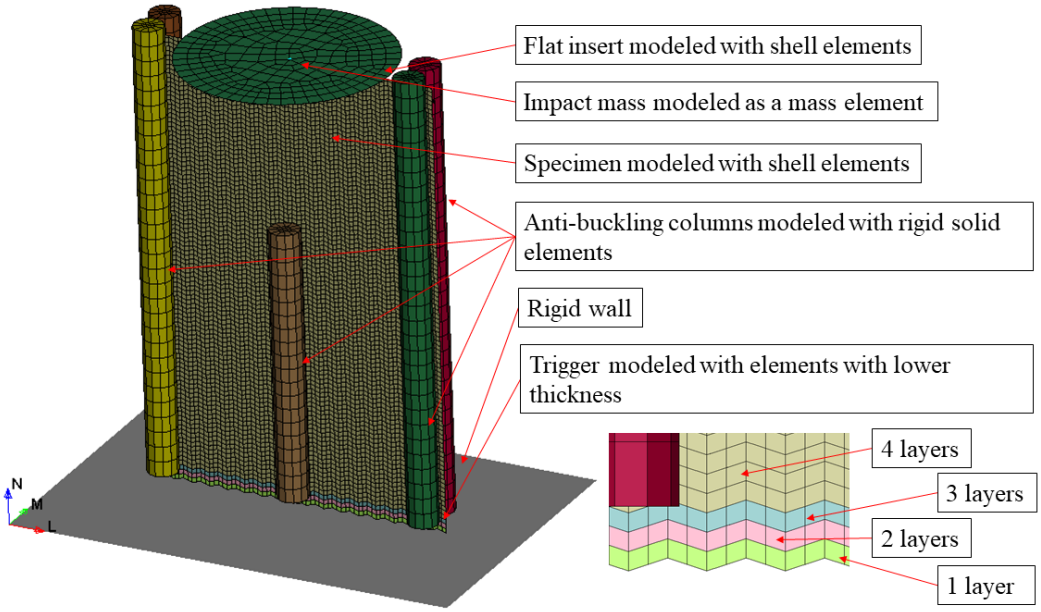


Figure 98: Single shell layer model setup.

Between the several material cards available to simulate the failure of composites, MAT54 was chosen because is the most used in the literature for these applications and the simplest to be set up thanks to the lower number of parameters and experimental data required. The material parameters used to build the model are reported in Table 9. Some parameters were available from material standard characterization tests whose results are summarized in Table 1, other parameters required calibration comparing the simulation results to experimental data. The comparison mainly involved the two force-displacement curves, the energy absorption level during the test and the visual aspect of the failure.

**Table 9**: MAT45 material card used to simulate the crashworthiness test.

| **Parameter** | Value | Comments |
|---|---|---|
| **RO** | 1.729e-6 | Material density, measured |
| **EA** | 58.8 | Elastic modulus, 0° direction, average of tensile and compression test results from Table 1 |
| **EB** | 58.8 | Elastic modulus, 0° direction, average of tensile and compression test results from Table 1 |
| **PRBA** | 0.074 | Poisson modulus, from Table 1 |
| **GAB, GBC, GCA** | 3.7 | Tangential moduli, from Table 1 |
| **2WAY** | 1 | Considers 2-way fiber behavior |
| **DFAILM** | - | Unused when 2WAY=1, that means DFAILC and DFAILT are used in both 0° and 90° directions |
| **DFAILS** | Tuned | Maximum shear strain |
| **TFAIL** | 1e-6 | Initially calibrated by trial-and-error |
| **ALPH** | 0 | Not influent on crash results |
| **SOFT** | Tuned | Critical parameter of the *crashfront* algorithm |
| **FBRT** | 0 | Not influent on crash results |

| | | |
|---|---|---|
| **YCFAC** | 2 | Default value |
| **DFAILT** | Tuned | Maximum tensile strain |
| **DFAILC** | Tuned | Maximum compressive strain |
| **EFS** | 0 | Set to zero to control element deletion with DFAILT, DFAILC and DFAILS |
| **XC** | 0.334 | Compression strength in 0° direction, from Table 1 |
| **XT** | 0.911 | Tensile strength in 0° direction, from Table 1 |
| **YC** | 0.334 | Compression strength in 90° direction, from Table 1 |
| **XT** | 0.911 | Tensile strength in 90° direction, from Table 1 |
| **SC** | 0.065 | Shear strength, from Table 1 |
| **BETA** | 0 | Not influent on crash results |
| **PEL** | 100 | Default value |
| **SLIMC1** | Tuned | Factor to determine the minimum stress limit after stress maximum |
| **Other** | Default | - |

Some preliminary investigations were performed with a tentative material card to set up properly the model before parameters identification trials. Several details of the model were found to be influent on the test results, pointing out the importance of minimizing the number of modifications between different models whose results need to be compared.

Different mesh architectures were tested to understand their effect on the simulation results. A structured mesh made of perfectly squared elements provided an irregular force signal due to the progressive deletion of rows of elements covering the full width of the specimen; the result is a force signal that bounces between zero (contact loss when a row of elements is deleted) and a maximum. These force oscillations can be filtered to better visualize the force curve, but caused in some cases unrealistic failures on the upper part of the specimen due to peak force higher than in experiments. To avoid these unwanted

effects, a waved mesh was employed obtaining a self-filtered signal and a lower probability of unrealistic failures. Two types of waves here called small wave (with a period of two elements, still affected by failures on the top of the specimen) and large wave (period of four elements) were tested finding better results with the latter. An interesting result of this investigation on structured mesh is that the average force calculated using the different types of mesh changed significantly, and another different result was obtained with a random mesh generated with the Auto Mesher command in LS-Prepost (Figure 99). This result pointed out the necessity of further investigation on the mesh effect on the results, that was assessed with a convergence analysis on the different meshes.

The mesh architecture and size were found to be influent on the results as plotted in Figure 99, and a convergent trend is not clearly visible. Focusing on the mesh that gives the best results (large wave mesh), its average crash force oscillates around a value of about 9.5 kN with an amplitude of 1.5 kN, while the solution time increases exponentially for smaller elements. Given the necessity of using the same mesh to run long optimization runs and to simulate larger components, a mesh size of 1.5 mm was chosen to limit the calculation time without getting too far from the average value of 9.5 kN.

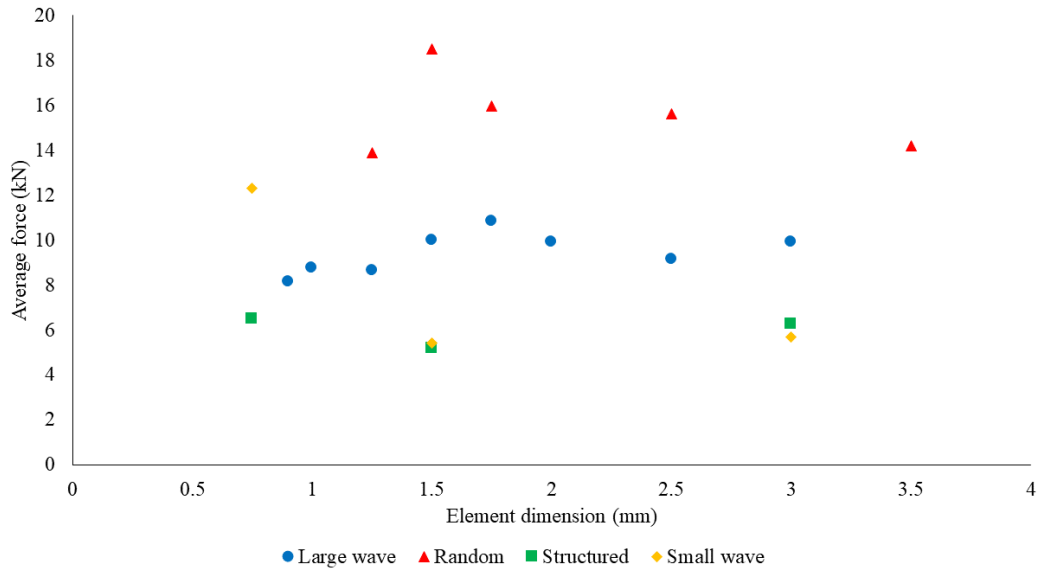


Figure 99: Effect of the mesh size on the average crash force in a single shell layer models with different meshes.

Several element formulations are available in LS-Dyna and can be suited for different applications. Different element formulations were tested to understand their effect on results and calculation time, finding non negligible differences. The fully integrated shell formulation (Formulation 16 fast or -16 accurate) were found to be more expensive and less sensitive to material card parameters than formulation 8 (Belytschko-Leviathan shell), that was then used in most of the work carried out. Another parameter influencing the crash curve was the number of integration points on the thickness, whose increment strongly also increases the calculation time. A number of integration points equal to the number of layers was adopted according to the LS-Dyna defaults.

Several strategies were tried to better simulate the trigger, which is necessary to start the failure in the lower part of the specimen. Reproducing the exact triangular geometry of the specimen was not effective because excessively reduced the resistance in the trigger area. A better approach to simulate the reduction of the cross section interested by the failure was the reduction of the thickness of the lower three rows of elements respectively from four layers to three, two and a single layer (Figure 98).

### 5.2.2 Double shell element model with cohesive elements

A more complex and realistic representation of the crashworthiness test was realized with a different model consisting of two layers of shell elements bonded by cohesive elements. This model can reproduce delamination, which is the main failure mechanism of the splaying test and allows to differentiate between intra-laminar behavior (shell elements) and inter-laminar behavior (cohesive elements), getting a more accurate representation of crash phenomenon as represented in Figure 100.

a) b)

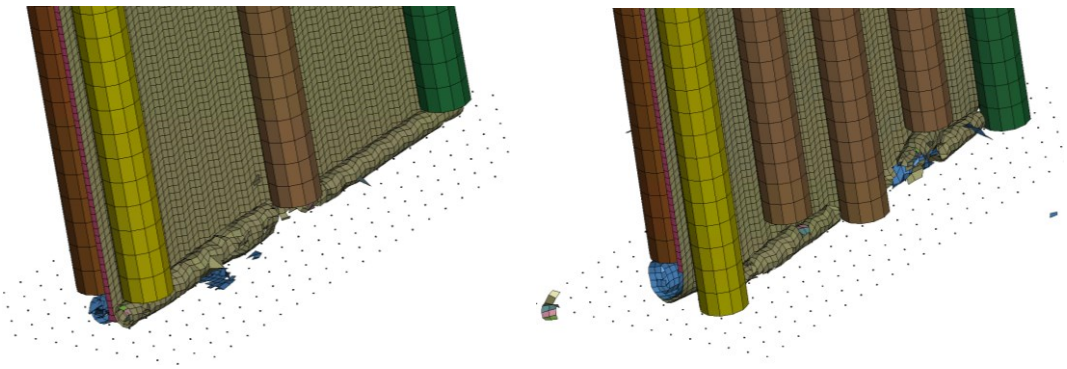

Figure 100: Different failure modes obtained using the model with cohesive elements: a) splaying test, b) tearing test.

Element formulation 8 and MAT54 were used in the shell elements and MAT138 for the cohesive elements, while the other aspects of the model remained unchanged respect to the single shell element model. The parameters of the MAT138 card are reported in Table 10: MAT138 material card used to simulate the intra-laminar behavior of the composite laminate.Table 10.

**Table 10**: MAT138 material card used to simulate the intra-laminar behavior of the composite laminate.

| Parameter | Value | Comments |
|---|---|---|
| **EN** | 3.2 | Normal stiffness, from [98] |
| **ET** | 2 | Tangential stiffness, from [98] |
| **GIC** | Tuned | Energy release rate for mode I |
| **GIIC** | 0.0015 | Energy release rate for mode II |
| **T** | Tuned | Peak tensile stress in normal direction, initially set to 0.075 as indicated in [98], then further calibrated |

| | | |
|---|---|---|
| **S** | 0.0375 | Estimated as T/2 |
| **UND** | Tuned | Ultimate displacement in the normal direction |
| **UTD** | 0.2 | Ultimate displacement in the tangential direction, initially calibrated by trial and error |

Due to the higher number of elements the solution time increased significantly compared to the single shell element model.

### 5.2.3 Material parameters identification

After a working model is built with tentative parameters, to get good agreement with the experimental data it is necessary to tune some material card parameters that are not representing the physical properties obtained from standard material tests, but are necessary to describe the crash failure through the so-called *crashfront* algorithm. In MAT54, these parameters are [76]:

- the strain failure values (DFAILT, DFAILC, DFAILS, DFAILM and EFS, see Table 9), that cause the element deletion and are then directly related to the energy absorption of the material;
- SOFT, an essential parameter of the *crashfront* algorithm to transmit the load from a failed element to its neighbor element;
- TFAIL is another parameter controlling the deletion of elements based on their time step;
- SLIMC1 allows to reduce the compression strength of the element after the peak strength, obtaining a force plateau until the element strain reaches the value set using DFAILC; similar values are available for the tensile and shear behaviors but are not considered here because they showed very low influence on the crash behavior.

To reduce the number of parameters to the most influent on the result and simplify the work of the optimizer, TFAIL was initially calibrated by trial and

error, EFS was set to zero to control the element deletion with specific values in the tensile, compression and shear direction, and DFAILM was not used because using the 2WAY flag the algorithm works with same properties in both fiber and matrix directions (option used to simulate fabrics as in the case of GG630T prepreg). In a first sensitivity analysis, DFAILT and DFAILS showed very low influence on the results because the elements failed under compression load, the optimization was then set to optimize only DFAILC, SLIMC1 and SOFT.

A first optimization run was performed using the Sequential optimization with Domain Reduction (SRSM) in LS-Opt, considering only the splaying test and obtaining a good matching with the experimental curve. A schematic representation of the optimization setup is given in Figure 101. The parameters found were not able to predict the different results obtained with the tearing tests.

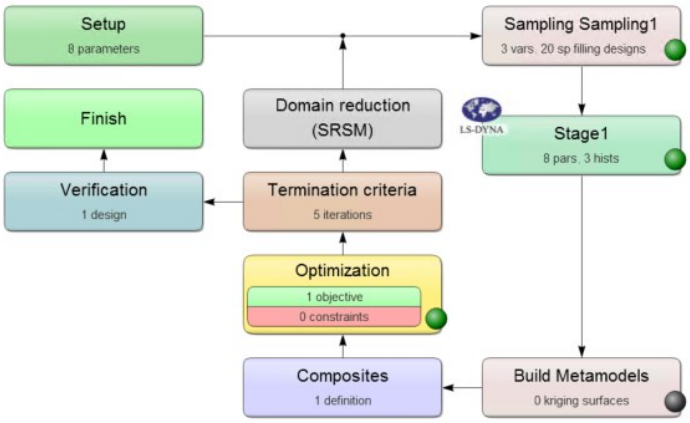


Figure 101: Optimization setup based on the splaying test in LS-Opt.

For this reason, a new optimization was set up combining both splaying and tearing tests in the same objective function, that was then the sum of the mean square difference between the simulated and experimental splaying test and the mean squared difference between the simulated and experimental tearing test (Figure 102). The new set of parameters obtained in this way should be able to reproduce both the splaying and tearing behaviors of the material.

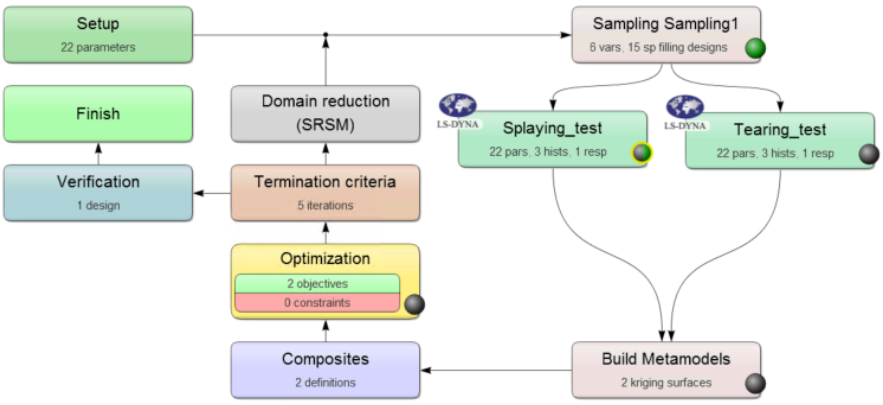


Figure 102: Optimization setup based on splaying and tearing test in LS-Opt.

The combined optimization based on splaying and tearing test was also performed using the model with cohesive elements; the optimized parameters in this case were again DFAILC, SLIMC1 and SOFT with the addition of DFAILT to describe the tensile behavior of the material and T, UND and GIC that describe the peel behavior of the adhesive layer (**Errore. L'origine riferimento non è stata trovata.**).

### 5.2.4 Model of the test of the waved specimen

To verify the effectiveness of the numerical model to predict the behavior of a different structure after the calibration of the material parameters based on the crashworthiness test on flat specimens, a new model was built to reproduce the crash test on the waved specimen described in Paragraph 4.2.3. The model (Figure 103) is as similar as possible to the previously described models (same mesh architecture, testing conditions, contact and material parameters, two versions with and without cohesive layer), and reproduces the waved specimen test (no anti-buckling system, trigger in the upper part, fixed constraint on the bottom).

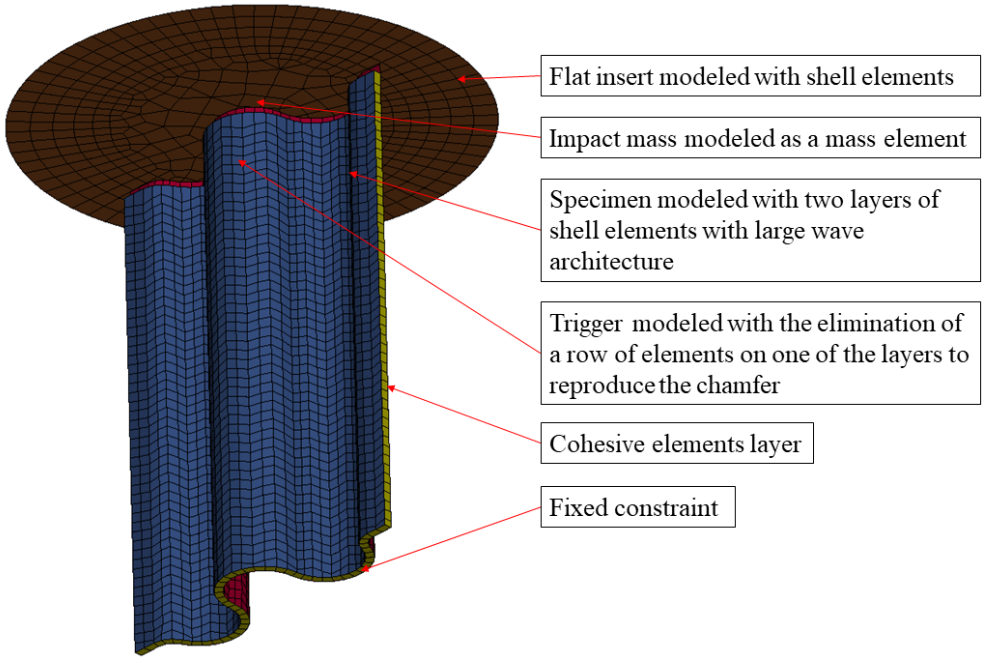


Figure 103: Setup of the waved specimen crash test simulation.

In the single shell layer model the trigger is simulated imposing reduced thickness in the upper elements raw (half thickness), while in the model with cohesive elements the first row of shell elements of one layer is deleted.

## 5.3 Simulation results

This chapter presents the results obtained from the simulations described in the previous pages. Between the several outputs of the numerical models, the attention was mainly focused on the force-displacement curves, that well characterize the phenomenon and provide an immediate comparison with the experimental curves. The SEA calculated from the simulated curves was used to have a quantitative evaluation of the similitude of the simulated curve with the experimental one.

The simulated force-displacement curve was obtained as the combination of the displacement of the impactor (vertical displacement of the node where the impactor mass is applied, from the nodal output NODOUT database) and the

contact force between the specimen and the impactor (using a FORCE_TRANSDUCER_PENALTY card). The experimental force signal was filtered as described in Paragraph 3.1.6, while a Butterworth filter with cutting frequency of 300 kHz was used to filter the simulated force signal.

### 5.3.1 Parameters identification

A preliminary parameter identification was performed considering only the splaying test. The simplest model built with a single layer of shell elements was able to reproduce quite accurately the experimental force-displacement curve (Figure 104), with an initial force peak followed by a plateau. The optimal curve obtained from the model with cohesive elements is also shown in Figure 104. Both curves overlap the force plateau with good accuracy. However, they do not overlap the experimental curve in its initial part, meaning that the trigger could be modeled in a more realistic way. The single shell model shows higher oscillations of the force signal, that are reduced by the model with cohesive elements. The failure mode consists of simple deletion of elements in the single shell model, and becomes more realistic with delamination and formation of small circular fronds in the model with cohesive elements (Figure 105).

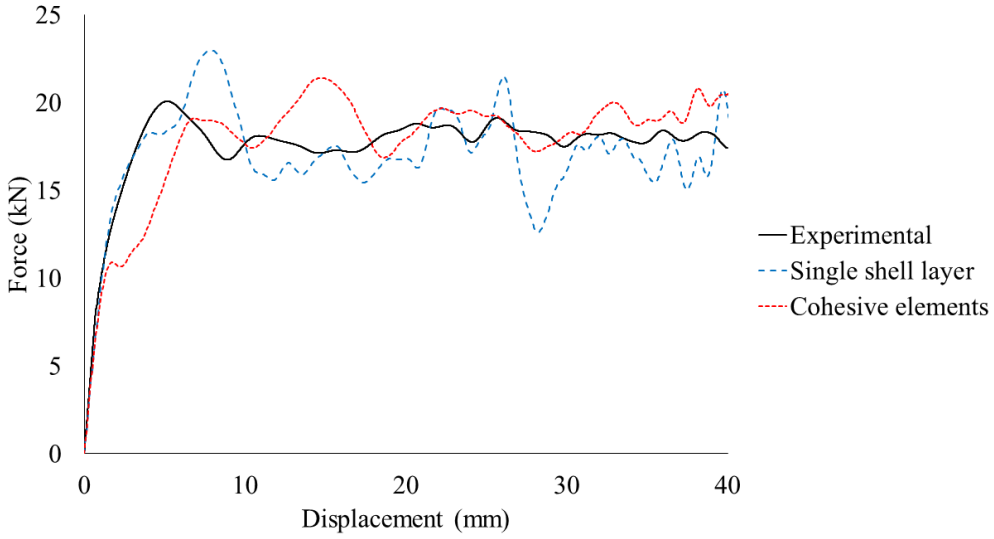


Figure 104: Results of the optimization of the model using MAT54 based on the splaying experimental test.

a) b) c)

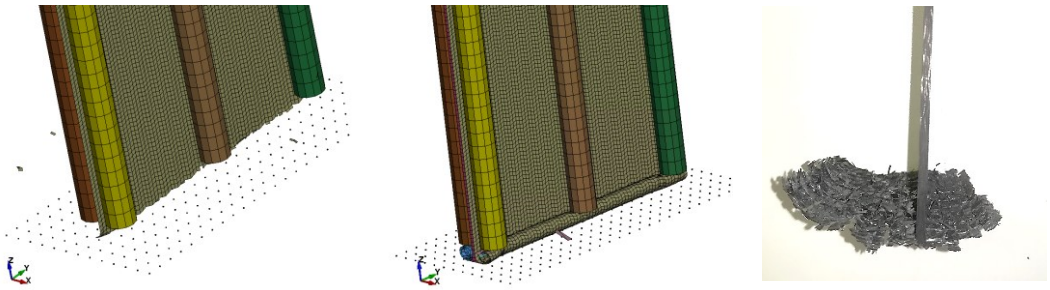

Figure 105: Failure modes of the model using MAT54 optimized based on the splaying experimental test compared with the real failure mode: a) single shell simulation, b) simulation with cohesive elements, c) failure mode observed during experiments.

The results of some trials to reproduce the tearing test using the single shell layer strategy are not reported here because the behavior of the material was very similar to the splaying test, i.e. the elements failed under compression load and no tearing happens, causing the force plateau to remain at the same level. Because of the better results achieved using cohesive elements, that can differentiate between inter-laminar and intra-laminar behavior, the combined optimization based on both splaying and tearing test was performed only on this model. The result (Figure 106) is a material card able to reproduce quite well the splaying test but not the tearing test. Figure 106 clearly shows that the force increase found experimentally is not reproduced in the simulation, where the tearing test shows lower force than the splaying test.

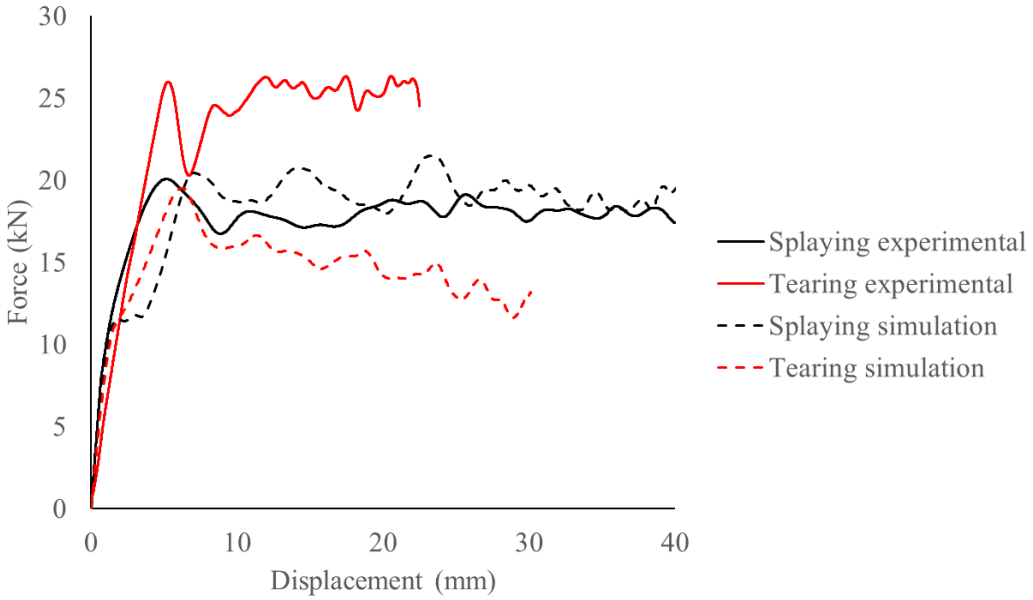


Figure 106: Results of the simulation of the splaying and tearing tests after combined optimization based on the experimental results of the two tests.

The result is probably explained by the fact that the tearing failure mechanism, that causes fibers failure and force increase in the tearing test, is not reproduced by the material formulation, that causes the element to fail under compression load.

### 5.3.2 Prediction of the crash behavior of a sinusoidal specimen

To test the effectiveness of the developed material cards to simulate different structures with complex geometry predicting their crash behavior and SEA, the test carried out on the waved carbon/epoxy specimens was modeled following the same approaches used for the flat specimen described in Paragraph 5.2. The results are summarized by the force-displacement curves plotted in Figure 107, that shows significantly lower force than the experiments. The evaluation of the SEA in the range between 10 mm and 20 mm gives then a lower result of 43.6 kJ/kg for the model with single shell layer and 33.5 kJ/kg for the model with cohesive elements.

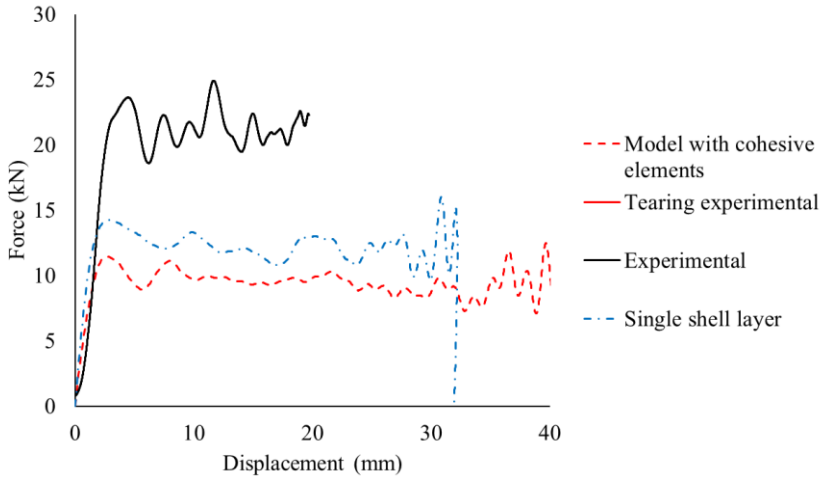


Figure 107: Results of the simulation of the crash test on waved specimens with parameters tuned based on the test of flat specimens.

The failure mode is similar to those shown by the tearing tests presented in Paragraph 5.3.1 (Figure 108), with elements deletion due to compressive failure without formation of fronds or evident tears in the failed material.

a) b)

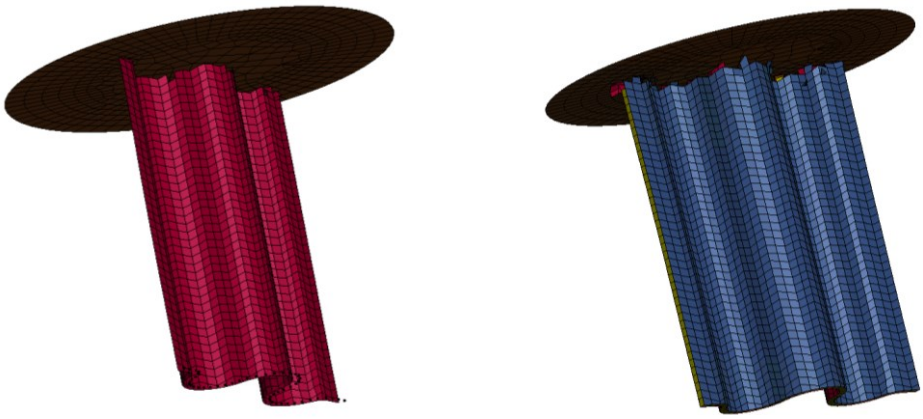

Figure 108: Failure modes of the simulation of the crash test on waved specimen: a) model with single shell layer, b) model with two shell layers bonded by cohesive elements.

Table 11 reports a summary of the obtained results with the percentage error respect to the experimental results.

**Table 11**: Summary of SEA results obtained from experiments and simulations.

| | **Splaying test** | | **Tearing test** | | **Waved specimen** | |
|---|---|---|---|---|---|---|
| | **SEA (kJ/kg)** | **Error** | **SEA (kJ/kg)** | **Error** | **SEA (kJ/kg)** | **Error** |
| Experimental | 48.1 | - | 69.3 | - | 79.1 | - |
| Single shell layer | 44.6 | -7% | - | - | 43.6 | -45% |
| Cohesive elements | 52.5 | 9% | 42.1 | -39% | 33.5 | -58% |

The results reported in this chapter clearly point out the difficulties that the material model exhibits when it must reproduce different failure modes with different effectiveness of energy absorption. The careful observation of the failure process in the simulations and the several studies carried out by changing various parameters in the model have not given a clear explanation of the presented results.

From the results described in this paragraph, some conclusions can be drawn:

- Optimization can give a set of material card parameters that simulates with good accuracy a crash test used as target by the curve matching algorithm.
- Trying to find a set of parameters able to reproduce more failure conditions using the same material card is a difficult task for the optimizer; more work will be necessary in future to find faster and more accurate parameters identification strategies.
- The predictive capabilities of the material cards for very different tests than the one used for parameter identification showed to be very

inaccurate; more work and probably more complex material models are necessary to obtain good predictive capabilities.

### 5.3.3 Use of the material model MAT262

The last step of this chapter is the evaluation of the capabilities of a more recent and complete material model to reproduce the different failure modes, that according to the results presented in the past pages seems to be the main issue with MAT54.

The most complete and lately developed material model in LS-Dyna is MAT262, based on the fracture mechanics formulation proposed by Maimì, Camanho et al. [114, 115]. This model requires several parameters that can be obtained from fracture mechanics tests [116] that were not available for the GG630 carbon/epoxy laminate, and needed to be found through parameters identification like the non-physical parameters of MAT54.

Six parameters of the material model (GXC, GXC0, GXT, GXT0, GYC, GYC0) were initially set as indicated in [116] for another carbon/epoxy material and later adjusted with a combined optimization based on the splaying and on the tearing test, similarly to the one represented in Figure 102.

This model showed that the simulated force curve increases of about 30% when moving from the splaying to the tearing test, in agreement with the experimental observation. This trend is visible from the two dashed curves in Figure 109. The same figure shows also that more efforts are needed to find values to match with more accuracy the experimental curves (initial peaks and average force in the sustained crash region), but the capacity of MAT262 to give a force increase when the failure mode becomes tearing seems to indicate a good potential for the prediction of the crash behavior of complex structures.

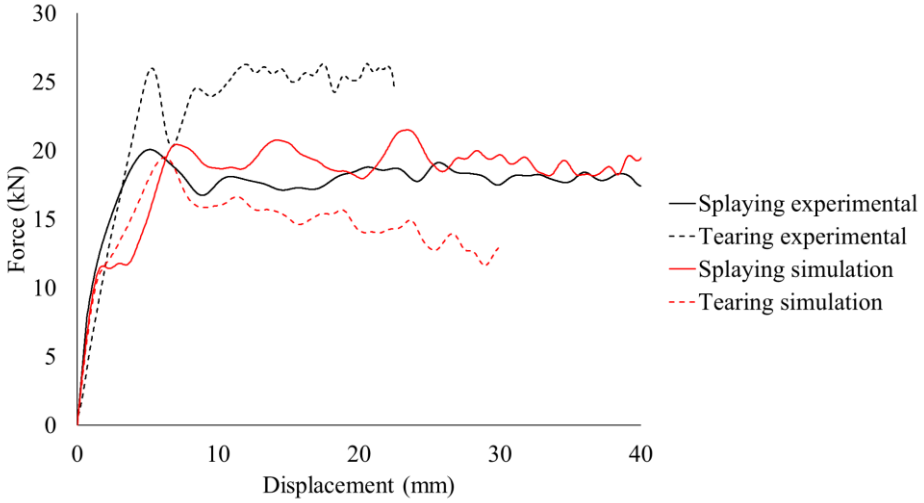


Figure 109: Results of the simulation using MAT262 of the splaying and tearing tests after combined optimization based on the experimental results of the two tests.

The failure mode (Figure 110) is similar to the experimental observations in the tearing test, with material flowing in the gaps between the columns and tearing because of the constraints (Figure 110b), while the element deletion for compression failure in the splaying test (Figure 110a) indicates a non-perfect balance between the failure of cohesive and shell elements, that needs to be optimized.

a) b)

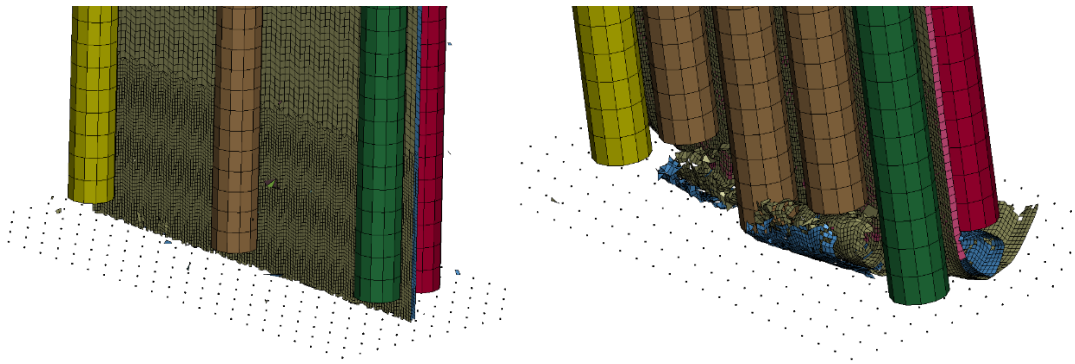

Figure 110: Failure modes of simulations using MAT262: a) splaying test, b) tearing test.

The results presented in this chapter leave several open points that will be assessed in future research. The crash simulation of composites is a complex field and deserves deeper investigations than what is reported in this work. What clearly comes out form these results is the importance of studying different failure modes in order to obtain really predictive capabilities from a model using a specific material card. For this reason, running tests obtaining different failure modes is extremely important, and the results show that the splaying and tearing tests on flat specimens and the crash test of the waved specimen are all good targets for material card parameters identification or validation.

# Chapter 6

# Conclusions and further research

This work has demonstrated how the assessment of the crashworthiness of composites is a complex and actual theme. The first part of the work aimed at identifying the issues that are slowing down the diffusion of composites for crashworthiness, identifying the absence of standard testing procedures and properties databases, the high development costs, the uncertainty on the failure process and the low predictive capabilities of FEM codes as the most critical aspects.

To address these issues, an innovative testing procedure has been developed to measure the SEA of material samples and study their failure process. The tests performed using the original testing setup to characterize a carbon/epoxy laminate have shown the influence of several factors on the energy absorption level of the same material. Summarizing, the higher the level of fragmentation of the material or the number of tears forcing fibers failure, the higher is the energy absorbed. The different kinds of failure can be triggered by external constrains, like those imposed by the developed testing fixture, or by the specimen geometry itself, as it is witnessed by the tests of waved specimens or of a full-scale component that were carried out. The failure mode has proven to be the main parameter influencing the SEA, while other parameters like the impact velocity and the

testing temperature showed a less dramatic influence, but need to be always considered.

The testing procedure has been developed to get the best compromise between research and industrial needs. The choice of using a flat specimen makes easier and cheaper the specimen production process, and the imposition of specific constraints allows to study different failure modes to have the most complete understanding of the behavior of the material. This choice and the decision to develop the fixture as an accessory of a drop tower testing machine found good interest both in the research and industrial fields, and the collaboration with other companies, universities and research institutions allowed to get new ideas that have been implemented in the last version of the device. Now it is ready to be used by anyone for future studies on new materials, or on the effect of the manufacturing process, layups, presence of defects or new testing conditions.

The study of the material models for composites in LS-Dyna is the part of this work that has encountered more difficulties, and this was mainly due to the good comprehension of the material behavior gained with experiments, that was hard to simulate numerically. While a procedure to easily and automatically identify the material parameters to simulate a specific test has been developed, the objective of getting a unique material card that could reproduce all the effects met during experiments was not reached. The experimental framework proved to be a good benchmark for building material models able to stress the capacities of the model; a material card able to reproduce all the different behaviors explained in this work will certainly be a good candidate for the prediction of the crash behavior of more complex structures.

# References


1. CMH-17 (2012) Crashworthiness and Energy Management. In: Composite Materials Handbook (CMH-17)

2. Böhler P (2019) Crash Management for the Mobility of Tomorrow. Light Des Worldw 12:52–57. https://doi.org/10.1007/s41777-019-0048-x

3. Park C-K, Kan C-D (Steve), Hollowell WT, Hill SI (2012) Investigation of Opportunities for Lightweight Vehicles Using Advanced Plastics and Composites. Natl Highw Traffic Saf Adm Report No.:416p

4. ASTM (2016) ASTM D3410-16: Standard Test Method for Compressive Properties of Polymer Matrix Composite Materials. https://doi.org/10.1520/D3410

5. (2018) ASTM D3763 − 18: Standard Test Method for High Speed Puncture Properties of Plastics Using Load and Displacement Sensors

6. (2018) ASTM D5628 − 18: Standard Test Method for Impact Resistance of Flat, Rigid Plastic Specimens by Means of a Falling Dart (Tup or Falling Mass)

7. (2000) ISO 6603-1: Plastics - Determination of puncture impact behaviour of rigid plastics - Part 1 : Non-instrumented impact testing

8. (2000) ISO 6603-2: Plastics — Determination of puncture impact behaviour of rigid plastics — Part 2: Instrumented puncture testing

9. (2015) ASTM D7136/D7136M − 15: Standard Test Method for Measuring the Damage Resistance of a Fiber-Reinforced Polymer Matrix Composite to a Drop-Weight Impact Event

10. (2017) ASTM D7137/D7137M − 17: Standard Test Method for Compressive Residual Strength Properties of Damaged Polymer Matrix

Composite Plates

11. Feraboli P, Deleo F, Garattoni F (2007) Efforts in the standardization of composite materials crashworthiness energy absorption. Am Soc Compos - 22nd Tech Conf Am Soc Compos 2007 - Compos Enabling a New Era Civ Aviat 1:741–759

12. Barnes G, Coles I, Roberts Ri, et al (2010) Crash Safety Assurance Strategies For Future Plastic and Composite Intensive Vehicles (PCIVs). US Dep Transp Natl Highw Traffic Saf Adm 130

13. Carruthers JJ, Kettle AP, Robinson AM (1998) Energy absorption capability and crashworthiness of composite material structures: A review. Appl Mech Rev 51:635–649. https://doi.org/10.1115/1.3100758

14. Lukaszewicz DH -J. A (2013) Automotive Composite Structures for Crashworthiness. In: Elmarakbi A (ed) Advanced Composite Materials for Automotive Applications: Structural Integrity and Crashworthiness. John Wiley & Sons, Ltd, Chichester, UK, pp 99–127

15. Farley GL, Jones RM (1989) Energy-Absorption Cabability of Composite Tubes and Beams. NASA Technical Memorandum 101634.

16. Hull D (1991) A Unified Approach to Progressive Crushing of Fibre-Reinforced Composite Tubes. Compos Sci Technol 40:377–421

17. Cutting RA, Rios-Tascon F, Goodsell JE (2020) Experimental investigation of the crush performance of prepreg platelet molding compound tubes. J Compos Mater 54:4311–4324. https://doi.org/10.1177/0021998320929418

18. Vigna L, Babaei I, Garg R, et al (2021) An innovative fixture for testing the crashworthiness of composite materials. Frat ed Integrità Strutt 15:76–87. https://doi.org/10.3221/IGF-ESIS.55.06

19. Feraboli P, Wade B, Deleo F, Rassaian M (2009) Composites : Part A Crush energy absorption of composite channel section specimens. Compos Part A 40:1248–1256. https://doi.org/10.1016/j.compositesa.2009.05.021

20. Farley GL (1991) The Effects of Crushing Speed on the Energy-Absorption Capability of Composite Tubes. J Compos Mater 25:1314–1329. https://doi.org/10.1177/002199839102501004

21. Chambe JE, Dorival O, Bouvet C, Ferrero JF (2018) Crushing of composite tubular structures and energy absorption for aircraft seats development.

ECCM 2018 - 18th Eur Conf Compos Mater 24–28

22. Kim JS, Yoon HJ, Shin KB (2011) A study on crushing behaviors of composite circular tubes with different reinforcing fibers. Int J Impact Eng 38:198–207. https://doi.org/10.1016/j.ijimpeng.2010.11.007

23. Jacob GC, Starbuck JM, Fellers JF, Simunovic S (2005) Effect of fiber volume fraction, fiber length and fiber tow size on the energy absorption of chopped carbon fiber-polymer composites. Polym Compos 26:293–305. https://doi.org/10.1002/pc.20100

24. Barnett PR, Hulett BM, Penumadu D (2021) Crashworthiness of recycled carbon fiber composites. Compos Struct 272:114232. https://doi.org/10.1016/j.compstruct.2021.114232

25. Cauchi Savona S, Hogg PJ (2006) Effect of fracture toughness properties on the crushing of flat composite plates. Compos Sci Technol 66:2317–2328. https://doi.org/10.1016/j.compscitech.2005.11.038

26. Hamada H, Coppola JC, Hull D (1992) Effect of surface treatment on crushing behaviour of glass cloth/epoxy composite tubes. Composites 23:93–99. https://doi.org/10.1016/0010-4361(92)90109-8

27. Bisagni C (2009) Experimental investigation of the collapse modes and energy absorption characteristics of composite tubes. Int J Crashworthiness 14:365–378. https://doi.org/10.1080/13588260902792954

28. Thornton PH (1979) Energy Absorption in Composite Structures. J Compos Mater 13:247–262

29. Heimbs S, Strobl F (2009) Crash Simulation of an F1 Racing Car Front Impact Structure. 7th Eur LS-DYNA Conf 1–8

30. Sigalas I, Kumosa M, Hull D (1991) Trigger mechanisms in energy-absorbing glass cloth/epoxy tubes. Compos Sci Technol 40:265–287. https://doi.org/10.1016/0266-3538(91)90085-4

31. Thuis HGSJ, Metz VH (1994) The influence of trigger configurations and laminate lay-up on the failure mode of composite crush cylinders. Compos Struct 28:131–137. https://doi.org/10.1016/0263-8223(94)90043-4

32. Dalli D, Varandas LF, Catalanotti G, et al (2020) Assessing the current modelling approach for predicting the crashworthiness of Formula One composite structures. Compos Part B Eng.

https://doi.org/10.1016/j.compositesb.2020.108242

33. Ueda M, Anzai S, Kubo T (2015) Progressive crushing of a unidirectional CFRP plate with V-shaped trigger. Adv Compos Mater 24:85–95. https://doi.org/10.1080/09243046.2014.882540

34. Bru T, Waldenström P, Renaud G, et al (2017) Development of a test method for evaluating the crushing behaviour of unidirectional laminates. J Compos Mater 29:4041–4051. https://doi.org/https://doi.org/10.1177/0021998317697811

35. Lavoie JA, Morton J (1993) Design and Application of a Quasistatic Crush Test Fixture for Investigating Scale Effects in Energy Absorbing Composite Plates. NASA Contractor Report 4526.

36. Feraboli P (2009) Development of a Modified Flat-plate Test Specimen and Fixture for Composite Materials Crush Energy Absorption. J Compos Mater 43:1967–1990. https://doi.org/https://doi.org/10.1177/0021998309343025

37. Babaei I, Garg R, Vigna L, et al (2020) Newly Developed Anti-Buckling Fixture to Assess the In-Plane Crashworthiness of Flat Composite Specimens. Appl Sci 10:7797. https://doi.org/10.3390/app10217797

38. Czaplicki MJ, Robertson RE, Thornton PH (1991) Comparison of bevel and tulip triggered pultruded tubes for energy absorption. Compos Sci Technol 40:31–46. https://doi.org/10.1016/0266-3538(91)90041-M

39. Jiménez MA, Miravete A, Larrodé E, Revuelta D (2000) Effect of trigger geometry on energy absorption in composite profiles. Compos Struct 48:107–111. https://doi.org/10.1016/S0263-8223(99)00081-1

40. Siromani D, Henderson G, Mikita D, et al (2014) Composites : Part A An experimental study on the effect of failure trigger mechanisms on the energy absorption capability of CFRP tubes under axial compression. Compos PART A 64:25–35. https://doi.org/10.1016/j.compositesa.2014.04.019

41. Chambe JE, Bouvet C, Dorival O, et al (2020) Effects of dynamics and trigger on energy absorption of composite tubes during axial crushing. Int J Crashworthiness 26:549–567. https://doi.org/10.1080/13588265.2020.1766175

42. Siviour CR, Jordan JL (2016) High Strain Rate Mechanics of Polymers: A

Review. J Dyn Behav Mater 2:15–32. https://doi.org/10.1007/s40870-016-0052-8

43. Ma L, Liu F, Liu D, Liu Y (2021) Review of strain rate effects of fiber-reinforced polymer composites. Polymers (Basel) 13:. https://doi.org/10.3390/polym13172839

44. Zabala H, Aretxabaleta L, Castillo G, et al (2014) Impact velocity effect on the delamination of woven carbon – epoxy plates subjected to low-velocity equienergetic impact loads. Compos Sci Technol 94:48–53. https://doi.org/10.1016/j.compscitech.2014.01.016

45. Aryal B, Morozov E V, Wang H, et al (2019) E ff ects of impact energy , velocity , and impactor mass on the damage induced in composite laminates and sandwich panels. Compos Struct 226:111284. https://doi.org/10.1016/j.compstruct.2019.111284

46. Duong AV, Rivallant S, Barrau JJ, et al Influence of speed on the crushing behavior of composite plates. In: 7th Asian-Australasian Conference on Composite Materials 2010, ACCM 2010. Taipei, Taiwan, pp 678–681

47. Zhang Z, Sun W, Zhao Y, Hou S (2018) Crashworthiness of different composite tubes by experiments and simulations. Compos Part B Eng 143:86–95. https://doi.org/10.1016/j.compositesb.2018.01.021

48. Boria S, Scattina A, Belingardi G (2015) Axial energy absorption of CFRP truncated cones. Compos Struct 130:18–28. https://doi.org/10.1016/j.compstruct.2015.04.026

49. Zhao X, Zhu G, Zhou C, Yu Q (2019) Crashworthiness analysis and design of composite tapered tubes under multiple load cases. Compos Struct 222:110920. https://doi.org/10.1016/j.compstruct.2019.110920

50. Bisagni C, Di Pietro G, Fraschini L, Terletti D (2005) Progressive crushing of fiber-reinforced composite structural components of a Formula One racing car. Compos Struct 68:491–503. https://doi.org/10.1016/j.compstruct.2004.04.015

51. Mischo F, Goergen C, Schmeer S, Mitschang P (2020) Use of recycled carbon staple fibers in an advanced thermoforming process and analysis of its crash performance. Adv. Manuf. Polym. Compos. Sci. 6:48–56

52. Feraboli P (2008) Development of a corrugated test specimen for composite materials energy absorption. J Compos Mater 42:229–256.

https://doi.org/10.1177/0021998307086202

53. Jackson A, Dutton S, Gunnion AJ, Kelly D (2011) Investigation into laminate design of open carbon-fibre/epoxy sections by quasi-static and dynamic crushing. Compos Struct 93:2646–2654. https://doi.org/10.1016/j.compstruct.2011.04.032

54. Tan W, Falzon BG (2016) Modelling the crush behaviour of thermoplastic composites. Compos Sci Technol 134:57–71. https://doi.org/10.1016/j.compscitech.2016.07.015

55. Joosten MW, Dutton S, Kelly D, Thomson R (2011) Experimental and numerical investigation of the crushing response of an open section composite energy absorbing element. Compos Struct 93:682–689. https://doi.org/10.1016/j.compstruct.2010.08.011

56. Dubey DD, Vizzini AJ (1998) Energy Absorption of Composite Plates and Tubes. J Compos Mater 32:158–176. https://doi.org/10.1177/002199839803200204

57. Daniel L, Hogg PJ, Curtis PT (2000) Crush behaviour of carbon fibre angle-ply reinforcement and the effect of interlaminar shear strength on energy absorption capability. Compos Part B Eng 31:435–440. https://doi.org/10.1016/S1359-8368(00)00026-3

58. Cauchi Savona S, Hogg PJ (2006) Investigation of plate geometry on the crushing of flat composite plates. Compos Sci Technol 66:1639–1650. https://doi.org/10.1016/j.compscitech.2005.11.011

59. Jacob GC, Michael Starbuck J, Simunovic S, Fellers JF (2003) New Test Method for Determining Energy Absorption Mechanisms in Polymer Composite Plates. Polym Compos 24:706–715. https://doi.org/10.1002/pc.10064

60. Jacob GC, Fellers JF, Starbuck JM, Simunovic S (2004) Crashworthiness of automotive composite material systems. J Appl Polym Sci 92:3218–3225. https://doi.org/10.1002/app.20336

61. Jacob GC, Starbuck JM, Fellers JF, et al (2006) Crashworthiness of various random chopped carbon fiber reinforced epoxy composite materials and their strain rate dependence. J Appl Polym Sci 101:1477–1486. https://doi.org/10.1002/app.24224

62. Jacob GC, Michael Starbuck J, Simunovic S, Fellers JF (2003) Energy

Absorption in Glass-Reinforced Continuous Strand Mat Composites. J Appl Polym Sci 90:3222–3232. https://doi.org/10.1002/app.12999

63. Lescheticky J, Barnes G, Schrank M (2013) System level design simulation to predict passive safety performance for CFRP automotive structures. SAE Tech Pap 2:. https://doi.org/10.4271/2013-01-0663

64. Aitharaju V, Kia HG, Aashat S, Pulugurtha VC (2016) Modeling of Crush Behavior of Carbon Fiber Composites. Proc Am Soc Compos - Thirty-first Tech Conf

65. Newcomb BA (2022) Dynamic crush response of compression molded planar isotropic carbon fiber reinforced composites. Polym Compos 1–13. https://doi.org/10.1002/pc.27155

66. Guillon D, Rivallant S, Barrau J, et al (2009) Experimental and numerical study of the splaying mode crush of CFRP laminates. ICCM Int Conf Compos Mater 27–31

67. Ueda M, Nishimura T (2010) Compressive failure of unidirectional CFRP plate under progressive crushing. 25th Tech Conf Am Soc Compos 14th US-Japan Conf Compos Mater 2010 2:1658–1668

68. Feindler N (2014) Charakterisierungs- und Simulationsmethodik zum Versagensverhalten energieabsorbierender Faserverbundstrukturen: Zugl.: München, Techn. Univ. München, Diss., 2012. PhD Diss Tech Univ München 2:

69. Reuter C, Sauerland KH, Tröster T (2017) Experimental and numerical crushing analysis of circular CFRP tubes under axial impact loading. Compos Struct 174:33–44. https://doi.org/10.1016/j.compstruct.2017.04.052

70. Lausch J, Takla M, Schweiger HG (2020) Crush testing approach for flat-plate fibrous materials. Compos Part B Eng 200:. https://doi.org/10.1016/j.compositesb.2020.108333

71. Lausch J, Takla M, Schweiger HG (2021) Crush characteristics of flat-plate discontinuous carbon composites. Compos Part A Appl Sci Manuf 147:106431. https://doi.org/10.1016/j.compositesa.2021.106431

72. Lausch J, Takla M, Schweiger HG (2022) Insight into crush performance comparison of composite profiles and flat plates. Compos Part B Eng 233:109643. https://doi.org/10.1016/j.compositesb.2022.109643

73. Boria S (2016) Lightweight design and crash analysis of composites. In: Lightweight Composite Structures in Transport. Elsevier Ltd

74. Rabiee A, Ghasemnejad H (2022) Finite Element Modelling Approach for Progressive Crushing of Composite Tubular Absorbers in LS-DYNA : Review and Findings

75. Arteiro A, Catalanotti G, Reinoso J, et al (2019) Simulation of the Mechanical Response of Thin-Ply Composites: From Computational Micro-Mechanics to Structural Analysis

76. Livermore Software Technology (2014) Keyword user ’s manual volume II - Material models. Livermore Software Technoloy Corporation (LSTC)

77. Chang F-K, Chang K-Y (1987) Laminated Composites Containing. J Compos Mater 21:834–855

78. Feraboli P, Wade B, Deleo F, et al (2011) LS-DYNA MAT54 modeling of the axial crushing of a composite tape sinusoidal specimen. Compos Part A Appl Sci Manuf 42:1809–1825. https://doi.org/10.1016/j.compositesa.2011.08.004

79. Deleo F, Feraboli P (2011) Crashworthiness energy absorption of carbon fiber composites: Experiment and simulation. Soc Plast Eng - 11th-Annual Automot Compos Conf Exhib ACCE 2011

80. Cherniaev A, Montesano J, Butcher C (2018) Modeling the Axial Crush Response of CFRP Tubes using MAT 054, MAT058 and MAT262 in LS-DYNA. In: 15th International LS-DYNA Users Conference

81. Liu Z, Xia Y (2019) Development of a numerical material model for axial crushing mechanical characterization of woven CFRP composites. Compos Struct 230:111531. https://doi.org/10.1016/j.compstruct.2019.111531

82. Boria S (2019) Sensitivity Analysis of Material Model Parameters to Reproduce Crushing of Composite Tubes. J Mater Eng Perform 28:3267–3280. https://doi.org/10.1007/s11665-019-04047-6

83. Boria S, Obradovic J, Belingardi G (2015) Experimental and numerical investigations of the impact behaviour of composite frontal crash structures. Compos Part B 79:20–27. https://doi.org/10.1016/j.compositesb.2015.04.016

84. Raponi E, Fiumarella D, Boria S, et al (2021) Methodology for parameter

identification on a thermoplastic composite crash absorber by the Sequential Response Surface Method and Efficient Global Optimization. Compos Struct 278:114646. https://doi.org/10.1016/j.compstruct.2021.114646

85. Bonnie Wade (2014) Capturing the Energy Absorbing Mechanisms of Composite Structures under Crash Loading. PhD Diss Univ Washingt

86. Hashin Z (1980) Failure Criteria for Unidirectional Fiber Composites. J Appl Mech 47:329–334

87. Scazzosi R, Manes A, Giglio M (2019) An enhanced material model for the simulation of high-velocity impact on fiber-reinforced composites. Procedia Struct Integr 24:53–65. https://doi.org/10.1016/j.prostr.2020.02.005

88. Xiao X, Botkin ME, Johnson NL (2009) Axial crush simulation of braided carbon tubes using MAT58 in LS-DYNA. Thin-Walled Struct 47:740–749. https://doi.org/10.1016/j.tws.2008.12.004

89. Zhou G, Sun Q, Fenner J, et al (2020) Crushing behaviors of unidirectional carbon fiber reinforced plastic composites under dynamic bending and axial crushing loading. Int J Impact Eng 140:103539. https://doi.org/10.1016/j.ijimpeng.2020.103539

90. Livermore Software Technology (2020) Keyword user ’s manual volume I

91. Fang J, Sun G, Qiu N, et al (2017) On design optimization for structural crashworthiness and its state of the art. Struct Multidiscip Optim 55:1091–1119. https://doi.org/10.1007/s00158-016-1579-y

92. Wang J, Yang N, Zhao J, et al (2016) Design and experimental verification of composite impact attenuator for racing vehicles. Compos Struct 141:39–49. https://doi.org/10.1016/j.compstruct.2016.01.013

93. Castro JMPBC, Fontana M, Araujo AL, Madeira JFA (2021) Optimization of a composite impact attenuator for a formula student car. Mech Adv Mater Struct 28:1858–1868. https://doi.org/10.1080/15376494.2020.1712627

94. Boria S, Obradovic J, Belingardi G (2017) On design optimization of a composite impact attenuator under dynamic axial crushing. FME Trans 45:435–440. https://doi.org/10.5937/fmet1703435B

95. Stander N, Basudhar A, et. al. (2019) LS-OPT User ’ s Manual: a design optimization and probabilistic analysis tool for the engineering analyst

96. Babaei I (2020) Structural Testing of Composite Crash Structures. PhD Diss Politec di Torino 1–110

97. Garg R (2021) A Methodology to Predict the Impact Behavior of Automotive Components made of Carbon Fiber / Epoxy Composite. PhD Diss Politec di Torino 1–132

98. Garg R, Babaei I, Paolino DS, et al (2020) Predicting Composite Component Behavior Using Element Level Crashworthiness Tests, Finite Element Analysis and Automated Parametric Identification. Materials (Basel) 13:4501. https://doi.org/10.3390/ma13204501

99. Instron Drop Weight Impact Testing Machine. https://www.instron.com/en-gb/products/testing-systems/impact-systems/drop-weight-impact-testing-machine?region=United Kingdom&lang=en-GB. Accessed 25 Aug 2022

100. Microtex Composites GG 630 T. https://microtexcomposites.com/products/gg-630-t-2/. Accessed 13 Mar 2023

101. Microtex Composites E3-150. https://microtexcomposites.com/products/e3-150/. Accessed 13 Mar 2023

102. Carbon Mind Carbon Mind. https://www.carbon-mind.com/. Accessed 13 Mar 2023

103. National Electrical Manufacturers Association (1998) NEMA LI-1-1998 (R2011): Industrial Laminated Thermosetting Products

104. Demezzi SAS Vetro epossidico NEMA FR4. http://www.demezzi.it/termici/fr4.php. Accessed 13 Oct 2020

105. Destefanis R (2021) Modellazione agli elementi finiti del test di impatto di un provino composito ed ottimizzazione dei parametri dell’impattatore. MS thesis, Politec di Torino

106. Vigna L, Calzolari A, Galizia G, et al (2021) Effect of impact speed and friction on the in-plane crashworthiness of composite of composite plates. Procedia Struct Integr 33:623–629. https://doi.org/10.1016/j.prostr.2021.10.069

107. Vigna L, Calzolari A, Galizia G, et al (2022) Effect of friction on a crashworthiness test of flat composite plates. Forces Mech 6:. https://doi.org/10.1016/j.finmec.2021.100070

108. Schön J (2004) Coefficient of friction and wear of a carbon fiber epoxy matrix composite. Wear 257:395–407. https://doi.org/10.1016/j.wear.2004.01.008

109. Vigna L, Calzolari A, Galizia G, et al (2022) Influence of the trigger geometry in the crash behavior of a carbon fiber laminate. In: ECCM20

110. Colonna E (2022) Sviluppo di un algoritmo per il calcolo della Specific Energy Absorption di laminati compositi impiegati in applicazioni Crashworthiness. MS thesis, Politec di Torino 1–125

111. (2019) ISO 11343 Adhesives – Determination of dynamic resistance to cleavage of high-strength adhesive bonds under impact wedge conditions – Wedge impact method ( ISO 11343 : 2019 )

112. Boria S, Belingardi G, Giannoni F (2014) A crashworthy problem on composite structures using a mathematical approach. Procedia Eng 88:125–132. https://doi.org/10.1016/j.proeng.2014.11.135

113. Thornton PH, Harwood JJ, Beardmore P (1985) Fiber-reinforced plastic composites for energy absorption purposes. Compos Sci Technol 24:275–298. https://doi.org/10.1016/0266-3538(85)90026-0

114. Maimí P, Camanho PP, Mayugo JA, Dávila CG (2007) A continuum damage model for composite laminates: Part I - Constitutive model. Mech Mater 39:897–908. https://doi.org/10.1016/j.mechmat.2007.03.005

115. Maimí P, Camanho PP, Mayugo JA, Dávila CG (2007) A continuum damage model for composite laminates: Part II - Computational implementation and validation. Mech Mater 39:909–919. https://doi.org/10.1016/j.mechmat.2007.03.006

116. Nishi M, Nishihara T, Iimori M, et al (2020) Modeling and Validation of Failure Behaviors of Composite Laminate Components using MAT_262 and User Defined Cohesive Model. 16 th Int LS-DYNA ® Users Conf 1–11